NOVEL APPROACHES FOR THE CHROMATOGRAPHIC AND ELECTROPHORETIC SEPARATION OF MOLECULES

by

AMANDA R. MEYER

B.S., Kansas State University, 2004

AN ABSTRACT OF A DISSERTATION

submitted in partial fulfillment of the requirements for the degree

DOCTOR OF PHILOSOPHY

Department Of Chemistry
College of Arts and Sciences

KANSAS STATE UNIVERSITY
Manhattan, Kansas

2008

Abstract

High-performance liquid chromatography (HPLC) and capillary electrophoresis (CE) are two well-established analytical separation techniques that are continuously being adapted for performing distinctive separations and analyses of multitudes of complex and/or unique samples. Since their introduction, these techniques have been pivotal in the discovery, analysis, and understanding of a variety of samples and still prove to be key analytical tools for biological investigation.

Using these techniques, one can obtain a wide-range of valuable sample information from the hydrophobicity and molecular weights to size and charge distributions. Furthermore, these techniques allow for sample analysis, purification, and collection for additional sample analysis, such as mass spectrometry analysis. My doctoral dissertation encompasses the full scope of these two techniques and novel approaches for the investigation of distinct, relevant samples.

Described herein is the fabrication of glass microfluidic devices used for CE and their diversity for numerous investigations. Chapter 2 shows that the resolution of the photomasks used in microchip fabrication does not alter the separation efficiency of the devices, as the separations remain diffusion-limited. Using an in-house built capillary electrophoresis system, wheat proteins were separated more than 25% faster than previously reported in literature, and the electropherograms used for sample varietal identification. The fabrication of a robust, portable CE system capable of performing biological analysis in microgravity and hypergravity environments is also discussed. The need for and features necessary to achieve a reliable, robust, automated system is further described in Chapter 4. Isolation and analysis of the pea aphid

(*Acyrthosiphon pisum*) salivary secretions was completed for the first time using HPLC. By altering the aphid environment and the sample treatment parameters, sample concentrations were increased above the limit of detection. Coupled with mass spectrometry, identification of pea aphid salivary proteins such as exopeptidase, angiotensin converting enzyme, and *Buchnera* proteins has been achieved. Finally, a simplified contact conductivity detection system for the detection of jurkat cells was developed that surpasses current, complex optical systems. The experiments described in this dissertation demonstrate novel approaches for the preparation, separation, analysis, and identification of a wide variety of common, and uncommon, samples.

NOVEL APPROACHES FOR THE CHROMATOGRAPHIC AND ELECTROPHORETIC SEPARATION OF MOLECULES

by

AMANDA R. MEYER

B.S., Kansas State University, 2004

A DISSERTATION

submitted in partial fulfillment of the requirements for the degree

DOCTOR OF PHILOSOPHY

Department of Chemistry
College of Arts And Sciences

KANSAS STATE UNIVERSITY
Manhattan, Kansas

2008

Approved by:

Major Professor
Christopher T. Culbertson

Abstract

High-performance liquid chromatography (HPLC) and capillary electrophoresis (CE) are two well-established analytical separation techniques that are continuously being adapted for performing distinctive separations and analyses of multitudes of complex and/or unique samples. Since their introduction, these techniques have been pivotal in the discovery, analysis, and understanding of a variety of samples and still prove to be key analytical tools for biological investigation.

Using these techniques, one can obtain a wide-range of valuable sample information from the hydrophobicity and molecular weights to size and charge distributions. Furthermore, these techniques allow for sample analysis, purification, and collection for additional sample analysis, such as mass spectrometry analysis. My doctoral dissertation encompasses the full scope of these two techniques and novel approaches for the investigation of distinct, relevant samples.

Described herein is the fabrication of glass microfluidic devices used for CE and their diversity for numerous investigations. Chapter 2 shows that the resolution of the photomasks used in microchip fabrication does not alter the separation efficiency of the devices, as the separations remain diffusion-limited. Using an in-house built capillary electrophoresis system, wheat proteins were separated more than 25% faster than previously reported in literature, and the electropherograms used for sample varietal identification. The fabrication of a robust, portable CE system capable of performing biological analysis in microgravity and hypergravity environments is also discussed. The need for and features necessary to achieve a reliable, robust, automated system is further described in Chapter 4. Isolation and analysis of the pea aphid

(*Acyrthosiphon pisum*) salivary secretions was completed for the first time using HPLC. By altering the aphid environment and the sample treatment parameters, sample concentrations were increased above the limit of detection. Coupled with mass spectrometry, identification of pea aphid salivary proteins such as exopeptidase, angiotensin converting enzyme, and *Buchnera* proteins has been achieved. Finally, a simplified contact conductivity detection system for the detection of jurkat cells was developed that surpasses current, complex optical systems. The experiments described in this dissertation demonstrate novel approaches for the preparation, separation, analysis, and identification of a wide variety of common, and uncommon, samples.

Table of Contents

List of Figures

List of Tables

Acknowledgements

To all the people who have helped me complete this work, I could not have accomplished it without your encouragement and guidance. Thank you.

Chris Culbertson, thank you for taking me in years ago and teaching me a tremendous amount about separation science and providing the resources for me to become a better scientist. Your ability to think ‘outside the box’ and come up with multiple ideas simultaneously is inspiring and has propelled me forward. Thank you for your patience, guidance, and enthusiasm.

My group members, thank you for teaching me things and helping me brainstorm. Most of all to the boys - thanks for all of the laughs, teasing, and playful behavior – you made the lab a fun place to be! Greg and Pernilla, thank you for everything you have taught me, for always helping me when I needed it, and for being my friend. I have learned so much from knowing all of you that I will carry with me forever.

Faculty, students, and staff in the chemistry department and the university, I appreciate your time and camaraderie throughout the years. You have made the department a pleasant place to be. Especially to Jim Hodgson, Ron Jackson, and Tobe Eggers, thank you for trying to understand my oftentimes-weird ideas, helping me make things, and just being genuine and fun people to be around. Earline Dikeman, thank you for always listening to me, giving me advice, and letting me teach classes that have helped me become a better educator.

Dr. George Lookhart, thank you for your knowledge on the wheat project and for acquiring so many samples for the project. Timothy J. Sobering and David Huddleston (KSU Electronics Design Lab), thank you for your assistance in the design and fabrication of the electronics for the NASA instrument and the conductivity detector. Dr. Steven Gonda, Dr. Janice Huff, Sandra Geffert, and all the staff of NASA’s Microgravity Research Project, thank you for the support and involvement in making the microgravity experiments possible. Dr. Tomich and Yasuaki Hiromasa, thank you for performing the mass spectrometry experiments in your facility and for being patient with me while I was learning how to analyze the data. Dr.

Gerald Reeck and Dr. John Reese, your insight into the world of the pea aphid has helped make this project successful. Thank you for the aphids, your time, and many insightful discussions.

Scott Bean and Brian Ioerger, thank you for letting me use your equipment and sharing with me your immense knowledge of HPLC. Your thought-provoking discussions and willingness to help when I didn't really know what I was doing is greatly appreciated.

Rhonda Reist and Greg Kifer, thank you for being passionate about education and showing me that science is more than a textbook. You taught me that creativity exists in science and its good question what is going on in the world around me. Without your enthusiasm and encouragement to 'play' I would not be where I am today. Thank you.

My friends and 'family' back home, thank you for your continued support and always helping me see the bigger picture. Your passion for life is infectious, and I have come along way with your help and guidance. Through you, I have learned that it's ok to ask for help, and at some point in time everyone needs it! Thank you for always caring, motivating me, and helping me laugh often – especially when I am being stubborn.

Mom and Dad, you taught me so much over the years that has shaped the person that I am today. You have instilled in me the drive and motivation to do whatever I set my mind to, and have had the patience to teach me countless things along the way that have helped me become a better experimentalist and more importantly, a better person. Deseree, Dede, Ashley, and Colin – you are the best siblings a girl could ask for. Thank you for always being there for me. You have made my life a brighter place with your creativity, thoughtful advice, silliness and laughter.

Dedication

This work is dedicated to those who have helped me achieve it and to those whom it may inspire.

Preface

If the term education may be understood in so large a sense as to include all that belongs to the improvement of the mind, either by the acquisition of the knowledge of others or by increase of it through its own exertions, we learn by them what is the kind of education science offers to man. It teaches us to be neglectful of nothing — not to despise the small beginnings, for they precede of necessity all great things in the knowledge of science, either pure or applied.

\- Michael Faraday

'*Science as a Branch of Education*' lecture to the Royal Institution, June 11,1858

CHAPTER 1 - Introduction

Separation science is important for the advancement of all branches of science. It is a critical component not only in research and development, but also in discovery, manufacturing, quantification, and purification of compounds. Though they are still relatively 'young' separation techniques, high performance liquid chromatography (HPLC) and capillary electrophoresis (CE) have proven to be critical in the identification and analysis of a multitude of biological and pharmaceutical compounds.[1] Adaptations and improvements, in instrumentation as well as the approaches used, are continuously evolving, aiding in the analysis of small-scale samples. This is especially important for the analysis of biological samples where small amounts are commonly obtained, and thus small volume sampling challenges continue to exist. As CE is discussed in detail in subsequent chapters, this introduction will primarily cover the background and principles necessary to understand the HPLC separation parameters discussed in the later chapters. This is especially significant, as HPLC remains the principal technique for analysis of most classes of biomolecules, simple and complex, such as amino acids, peptides, proteins, and nucleic acids.

HPLC is defined by and consists of a separation of soluble molecules using (1) a column packed with small diameter particles, (2) a pump with the ability to push solvents through the column bed, and (3) a detector capable of quantitating the compounds of interest. With any technique numerous advantages and limitations exist, and this holds true for HPLC. HPLC possesses numerous features that make it superior to column chromatography such as: (1) increased analysis speed (minutes vs. hours), (2) increased resolution and reproducibility and accuracy, (3) adequate sensitivity for native samples (fg-ng), (4) sample recovery post-analysis, and (5) automated system operation. Limitations include: (1) higher equipment costs, (2) greater system and operation complexity, and (3) occasional difficulties in serial analysis, compound adsorption, and compound coelution.[1]

Chromatographic separations in HPLC require the use of two phases, a stationary and a mobile phase. The stationary phase is generally composed of small diameter spherical particles (ie: silica) that can have a stationary phase support adsorbed or bonded onto the surface. These particles are tightly packed into a stainless steel tube with a specific diameter. These stationary phase particles and the respective tube compose what is called a separation column. The mobile phase consists of the solvent(s) passed through the column to remove, or elute, the solute from the stationary phase. As the solute molecules pass through the column they are transported to the detector by the mobile phase. The eluted analytes possess signals recorded as Gaussian-shaped curves (or peaks). An illustration of a chromatogram with its characteristic features can be seen in **Figure 1.1**. The mobile phase volume (or dead volume) V_M, is the volume of the mobile phase in the column. The time required for this volume (dead volume) is called the dead time (t_o). V_R describes the retention volume, which is the volume of mobile phase that passes through the column from the time of sample injection to the point of peak detection. The time required for the solute peak to be detected is the retention time and is described as t_R. Additionally, the peak width (w) and standard deviation (σ) can be approximated from the chromatogram as shown.

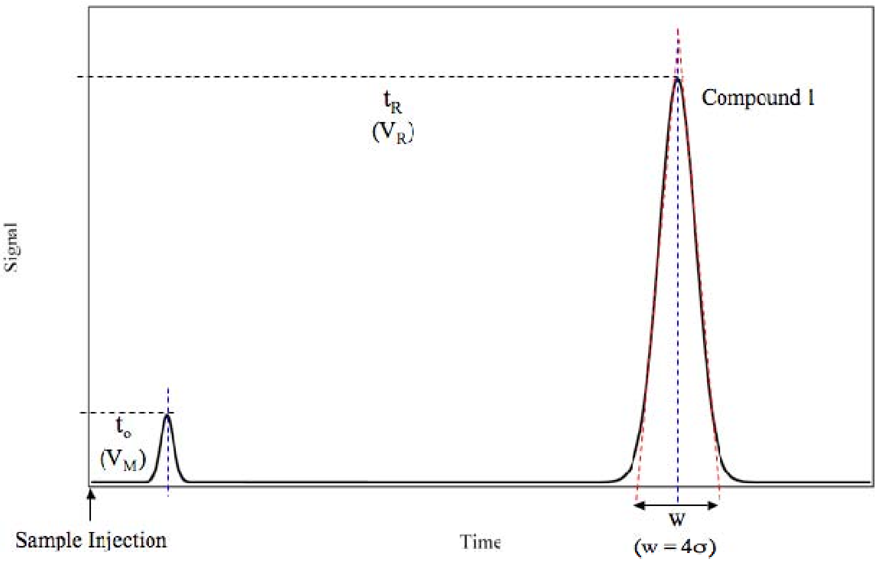

Figure 1.1 Drawing of a chromatogram with its characteristic features.

Separation occurs when the solute molecules travel in a mobile phase and interact with the stationary phase. For liquid-liquid partitioning chromatography, the solute molecules partition into and out of the stationary phase as they move through the column. This interaction is called retention. The longer the molecules spend in the stationary phase, the longer they are retained. The degree to which the solute molecules are retained is determined by the retention (or capacity) factor, k, as seen in equation 1.1:

$$k = K\frac{V_S}{V_M} \qquad (1.1)$$

where K is the partition coefficient, V_S and V_M and the volumes of the stationary and mobile phases, respectively.

The retention factor is measured from the retention time of the analytes (t_R). The retention time is the time required for the peak to be detected, measured at its apex:

$$k = \frac{V_R - V_M}{V_M} = \frac{t_R - t_o}{t_o} = \frac{t_S}{t_o} \qquad (1.2)$$

where V_R and V_M are the retention and mobile phase (dead) volumes, respectively. The dead time (t_o) is the time required for the dead volume to traverse through the column. The volume of solvent that moves through the column from the point of sample injection to the time where the peak is detected defines the retention volume, again measured at the peak apex. From this equation, it is clear that the retention factor is a ratio of the time the solute spends in the stationary phase to that in the mobile phase.

For good quality chromatography, selectivity (α) is one of the most important factors. The ratio of the retention factors of a highly retained compound (k_2) to that of a less retained compound (k_1) determines the selectivity, as shown in equation 1.3.

$$\alpha = \frac{k_2}{k_1} \qquad (1.3)$$

Because selectivity depends on the retention factors of the solute compounds, it is apparent that it is determined by the structures of the solute molecules as well as the composition of the stationary and mobile phases. As such, selectivity is independent of instrumental parameters such as flow rate and column dimensions. In order for a separation to occur, the selectivity must be greater than 1 ($\alpha > 1$). In some instances, it is difficult to determine if complete peak separation has occurred. The degree to which two peaks are separated is defined by the resolution (R_s). The resolution between two peaks can be seen if **Figure 1.2** and calculated using equation 1.4.

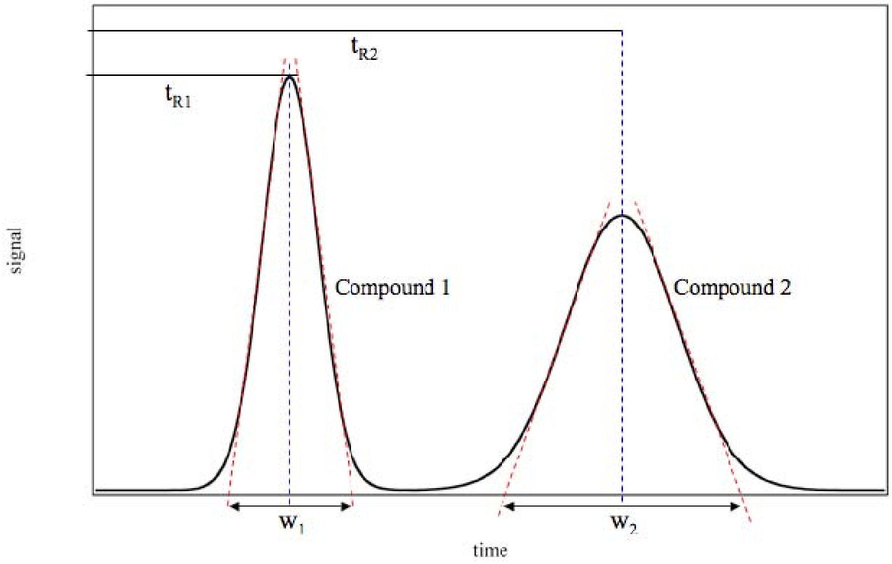

Figure 1.2 A chromatogram illustrating the resolution of two neighboring peaks (1 and 2) using the retention times (t_1 and t_2) and the peak widths (w_1 and w_2).

$$R_s = \frac{2(t_{R2} - t_{R1})}{w_2 + w_1} \qquad (1.4)$$

The retention times for the first and second peaks are given as t_1 and t_2, respectively. The peak widths of the two neighboring peaks (1 and 2) are given as w_1 and w_2, respectively. When the resolution is equal to 1, the peaks are 98% resolved. To improve the resolution one can make their peaks narrower or increase the selectivity.

Resolution is specific to two neighboring compounds in the sample. Often times, a more generic method to relate the separation performance to the fundamental mechanisms of partitioning and band broadening is preferred. In these instances, separation efficiency can be used. Separation efficiency is a measure of how well a column is separating the analytes of interest. Additionally, separation efficiency describes the fundamental processes of band broadening and retention. Separation efficiency can be determined as a function of the column length to allow for comparison of columns of any geometry. This is done calculating the plate height (H) using the column length (L) and/or the peak standard deviation (σ) as seen by equation 1.5. Again, as seen previously in **Figure 1.1**, the standard deviation of a peak is approximately one-fourth of the peak width.

$$H = \frac{\sigma^2}{L} \qquad (1.5)$$

As seen in this equation the plate height is a measure of band broadening per unit length. Additionally, from these equations it is evident that to achieve a high efficiency separation the peak width should remain as sharp (or narrow) as possible as it traverses the column length. This is to say that the peak broadening should be minimized. Band broadening mechanisms fall into three categories as they relate to the mobile phase flow. This is because faster, good-quality separations are ideal. The sum of these three band broadening contributions (A, B, and C terms) as related to the plate height are accounted for in the van Deemter equation shown below:

$$H = A + \frac{B}{u} + Cu \qquad (1.6)$$

where H is the plate height is determined by the linear flow velocity (u) in the presence of these three terms: (A) flow path variations of the solute molecules through the packed bed, (B) axial and longitudinal diffusion of the solute, and (C) solute peak broadening due to mass transfer kinetics will be further discussed.

The effect of band broadening due to flow path variation is due to the contributions of eddy diffusion and variations in laminar flow. The band broadening contribution due to Eddy diffusion can be defined by the equation:

$$H_{eddy} = A_{eddy} d_p \qquad (1.7)$$

where d_p is the particle diameter and A_{eddy} is a measure of the flow path inequality. This term can be significant if the column is not well-packed, resulting in similar solute molecules that will possess dissimilar flow paths (ie: longer or shorter travel lengths). Laminar flow band broadening ($H_{laminar}$) results because solute molecules move slower along the surface of the particles and the column wall and fastest when in the midpoint between two particles. This broadening contribution is described by the following equation:

$$H_{la\min ar} = \frac{A_{la\min ar} d_p^2 u}{D_M} \qquad (1.8)$$

where d_p is the particle diameter, u is the linear flow velocity, and D_M is the diffusion coefficient of the solute and for small molecules is on the order of 10^{-5}. These two contributions are not independent and can be combined into the following equation:

$$H_{flow} = Ad_p \left(\frac{ud_p}{D_M} \right)^{0.33} \qquad (1.9)$$

where A_{dp} is a measure of the column packing. Thus, packing the column with smaller diameter particles will reduce the interparticle fluid regions, which will minimize variations in laminar flow.

The second term of the van Deemter equation describes the effects of axial and longitudinal diffusion. All molecules will diffuse in flow or stagnant conditions when another solvent (ie: the mobile phase) is present. The larger the amount of time the solute and solvent are in contact, the higher the degree of molecular diffusion. This is to say that at low HPLC flow rates, a higher degree of molecular will occur. This axial band broadening contribution (H_{axial}) can be seen in the equation 1.10.

$$H_{axial} = \frac{B_{mp} D_M}{u} \qquad (1.10)$$

where B_{mp} is a constant obstruction factor related to the axial diffusion in the mobile phase. If the solute retention factor (k) is vary large or the stationary phase is very thick, diffusion can also occur. This term is negligible for most modes of HPLC, but can be illustrated in the following equation:

$$H_{axial-sp} = \frac{2kB_{sp} D_s}{u} \qquad (1.11)$$

where B_{sp} is a constant related to the stationary phase and D_s is the diffusion in the stationary phase.

The major contribution to band broadening in HPLC lies in the third term of the van Deemter equation, relating to mass transfer kinetics. This occurs from the finite amount of time required for equilibration of the solute molecule with the stationary phase. The solute molecules in the stationary phase are being temporarily immobilized while the solute in the mobile phase is allowed to move forward through the column. The solute diffuses into the pores on the stationary phase. The mobile phase in these pores is not effectively pumped and is stagnant. This behavior slows the kinetics of the mobile phase transfer and thus causes solute molecules to move slower than identical non-stagnant solute molecules, resulting in band broadening defined by:

$$H_{pores} = \frac{C_m d_p^2 u}{D_M} \qquad (1.12)$$

where C_m is a mass transfer constant dependent upon the retention factor and stationary phase porosity. When all of the significant terms of band broadening are combined, and expanded van Deemter equation is achieved as seen below in equation 1.13.[1-3]

$$H = Ad_p\left(\frac{ud_p}{D_M}\right)^{0.33} + \frac{BD_M}{u} + \frac{Cd_p^2 u}{D_M} \qquad (1.13)$$

In an isocratic separation the separation efficiency of the column defined by the plate height is a relative term. A more absolute measure of the solute partitioning in and out of the stationary and mobile phases can be given as the number of theoretical plates (N). The number of theoretical plates is a kinetic parameter used to measure the separation efficiency. This measurement holds true for Gaussian peaks and the efficiency can be determined from a chromatogram using the following equation:

$$N = 16\left(\frac{t_R}{w}\right)^2 \qquad (1.14)$$

were t_R is the peak retention time and w is the peak width. Because the peak width is approximately four times the peak standard deviation (σ), this equation can also be written as:

$$N = \left(\frac{t_R}{\sigma}\right)^2 \qquad (1.15)$$

It is important to note that the separation efficiency given in this manner is dependent upon the separation conditions. To accurately describe the efficiency, this value must be accompanied by: (1) the column length and internal diameter, (2) the sample compound, retention factor and size, (3) stationary and mobile phases, (4) the mobile phase flow rate and (5) the column temperature.

As discussed previously the separation speed, solute retention, and resolution are interrelated parameters. Oftentimes, improving one parameter will compromise another. Within these parameters are additional interrelated components. Specifically, resolution is dependent upon the combination of three factors: separation efficiency, selectivity, and retention. Each factor can improve or degrade the separation resolution and the impact of each can be investigated individually using the Purnell equation below (1.16).

$$R = \frac{\sqrt{N_2}}{4}\left(\frac{\alpha - 1}{\alpha}\right)\left(\frac{k_2}{1 + k_2}\right) \qquad (1.16)$$

From this equation, resolution can be calculated as a function of retention, selectivity, and efficiency. Additionally, the relative effect of each parameter can be examined. For a separation to occur, the solute molecules must be retained on the column. However, if the solute is highly retained, there is an increase in analysis time that can also be considered detrimental. At values of $k > 5$, there are no significant increases in resolution because this term approaches 1. The second parameter effecting resolution, selectivity, can have a range of 10^3 and can cause the most significant changes in resolution. Because of this, selectivity should be the main focus of separation optimization. These two parameters can be altered by adjustments in the mobile and/or stationary phases. The third term, separation efficiency, also plays a role in the resolution. However, because the resolution is proportional to the square root of the plate number, this parameter does not have a tremendous impact. Additionally, the plate number is generally increased by the use of a longer column, which will increase the column pressure and analysis time. Because of this, the separation efficiency is not the most favorable means for resolution improvement.

When solute mixtures contain many components, it is more important to determine how many peaks can be separated than solely looking that the resolution of two peaks. This can be found using the peak capacity equation below. Peak capacity is defined by the number of peaks (n_c) that can be separated with a resolution (R_s) over a path length of L or over an elution volume range of V_{max}-V_{min}.[4]

$$n = \frac{L}{w} = \frac{L}{4\sigma} \qquad (1.17)$$

In some cases, complete peak resolution is not necessary, and R_s values are adequate. In these situations, the peak capacity increases as shown by:

$$n_c = \frac{L}{4\sigma R_s} \qquad (1.18)$$

and when the migration distance is replaced by L this equation reduces to:

$$n_c \sim \frac{N^{1/2}}{4} \qquad (1.19)$$

In chromatography, new peaks can be resolved with each successive volume sweep, causing peak capacity values to be larger than anticipated if using the above equations. For chromatographic separations, the peak capacity can be approximated using equation 1.20, incorporating the largest and smallest volumes in which peaks can be eluted, V_{max} and V_{min}, respectively:

$$n_c = 1 + \frac{N^{1/2}}{4} \ln \frac{V_{\max}}{V_{\min}} \qquad (1.20)$$

The separation efficiency equations above hold true for isocratic separations, where the mobile phase consists of only one solvent. When a combination of analytes need to be separated, isocratic separations are generally not possible if the analytes have a wide range of hydrophobicities/hydrophilicities. This is especially true for separations of complex biological samples. Such a sample is discussed in Chapter 5. In these cases, gradient elution is used and consists of a process where at least two different solvents with varying elution strengths are continuously blended over the elution period. Commonly two solvents are used: water and an organic modifier. In reversed phase chromatography, the average value of retention (k*) obtained using a gradient can be determined by:

$$k^{*} = 0.87 t_G \left[\frac{F}{V_M \Delta\Phi S} \right] \qquad (1.21)$$

where t_G is the gradient time, F is the flow rate, V_M is the total mobile phase volume in the column, $\Delta\Phi$ is the change in solvent strength, and S is a constant that is specific to the mobile phase solvent combination. From this equation it is evident that the peak elution time can be decreased by increases in the solvent strength of the mobile phase or the gradient. It should also be pointed out that the retention factor is now a function of flow rate and mobile phase volume, which was not the case in the isocratic separations described above. And again because of an interrelationship of multiple terms, the gradient can create a variety of effects on the peak resolution.

As discussed above, gradient elution can improve the separation of complex analytes based on altering the mobile phase composition. Changes in the mobile phase composition will alter the analyte affinity for the stationary phase based through hydrophobic interactions. Because a large percentage of peptides and proteins are water-soluble and contain some hydrophobic amino acid residues, these charged portions will also interact with the stationary phase and can create similar charge-interaction variations. Additionally, because proteins and peptides also possess a large amount of hydrophilic (and in some cases charged) amino acid regions, it is beneficial to alter the hydrophobic characteristics of the analytes or the stationary phase. This can be done by addition of an ion-pairing agent to the mobile phase solvents. The ion-pairing agent can bind to charged analytes in the mobile phase, forming a neutralized complex that will have an increased affinity for the stationary phase. This mobile phase ion-pair formation mechanism can be illustrated by:

$$S_M^+ + P_M^- \rightarrow (S^+P^-)_M$$
$$(S^+P^-)_M \rightarrow (S^+P^-)_S$$

where S_M^+ is the positively charged solute molecule and P_M^- is the negatively charged ion-pairing agent in the mobile phase, and $(S^+P^-)_{M/S}$ is the neutralized complex in the mobile phase (M) or the stationary phase (S).

Interaction between the ion-pairing agent and the stationary phase is also possible through hydrophobic binding, though this phenomenon is much less common. This binding leaves the ionic portion of the ion-pairing agent protruding into the mobile phase region, which can create ion-exchange interactions with charged solutes (dynamic ion exchange). In this case, the negatively-charged ion-pairing agent binds to the stationary phase (P_S^-) and can then create a neutral complex on the stationary phase $(S^+P^-)_S$ as shown in the following mechanism.

$$P_M^- \rightarrow P_S^-$$
$$S_M^+ + P_S^- \rightarrow (S^+P^-)_S$$

In the following experiments, the ion-pairing agent used was trifluoroacetic acid (TFA), which lowers the pH of the mobile phase and neutralizes charges on the charged amino acids of proteins and peptides, making them more hydrophobic. This increased hydrophobicity increases the interaction (and thus retention) of the proteins and peptides with the stationary phase. Additionally, TFA is an excellent ion-pairing agent due to its volatility if the samples are to be further analyzed after HPLC separation.

Numerous modes are possible for analyte detection following the chromatographic separation. Most commonly in HPLC, Ultraviolet/Visible (UV/Vis) detection is used. UV/Vis is a powerful detection method because it offers high sensitivity (10^{-10} to 10^{-11}g) and selectivity and is nondestructive to samples. Additionally, it employs the used of well-developed UV/Vis spectrometers that operate according to Beer's Law:

$$A = \varepsilon bC = \log\frac{I_o}{I} \qquad (1.22)$$

where ε is the molar absorptivity, b is the cell path length, C is the sample concentration, Io is the intensity of the reference light, and I is the intensity of the sample. Molar absorptivity depends on the compound structure and the wavelength used for detection, making it specific for a given compound. Also, the path length is constant for the detection system. This means that fluctuations in the absorbance can be attributed to changes in concentration, thus UV/Vis can be a quantitative detection technique. Another advantage is that UV/Vis can be coupled with other detection and/or analysis techniques, such as mass spectrometry.

A mass spectrometer is composed of an ion source, a mass analyzer, and a detector. In Chapter 5, the mass spectrometry methods used consisted of a matrix-assisted laser desorption/ionization (MALDI) technique with a time-of-flight (TOF) analyzer. In MALDI, the sample is initially digested using trypsin to cleave proteins after the carboxyl groups following the lysine and arginine amino acid residues. The digested proteins are then mixed with the matrix solvent and the mixture is evaporated onto a steel plate, forming crystals. MALDI techniques use a laser beam to trigger the ionization and the matrix is used to protect the protein from being destroyed by the laser and also to promote sample vaporization and ionization (**Figure 1.3**).

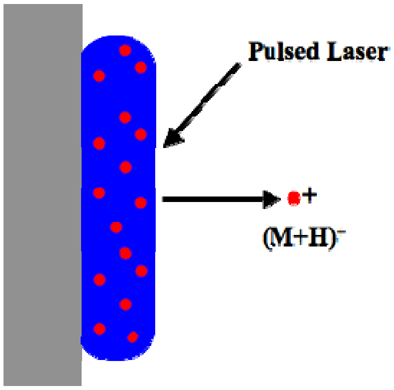

Figure 1.3 Schematic of the MALDI process showing the incoming pulsed laser irradiating the sample (red) and the matrix (blue) and creating a charged sample ion species that leaves the matrix.

Once the sample is ionized, the charged species enter the TOF mass analyzer. The mass analyzer is composed of an electromagnetic field region, which is used to accelerate the ions. Following acceleration, the ions then enter a field-free drift zone where they begin to separate based on their mass to charge ratios. The ions with a smaller mass have a higher velocity and will hit the detector before the slower ions with larger masses as diagramed below in **Figure 1.4**.

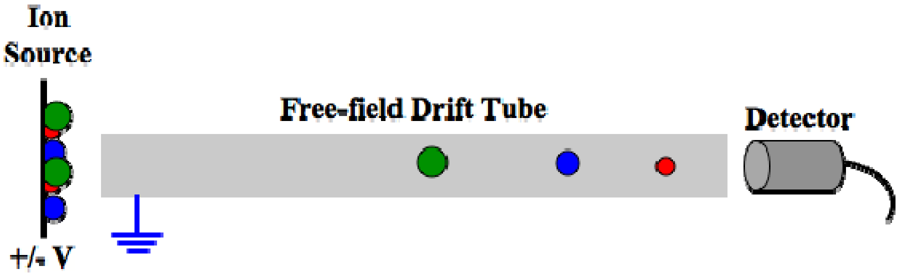

Figure 1.4 Schematic of a time-of-flight (TOF) mass analyzer with sample ions of varying masses illustrated by changes in spherical size.

In the experiments discussed in Chapter 5, UV/Vis was coupled with two specific mass spectrometry analyzing techniques: MALDI-TOF (MS) and MALDI-TOF-TOF

(MS/MS). In MALDI-TOF-TOF, the MS spectrum is acquired and a specific peptide of known mass can again be bombarded with the laser. When this occurs, the peptide is fragmented into its amino acid components and the charged species again enter the TOF analyzer for mass determinations. Following this, the amino acid sequence of the peptide can be acquired which will lead to increased certainty of the protein identification. The results as they pertain to the analysis and identification of pea aphid salivary proteins are further discussed in Chapter 5.

CHAPTER 2 - The Effect of Photomask Resolution on Separation Efficiency on Microfabricated Devices

2.1 Introduction

In most papers that report the use of microfluidic devices, the channel manifolds, or molds in the case of plastic devices, are fabricated via photolithographic patterning using chrome photomasks. Chrome masks produce smooth channels with nanometer-scale edge roughness. While such masks are commonplace they are expensive, fragile, and the thin layer of chrome is subject to pinholes and scratching. In rapid prototyping applications, several iterations of a design may be necessary to optimize operation. In addition, as more functional elements are integrated into a microfluidic device, the manifold gets increasingly complex and often several redesigns are necessary in order to optimally integrate the components; therefore, more economical options for mask production would be desirable. One option is to use laser photoplots or simple high resolution laser printing on transparencies. At the present time laser printer transparencies are not capable of adequately producing the 20 μm feature sizes that we desire, but laser photoplots are. Laser photoplots are fabricated by layering sub-micron silver halide crystals onto a film of Mylar or similar plastic. Patterns are then written by raster scanning a laser across the light sensitive film to produce an image.[5] The resolution of the mask features is a function of the silver halide grain size, the laser focus spot size, and the stepper motor resolution that controls the laser position. Resolution, generally measured as a plot density in dots per centimeter (dpc), ranges from 620 dpc to

> 6 200 dpc for these masks. The minimum feature sizes for such plots are ~12 to < 7 µm, respectively, and the distances between parallel edges of small geometric patterns can be maintained to tolerances within about three times the resolution of the plotter. The edge roughness of the 6 200 dpc photoplots is reported to be ~2 µm for both horizontal and vertical features. In general, the minimum feature size decreases and edge definition increases with increasing resolution.

Laser photoplots are 60 to 250 times cheaper than conventional electron beam and flash lamp produced chrome masks depending upon resolution (plot density) as can be seen in **Table 2.1** below.

Resolution	Size and Cost	Cost/cm^2
620 dpc [a] *1/4th mil*	25.4 x 30.48 cm $14.00	$0.01808
1 240 dpc *1/8th mil*	25.4 x 30.48 cm $10.45	$0.01350
3 100 dpc *1/20th mil*	25.4 x 30.48 cm $26.22	$0.03387
6 200 dpc *1/40th mil*	25.4 x 30.48 cm $65.01	$0.08397
Chrome	12.7 x 12.7 cm $800	$4.9600

Table 2.1 Cost comparison table of various photomasks. [a]The 620 dpc mask was purchased from a different company than the other photoplotted photomasks.

In addition to being less expensive than chrome photomasks, the photoplots are generally more opaque and have fewer pinhole defects than chrome masks. Because they are printed in a flexible matrix on a flexible substrate, we have also found them to be generally more robust than their chrome counterparts. The major drawback of these masks is the feature sizes that can be reliably printed. For the highest resolution laser photoplots, earlier studies have shown this to be ~ 7 µm.[5] For most of the applications in our lab, such feature sizes are more than adequate. In fact, laser photoplots have been successfully used to fabricate a variety of micro-scale devices for both microelectromechanical and microfluidics applications.[6] While laser photoplots have been used previously to fabricate microchips,[5,6] no study has been made as to how the increased edge roughness imparted to the channel sidewalls during the patterning process affects separation quality.

Numerous factors can affect separation efficiency on microfluidic devices. Many of these factors in some way involve the channel walls. As microchips fabricated from laser photoplots have channel sidewalls rougher than those fabricated from chrome masks, such roughness may affect the separation quality. Little has been published on the effects of surface roughness on separation quality, but the effects of surface roughness have been described by mathematical modeling.[7] In these studies, increases in surface roughness lead to variations of electroosmotic flow (EOF). Such variations in EOF would generate pressure differentials along the channel and, therefore, some type of parabolic flow profile, as opposed to the flat flow profile generated in channels with constant EOF. Such pressure-induced flows will lead to band broadening beyond that due to molecular (longitudinal) diffusion and, therefore, degrade separation quality.

There are several potential metrics that can be used to assess separation quality. These include the number of plates generated (N), plate height (H), the resolution between two analytes (Rs), and analyte peak height (h). Unfortunately, typical chip-to-chip and run-to-run variation in EOF and temperature can lead to significant variability in the experimentally obtained values that may have nothing to do with the separation channel roughness. In addition, small chip-to-chip changes in channel lengths, the optimal potentials for injection and injection plug length can further complicate the use of such metrics. In order to focus on the basic band broadening mechanisms and avoid some of these other variables, one can measure the dispersion (or apparent diffusion) coefficient of a series of analyte plugs as they travel through the channel. The dispersion coefficient includes the effects of basic longitudinal (or molecular) diffusion and other dynamic random processes that occur during a separation.[4] These random processes generally lead to Gaussian distributions of molecules in analyte bands (peaks), and dispersion coefficients (D_T) can be measured from these peaks using the Einstein-Smoluchowski equation:

$$\sigma_l^2 = 2D_T t \qquad (2.1)$$

where σ_l^2 is the spatial analyte band variance and t is the time over which the dispersion is measured; i.e. in our case the analyte migration time. By plotting the peak variance as a function of migration time, where the migration time is varied by changing the detection distance, the dispersion coefficients can be determined.[8] Such measurements are independent of variations in injection plug length, electric field, EOF, analyte mobility and migration time as might be common among a set of microchips. In addition, if the temperature varies among runs, such changes can be corrected based upon the Stokes-Einstein relationship[9] as shown in equation 2.2 below:

$$D_{25^\circ C} = D_{X^\circ C} \frac{T_{25^\circ C}\eta_{X^\circ C}}{T_{X^\circ C}\eta_{25^\circ C}} \qquad (2.2)$$

where T is the temperature and η is the viscosity of water at temperature X.

If the band broadening occurring during a separation is truly limited to longitudinal diffusion and if the diffusion coefficient is known, then the ratio of the dispersion coefficient to the diffusion coefficient provides a dimensionless parameter that can be used compare band broadening processes performed under different separation conditions. Unfortunately the diffusion coefficients for most analytes are not precisely known in many cases, so such dimensionless values cannot be calculated. Nonetheless simple comparisons of dispersion coefficients still allows for a fundamental comparison of band broadening among separations performed under different conditions where one wants to assess the various dynamic band broadening mechanisms that are occurring during a separation; e.g. molecular diffusion, potential pressure induced band broadening, Joule heating, rapid adsorption/desorption phenomena. These are the parameters that one might expect to be affected by channel surface roughness. Finally, the dispersion coefficient is directly related to the peak variance (eqn 2.1), and therefore, plays a fundamental role in describing the separation efficiency (N), analyte resolution (R_s), and peak height (h) as shown in equations 2.3, 2.4, and 2.5:

$$N = \frac{t^2}{\sigma_t^2} \qquad (2.3)$$

$$h = \frac{A}{\sigma_t \sqrt{2\pi}} \qquad (2.4)$$

$$Rs = \frac{t_2 - t_1}{2(\sigma_{t2} + \sigma_{t1})} \qquad (2.5)$$

where σ_t^2 is the temporal variance, σ_t is the temporal standard deviation, and A is the peak area. In all cases, the smaller the dispersion coefficient the better the separation performance.

In this chapter we report how the resolution of the photomask used to pattern a microchip manifold affects the separation quality by measuring the diffusion coefficients of FITC-labeled amino acids separated on the microchips.

2.2 Materials and Methods

2.2.1 Reagents and Fluorescent Derivatization

Arginine (Arg) and Serine (Ser) were obtained from INC Biomedicals Inc. (Aurora, OH). The α-lactalbumin was obtained from Sigma (St. Louis, MO). Fluorescein isothiocyanate (FITC) was obtained from Molecular Probes (Eugene, OR). Acetone, methanol, sodium tetraborate, sodium hydroxide and dimethylsulfoxide (DMSO) were obtained from Fisher (Pittsburgh, PA). 10 mM stock solutions of the amino acids and a 5 mM stock solution of α-lactalbumin were prepared in 150 mM sodium bicarbonate (pH 9). A 10 mM stock solution of FITC was prepared in DMSO. 100 µL of the FITC stock solution were added to 900 µL of each amino acid stock solution and vortexed for 1 min. The FITC stock solution was also added to the α-lactalbumin stock solution in a 1:1 molar ratio. The labeling solutions were then placed in the dark for 4 hrs at room temperature. After 4 hrs the labeled amino acids were frozen, and the labeled α-lactalbumin was placed in the refrigerator until needed. All labeling and buffer solutions were made using distilled deionized water from a Barnstead Ultrapure Water System (Dubuque, IA) and filtered using 0.45µm Millex®-LCR syringe driven filter units (Millipore Corporation; Bedford, MA). The labeled amino acids were diluted 1000-fold from the stock solution to a final concentration of ~1.3 μM in a 1mM sodium tetraborate solution at pH 9.1. The labeled α-lactalbumin was diluted 50-fold from the stock solution in 10mM sodium tetraborate, pH 9.1.

2.2.2 Microchip Design and Fabrication

A simple cross channel design was used in all experiments (**Figure 2.1**). Chip designs were drawn in-house using AutoCAD LT 2002 program from Thompson Learning (Albany, NY) and electronically sent to photomask fabricators for translation and fabrication. The 620 dots per centimeter (dpc) laser photoplot was obtained from Garrett Film Services (Grand Prairie, TX). Precision laser photoplots with resolutions of 1 240 dpc, 3 100 dpc, and 6 200 dpc were obtained from The Photoplot Store (Colorado Springs, CO). An electron beam written chrome mask was obtained from Advance Reproductions Corporation (Andover, MA).

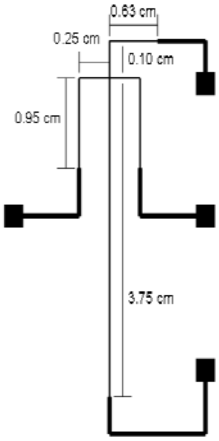

Figure 2.1 Schematic of the photomask and the resultant glass chips used for the amino acid separations.

Microchips were fabricated from 10.16 cm x 10.16 cm x 0.16 cm soda-lime photomask blanks coated with chrome and AZT positive tone photoresist (Telic Co.; Santa Monica, CA). The photomask blanks were patterned using the photomasks. The blanks were exposed to UV light for 10 s at an energy density of 45 $\mu J/cm^2$ using a flood exposure system (ThermoOriel; Stratford, CT). The exposed plate was then submerged in a stirred solution of Microposit Developer (Shipley Co.; Marlborough, MA) for 90 s, followed by a thorough rinse with 18 MOhm•cm water. The plate was subsequently submerged in a stirred solution of Chrome Mask Etchant (Transene, Co.; Danvers, MA) for 3 minutes, rinsed with 18 MOhm•cm water, and dried with inert gas. The exposed glass was wet chemically etched using a stirred, dilute buffered oxide etchant (Transene Co.; Danvers, MA). The buffered oxide etchant (NH_4F/HF, 10:1) was diluted with water and mixed with HCl in the volumetric proportions 1:4:2, respectively. The channel dimensions were periodically measured throughout the etching process using a stylus-based surface profiler (Ambios Technology; Santa Cruz, CA). Once the channels were the desired depth, the remaining photoresist was removed by rinsing the plate with acetone followed by a 18 MOhm•cm water rinse. The remaining chrome was then removed by immersing the plate in a stirred solution of Chrome Mask Etchant for 10 min followed by rinses in 1M sulfuric acid and 18 MOhm•cm water. The cleaned plate was then dried with inert gas and diced into 8 individual 2.54 cm x 5.08 cm slides using a dicing and cutting saw (Model EC-400; MTI Corp.; USA). Access holes were mechanically drilled into 10.16 cm x 10.16 cm x 0.15 cm cover plates (Technical Glass Inc.; Aurora, CO), then cut into 8 individual slides in a similar manner prior to bonding.

2.2.3 Microchip Bonding

The 8 top and bottom slides were cleaned thoroughly by swabbing with acetone followed by rinses with ethanol and 18 MOhm•cm water. The chips were then dried with inert gas. Next, the slides were submerged in a stirred 5M sulfuric acid solution for 5 min, rinsed with 18 MOhm•cm water, and then cleaned using the above described acetone/ethanol/water/inert gas procedure. In a laminar flow hood, the slides were immersed in a Versa-Clean Liquid soap solution (Fisher Scientific; Pittsburgh, PA), sonicated (3510 ultrasonic cleaner; Branson; Danbury, CT) for 15 minutes, rinsed with 18 MOhm•cm water and dried. The slides were then sonicated in acetone for 10 min, dried, and placed in the previously described dilute buffered oxide etch solution for 10 s. The slides were immediately rinsed with 18 MOhm•cm water and placed in a dilute hydrolysis solution (1:1:2 parts NH_4OH, H_2O_2, H_2O, respectively) for 12 minutes at 60 ^{o}C.[10] The slides were then rinsed with 18 MOhm•cm water and sonicated in flowing 18 MOhm•cm water for 60 s before joining. The etched slides were removed one at a time from the flowing water under a stream of 18 MOhm•cm water and placed on a Cleanroom Wiper (DURX 670; Great Barrington, MA). The drilled cover slides were removed from the flowing water and placed on top of the respective etched slide. Binder clips were fastened on the perimeter of the chip to ensure contact between the two surfaces, and water was removed from the channels with a vacuum hose. The joined chips were placed in the oven at 95 ^{o}C for 15 min to drive out any remaining water and then annealed at 565 ^{o}C to ensure proper bonding of the cover plate to the chip surface. In the past six months, we have successfully bonded 112 of 112 microchips using this method for a bonding success rate of 100%. Cylindrical glass reservoirs (~140 µL capacity) were attached using Epo-tek 353ND Epoxy (Epoxy Technologies, Inc.; Billerica, MA) where the access holes were located.

2.2.4 Separations and Detection

Electrophoretic separations of the FITC-labeled amino acids were performed using a 1 mM sodium tetraborate buffer. FITC-labeled α-lactalbumin separations were performed using a 10 mM sodium tetraborate buffer. Electric potentials for gated injections and separations were applied to the sample, buffer, and sample waste reservoirs using three independent and remotely programmable high-voltage (0-10 kV) power sources from EMCO (Sutter Creek, CA). The samples were injected into the separation channel using 0.02 s gated injections, and the proper potentials were calculated using Kirchhoff's rules and Ohm's Law.[11] The timing and magnitude of the electric potentials were controlled by an in-house written LabVIEW program and detected by laser-induced fluorescence (LIF) on a single point setup as previously described in the literature.[12,13]

2.2.5 Scanning Electron Microscopy

Images of nonbonded, etched microchannels were taken at the injection cross for each type of photomask used. The etched channel manifolds were first cut into one centimeter squares encompassing the cross intersection, and then a 40/60 noble metal mixture of palladium and gold was sputter coated (Desk II Sputter/Etch Unit; Denton Vacuum, LLC; Moorestown, NJ) onto the open-faced microchip to a thickness of 4 nm onto the wafers. SEM images of each chip were taken normal to the chip surface and at 40^{o} from the normal with a Scanning Electron Microscope (S-3500N; Hitachi Science Systems, Ltd; Ibaraki, Japan) using an Absorbed Electron Detector (S-6542; Hitachi

Science Systems, Ltd; Ibaraki, Japan). Images taken normal to the surface were magnified 500x while images taken at a 40° angle were magnified 800x.

2.2.6 Optical Microscopy

The microchips were imaged using a Nikon Eclipse TE2000E microscope with an epiluminescent illumination attachment. Photographs were taken using a 16-bit CCD camera (Princeton Instrument's Micromax; Roper Scientific; Trenton, NJ), and a Sony CCD color video camera (SSC-DC50A). The optical images of the chip intersection were taken with a 600x magnification.

2.2.7 Dispersion Coefficient Measurements

The dispersion coefficient measurements were taken in the center of the separation channel at distances of 1.25 cm, 1.56 cm, 1.88 cm, 2.19 cm, 2.50 cm, and 2.81 cm from the center of the injection cross. Five runs were made at each detection distance on a minimum of three chips fabricated from photomasks at each plot density. The analyte band variance was measured from the peak widths using Igor Pro (WaveMetrics, Inc.; Lake Oswego, OR) and plotted as a function of migration time. The dispersion coefficient was then obtained from the slope of the plot. Because the separations were performed on an unthermostatted system, temperature fluctuations were apparent and can cause a 2%/°C change in the measured dispersion coefficient.[8] Therefore, all of the dispersion coefficient measurements taken at temperature X were normalized to 25°C using equation 2.2 above.

2.2.8 Channel Roughness Measurements

The edge roughness of the channel wall was measured as a ratio by laying a line down along the edge of the channel on the SEM image and dividing that by the equivalent straight-line length. SEM images shown in **Figure 2.2 K-O** were enlarged and printed out on a high resolution printer. From the bottom of the injection cross on the print, a linear distance of 9 cm (actual microchip distance of 54.2 µm) was marked along each side of the channel wall. Non-elastic string was then conformed along the top of each side of the channel wall image for the 9 cm linear distance. The string was then removed, measured, and the average length determined. This average length was then divided by the linear constant distance of 9 cm.

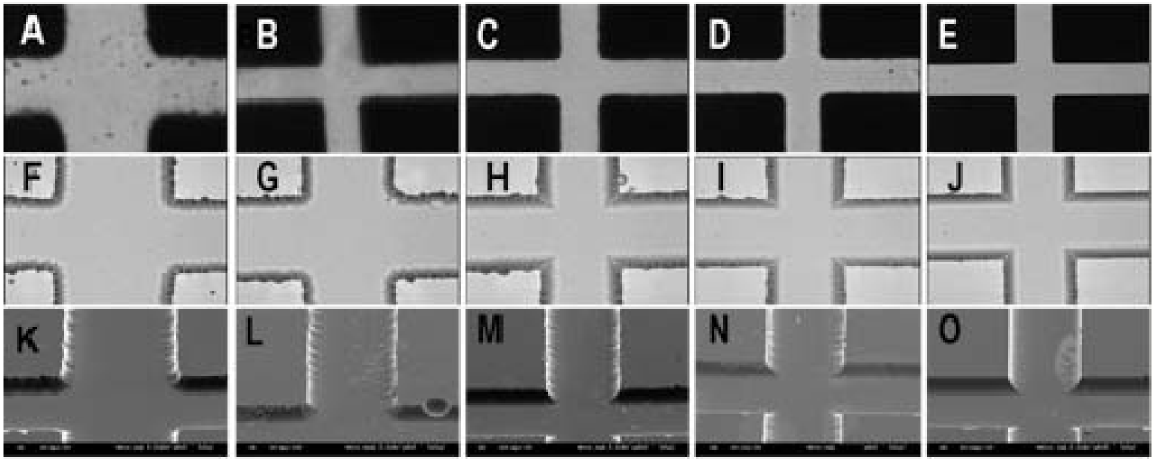

Figure 2.2 Optical microscope images taken at 600 x of the injection cross from photomasks (A) 620 dpc photoplot (B) 1 240 dpc photoplot (C) 3 100 dpc photoplot (D) 6 200 dpc photoplot (E) Chrome photomask. Optical microscope images of cross from bonded chips at 600x for (F) 620 dpc microchip (G) 1 240 dpc microchip (H) 3 100 dpc microchip (I) 6 200 dpc microchip (J) Chrome microchip. SEM Images of the non-bonded injection cross 40^{o} from normal (K) 620 dpc chip (L) 1 240 dpc chip (M) 3 100 dpc chip (N) 6 200 dpc chip and (O) chrome chip.

2.2.9 Data Analysis

In order to compare the diffusion coefficients obtained across the chips made from the different photoplots, a one-way analysis of variance (ANOVA) with Tukey multiple-comparison tests was used (SAS software; SAS Institute Inc.; Cary, NC). A probability level of $p < 0.05$ was used to determine whether the diffusion coefficients obtained on the different chips were significantly different from one another.

2.3 Results and Discussion

2.3.1 Mask Cost

The cost per square centimeter for each laser photoplot was calculated based on the fabrication expense for a 25.4 cm x 30.48 cm sheet. These are generally the smallest and most expensive photoplots available. The cost per square centimeter for the chrome photomask was calculated based on the cost of a standard 12.7 cm x 12.7 cm mask. These costs do not include any added fees one might incur for data processing tasks or file formatting. Such costs, however, would be similar for both laser and electron beam/flash lamp written masks. The cost/cm^2 for the photoplotted photomasks are 60 to 225 times less expensive than that of the chrome photomask depending upon the desired resolution as can be seen in **Table 2.1**.

2.3.2 Optical Comparison of Mask Resolution

The differences in laser photoplot resolution can be observed easily using optical microscopy. **Figure 2.2 A-E** shows the injection crosses of several different resolution laser photoplots and a chrome photomask magnified at 600x. The channel widths in all the patterns are nominally 25 µm. The chrome mask is of considerably superior quality with square corners, no measurable fluctuations in channel width, and no residue left in the channel area. These features begin to degrade as one moves to the laser photoplots and then down in resolution. The 620 dpc photoplot has pronounced rounded corners, variable channel widths, and significant silver halide residue throughout the channel pattern.

The photomasks in **Figure 2.2 A-E** were employed to pattern the channels onto the photoresist of the glass microchip substrates. The photoresist on the glass substrates were subsequently developed and channels were etched in the glass as described in the Material and Methods Section above. Both optical and SEM images of the etched channels were obtained. As can be seen in the optical microscope images in **Figure 2.2 F-O**, the photomask edge roughness was transferred to the etched glass chips. Qualitatively, the roughness of the glass sidewalls increased as the mask resolution (plot density) decreased. To try to get a more quantitative measure of the roughness introduced by the masking and patterning process, the length of the sidewall edge was measured from the SEM images of the channels as described in the Material and Methods Section. The results can be seen in **Table 2.2**, along with the average channel dimensions.

Resolution	Side Wall Roughness [a]	Avg. Injection Plug Length (cm) [b]	Avg. Channel Width (µm)	Avg. Channel Depth (µm)	Channel Ratio (Width/Depth)
Chrome	1.00	1.67×10^{-2}	48.85	11.63	4.21
6 200 dpc	1.05	1.66×10^{-2}	51.96	10.81	4.81
3 100 dpc	1.11	1.45×10^{-2}	53.56	10.98	4.88
1 240 dpc	1.04	1.61×10^{-2}	72.83	10.39	7.01
620 dpc	1.07	1.41×10^{-2}	80.06	11.52	6.95
Rough Chrome	1.06	N/A	45.66	10.69	4.27
Rough 3 100 dpc	1.17	1.40×10^{-2}	53.05	11.82	4.49

Table 2.2 Channel Surface Roughness Measurements and Dimensions. Roughness measurements were calculated from the corresponding SEM images captured at 40° from normal. Channel dimensions were measured from the channel profiles.

[a] These numbers represent a relative measure of the roughness of the side channels as explained in the Materials and Methods section.

[b] These numbers represent the injection plug length as explained in the Materials and Methods section.

While there is a measurable increase in surface roughness when moving from chips patterned using the chrome masks to chips patterned using the laser photoplots, the resolution of the photoplot used seemed to have little effect on the actual edge roughness. This is probably due to the fact that we were only able to measure a single line along the top edge of the sidewall. Unfortunately, because of the angle of the sidewall, we could not apply other methods such as AFM or stylus based profilers that are usually used to quantitate surface roughness. The sidewall roughness and the silver halide residue seen on the lower resolution photoplots did not measurably affect the roughness on the channel bottoms. Infrequently, however, some of the etched channels were also very rough on the bottom (**Figure 2.3**). Such roughly etched chips occurred over a range of mask resolutions and under a variety of etching conditions indicating that the roughness was due to some intrinsic factor in the glass rather than the channel-patterning step. Nonetheless, all of the microchips fabricated filled with fluid easily and the wall roughness did not lead to bubble nucleation and generation.

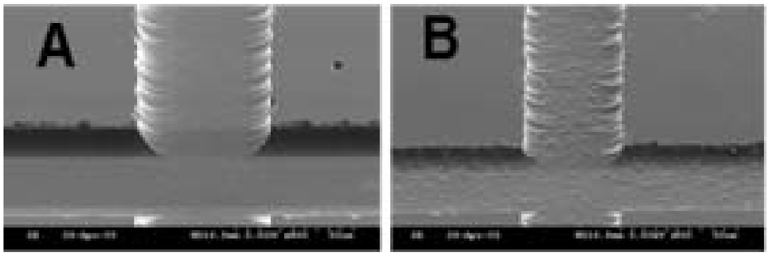

Figure 2.3 SEM images taken 40^o from normal of a non-bonded injection cross of roughly etched microchannels for (A) 3 100 dpc photomask and (B) chrome photomask.

2.3.3 Effects of Mask Resolution on Separation Quality

In order to determine the effects of the channel sidewall roughness on separation quality, electrophoretic separations of FITC-labeled Arg and Ser were performed, and the separated analytes were detected at several distances from the injection point. Plots of analyte band variance vs. migration time were made and the dispersion coefficients were measured from the slope of these plots as described in the Material and Methods Section. A typical plot is shown in **Figure 2.4**. Diffusion coefficients were measured on at least three chips patterned from each type of photomask, and the results are shown in **Figure 2.5**.

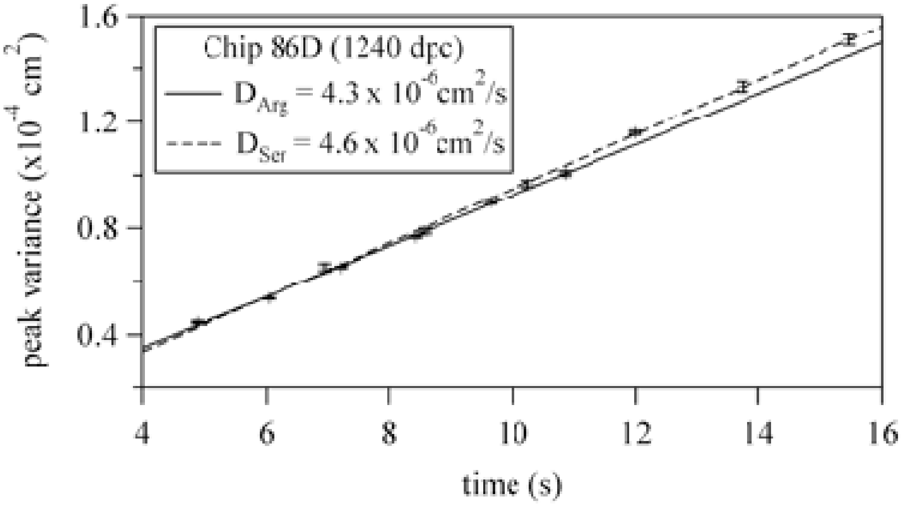

Figure 2.4 IGOR graph of peak variance *vs.* migration time with error bars for microchip 86D (1 240 dpc).

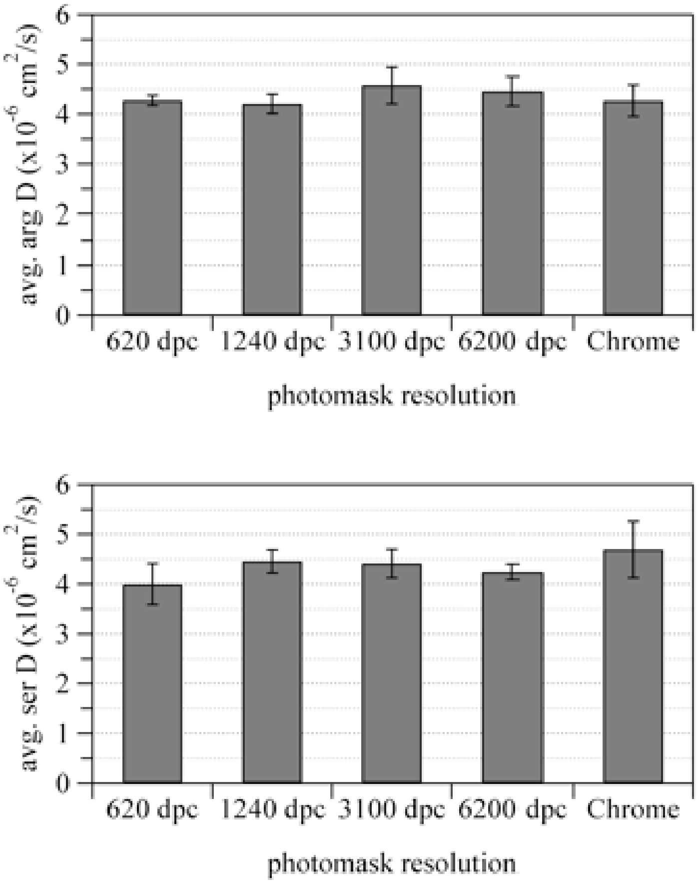

Figure 2.5 Average diffusion coefficients of FITC-arginine (top) and FITC-serine (bottom). The type of photomask is identified on the x-axis.

In order to determine whether there was a statistically significant difference in the diffusion coefficients measured from the different chips a one-way ANOVA was performed on the data. The probability levels (p) for the FITC-arg and FITC-ser diffusion coefficients were 0.1170 and 0.0910, respectively. Because $p > 0.05$, no significant difference exists in the experimentally determined dispersion coefficients for the chips fabricated from the different photomask resolutions. The average diffusion coefficient values for each set of chips were also within experimental error of previously published diffusion coefficient values for similarly sized small molecules like fluorescein and Rhodamine B (4.25 ± 0.01 x 10^{-6} cm^2 s^{-1} at 25°C),[8] indicating that the separations were all diffusion limited.

Similar separations were carried out using α-lactalbumin. The dispersion coefficients for α-lactalbumin measured on the lowest resolution photoplot (620 dpc) and chrome devices were 4.9 x 10^{-6} cm^2 s^{-1} and 4.8 x 10^{-6} cm^2 s^{-1}, respectively. While these results were within experimental error of one another, they were also both larger than the expected diffusion coefficient for α-lactalbumin. The excess band broadening, however, was not due to the difference in chip side wall roughness as it was of equal magnitude on both devices. Rather, it was probably due to some surface adsorption/desorption phenomena.

Finally, the y-intercept of the variance vs. migration time plot (**Figure 2.4**) is a measure of the injection width (σ_{inj}^2) and detection window length (σ_{det}^2) contributions to the overall peak variance as shown by equation 2.6:

$$\sigma_{y-\mathrm{int}}^2 = \frac{w_{inj}^2}{12} + \frac{w_{\mathrm{det}}^2}{12} \qquad (2.6)$$

where w_{inj} is the injection plug length and w_{det} is the width of the detection window. The detection window length can be calculated from the spatial filter size divided by the magnification (σ^2_{det} = 0.0025 cm^2 in our case). This allows one to determine the injection plug length from the y-intercept on the graph.[14] As can be seen in Table 1.2 the average injection width among the 5 different chips patterned from different resolution photoplots are within a very small range and within experimental error of one another.

This demonstrates that even the poor cross shapes of the lower resolution chips are still capable of generating small injection plugs.

The results for FITC and α-lactalbumin indicate that there is no correlation between the measured dispersion coefficients and increased channel roughness imparted by patterning chips with laser photoplots. Earlier results from PDMS devices cast from molds patterned with a 1 240 dpc laser photoplot also resulted in diffusion limited separations for a variety of analytes.[13] Other reports of microfluidic devices fabricated using laser photoplots have also yielded good separations and fluid transport capabilities.[13,15-19] One reason that the increased surface roughness imparted to the channels may not have impacted the separation quality is that the roughness is limited to the sidewalls of the channel. These sidewalls make up < 2/9 of the total surface area of the channel. We also, however, tested microchips that were roughly etched on the bottom of the channel. Approximately ½ of the channel surface on these chips were significantly rough, i.e. > 500 nm rms, as can be seen in **Figures 2.3 A and B**. The diffusion coefficients measured for the analytes on these microchips were also within experimental error of the dispersion coefficient measured on the chrome patterned chip. Based on this result it appears that analyte band dispersion and therefore separation quality is not adversely affected by increased surface roughness up to at least 500 nm rms.

In terms of the fabrication of microfluidic devices, the real limitation to how low of a resolution laser photoplot that one can use is the fidelity of the mask to the desired channel manifold design. A high resolution photomask is needed if the pattern details are pertinent to the experiment or when the features are small. These results do not at this time correlate well with some theoretical models of the effect of surface roughness on separation quality.[7] Further research is needed to bring the experimental and theoretical results in line with one another.

Finally, because the excitation and emission light enter and exit primarily through the smooth top and bottom of the channel (rather than through the side wall), no degradation in optical properties was seen among the different resolution chips tested above.

2.4 Conclusions

Based on experimental data reported above, microfluidic devices patterned using laser photoplots are able to produce separation quality equivalent to microchips patterned using chrome photomasks. For fabrication of microstructures greater than ~10μm, photoplotted photomasks offer numerous advantages such as significantly lower cost and increased durability.

CHAPTER 3 - Ultrafast Capillary Electrophoresis Separations of Wheat Gliadin Proteins for Rapid Varietal Identification

3.1 Introduction

Chemists have tried to relate the amount, composition, and structure of cereal proteins to the properties of the end-use product for more than 250 years.[20] Wheat (*Triticum aestivum*) is considered to be the most important cereal grain because it is the only grain that possesses the ability to form a cohesive, viscoelastic dough. Another documented feature of wheat dough is its ability to retain gas during fermentation, a necessity for bread making. This unique property is due to the endosperm (gluten) proteins. Gliadins and glutenins are the two main subclasses that make up the gluten proteins, which is approximately 80% of the total protein in wheat flour. The gliadins are small, monomeric proteins while the glutenins are massive polymers linked together by disulfide bonds through the amino acid cysteine. Why the gluten proteins interact with themselves and form this unique dough is still largely unknown. However, it is known that ratios of these proteins determine the cohesiveness, or mixing strength, of the dough and serve as an indicator of the bread-making quality for a particular type of wheat. These protein ratios in the endosperm are determined by the growing environment and genetics. Identification of the genetic aspect allows for control of about 50% of the end-use quality of the wheat.[21] Generally, the gliadin proteins are not greatly altered by environmental factors, and thus have been found a reliable experimental source for identification. Lookhart and Jones determined early on that the gliadin electropherograms were not significantly altered in environments ranging from severe frost to immature wheat to germination up to 44 hours.[22]

Researchers have been able to use high-performance liquid chromatography (HPLC), acid-polyacrylamide gel electrophoresis (A-PAGE), and sodium dodecyl sulfate-PAGE (SDS-PAGE) to create a catalogue of information for individual wheat cultivars by 'fingerprinting' the gliadin proteins.[23-25] This information includes: class, relative molecular size, relative charge, hydrophobicity, and separation times. HPLC and A-PAGE have been the methods of choice for analyzing wheat and other cereal proteins, with A-PAGE being the most functional method for grain identification.[26] Currently, the bread-making quality of wheat is determined by actually baking test loaves of bread. This batch process is time-consuming and wasteful on commercial scales if the wheat is not suitable for bread. Additionally, if the wheat has been bred to incorporate a specific rye translocation, the dough can be too sticky, causing damage to the mixers used to knead the dough.[26]

Within the past fifteen years, capillary electrophoresis (CE) has become an increasingly valuable tool for wheat protein analysis. CE is rapid, sensitive, versatile, and automated, yielding high-resolution separations. It has been noted that CE is advantageous to the previous methods because it is a less toxic (uses substantially less volumes of harmful solvents) and more complementary chromatographic technique.[27] Currently, a complete analysis of one wheat sample uses multiple laboratory processes such as visual inspection, HPLC, CE, IR spectroscopy, and baking test loaves because these methods are well developed for product quality assessment. These tests take multiple days to carry out in the lab, requiring extensive human manipulation and making them fairly expensive. Thus, it is important to identify ‘high quality’ wheat via rapid, inexpensive means, such as capillary electrophoresis, to allow operators at grain mills, elevators, and shipping ports to classify and sort the grains without baking test loaves. This reduction in analysis and sorting time will add substantial value to the product.

3.1.1 Capillary Electrophoresis Theory

Capillary electrophoresis (CE) has been emerging as an important tool for biochemical separation and analysis. Its uses extend into the realms of amino acids, peptides, proteins, and single cell analysis. The advantages of CE include: rapid separation and analysis, small reagent consumption and waste production, high sensitivity, versatility, compact geometries, and process automation. In capillary electrophoresis, applying a high voltage across the length of a capillary or microchannel creates an electric field that causes ions to separate. The velocity of an ion is given by:

$$v = \mu_e E \qquad (3.1)$$

where μ_e is the electrophoretic mobility and E is the applied electric field in volts/cm. The electric force (F_E) and frictional drag (F_F) the molecule experiences determine the electrophoretic mobility. Electric force is given by:

$$F_E = qE \qquad (3.2)$$

and a spherical ion’s frictional force is given by:

$$F_F = -6\pi\eta r v \qquad (3.3)$$

where q is the ion charge, η is the solution viscosity, r is the radius of the ion, and v is the velocity of the ion. Because a steady state is achieved during CE, these forces are equal and opposite, yielding:

$$qE = 6\pi\eta r v \qquad (3.4)$$

The electrophoretic mobility can then be described in terms of physical parameters by solving Equation 3.4 for velocity and substitution into Equation 3.1 to get:

$$\mu_e = \frac{V}{E} = \frac{q}{6\pi\eta r} \qquad (3.5)$$

From Equation 3.5 it can be shown that large, minimally charged species will have low mobilities while small, highly charged species will have higher mobilities.[28]

Another important factor in CE is the electroosmotic flow (EOF). Most channel surfaces possess a negative charge in aqueous solution that allows a solution double-layer to form. This surface charge creates a bulk solution flow when an electric field interacts with the solution double-layer. This bulk solution flow is termed the EOF and under normal conditions is toward the cathode. An interesting attribute of the EOF is its ability to cause almost all species (regardless of charge) to migrate in the same direction. Occasionally, the EOF is so fast that the sample elutes before the separation is complete. EOF can be controlled by a variety of means, including changes in buffer viscosity, composition, and pH. However, care must be taken to not negatively affect the sample mobility mentioned above.

Multiple detection methods have been developed for CE. Two of the most common detection modes for CE are ultraviolet (UV) and laser-induced fluorescence (LIF) detection. UV and LIF offer high sensitivity but are not universal detection methods. When using LIF, one must fluorescently label the species of interest. When performing capillary electrophoresis, this fluorescent label can alter the mass and charge that the overall species possesses, possibly introducing experimental errors. UV detection offers the advantage of detecting species in their native state (without use of labels). However, UV absorbance detection has a similar disadvantage in that not all species of interest have bonding structures capable of UV excitation. It should also be noted that UV detection on a microchip and small diameter capillary is very difficult because of their short pathlength, as UV absorbance detection is a pathlength dependent method. However, for wheat proteins, UV detection provides adequate sensitivity for wheat protein detection because we are not limited by sample amount, and the gluten proteins are in rather high concentrations.[29]

3.2 Materials and Methods

3.2.1 Samples

All wheat samples were obtained from the Hard Winter Wheat Quality Lab (HHWQL; Manhattan, KS). A majority of the samples were received as flours, while some were in whole kernel form. Samples received in whole kernel form were first ground into flour, in house, using a standard electric coffee grinder for approximately one minute. This yields flours of a similar particle size composition to those milled samples from the HHWQL.

3.2.2 Gliadin Protein Extaction

It has been found that a 10:1 ratio of solvent to flour yields the best sample reproducibility. Thus, wheat gliadins were extracted from 100 mg wheat flours using 1 mL of a 1:1 (v/v) solution of 1-propanol and water in an eppendorf tube as previously described.[30] The sample and extraction solvent were continually vortexed for 5 min on an Analog Mini Vortexer from Fisher Scientific (Pittsburg, PA). Following continual vortexing, the extractions were centrifuged using a Marathon 8K Centrifuge (Fisher Scientific; Pittsburgh, PA). After centrifugation, 0.5 mL of the liquid is removed and placed into a new eppendorf tube. The remaining 0.5 mL is discarded and the extraction procedure described above is repeated a second time, yielding 1.0 mL of extracted solvent containing gliadin proteins.

3.2.3 Capillary Electrophoresis

All separations were carried out in 25 μm fused silica capillary (Polymicro Technologies; Phoenix, AZ) using a non-commercial capillary electrophoresis setup, constructed in-house. The capillary lengths used were kept between 9-10 cm. The reservoirs were constructed from a 1 cm length of glass tubing with a 1/16" hole drilled into the side that was epoxied onto 1cm x 1 cm x 1 mm glass square. The capillary electrophoresis system consists of a Unicam 4225 UV Detector (Mississauga, Canada) and a Spellman CZE 1000R power supply (Spellman High Voltage Electronics Corp.; Hauppauge, New York). The samples were injected into the separation channel using hydrodynamic and electrokinetic injections as described in the Results and Discussion section and separated using field strengths of 975-1000 V/cm. An in-house written LabVIEW program controlled the timing and magnitude of the electric potentials, as well as collected the signal response.

Prior to the capillary electrophoresis separations, each capillary used was cleaned and prepared using the following steps. First, a 1:1 (v/v) solution of sodium hydroxide and methanol was pushed through the capillary for 5 minutes at a flow rate of 10 μL/min using a BS-8000 syringe pump (Braintree Scientific, Inc.; Braintree, MA). Following the previous cleaning step, water was then pushed through the capillary (same time and flow rate) to remove the base. The capillary was then coated using a solution of 0.5% hydroxypropyl methylcellulose (HPMC) for 5 minutes followed by the buffer solution in a similar manner. Separation buffers for performing wheat gliadin separations using capillary electrophoresis have been previously examined and optimized using commercial instruments.[26,30-32] From these experiments, a low pH sodium phosphate buffer was chosen for the following experiments. The buffer consisted of 50 mM sodium phosphate (pH 2.5), 20% acetonitrile, and 0.05% HPMC by volume. Sodium phosphate, acetonitrile, and HPMC were acquired from Fisher Scientific (Pittsburgh, PA). Because the sodium phosphate is a high conductivity buffer, ACN is necessary to serve as a cooling agent and prevent joule heating. Also at pH 2.5, the wheat proteins are primarily positively charged. To prevent surface interaction and adsorption to the negatively charged capillary surface, HPMC was needed to coat the capillary. Additionally, HPLC must be incorporated into the buffer to maintain a uniform coating throughout the separations.

3.3 Results and Discussion

3.3.1 Injection Methods

In capillary electrophoresis, there are two injection methods used to introduce sample into the capillary, electrokinetic or hydrodynamic injections.[33,34] To determine if our experiment was dependent up the injection style, both hydrodynamic and electrokinetic injections were carried out. To perform the hydrodynamic injections, the capillary was inserted into the sample and then elevated to a specific height for a determined length of time such that the sample will be siphoned into the capillary. The injection volume is dependent upon the change in the pressure between the two capillary ends. The exact height and length needed for a specific injection volume can be determined using equations 3.6 and 3.7:[34]

$$\Delta P = \rho g \Delta h \tag{3.6}$$

$$V = \frac{\Delta P \pi d^4 t}{128 \eta L_t} \tag{3.7}$$

where ΔP is the pressure difference between the ends of the capillary, ρ is the buffer density, g is the gravitational constant, Δh is the height difference between the two capillary reservoirs, d is the inner diameter of the capillary, t is the time in sample, η is the sample viscosity, and L_t is total capillary length. These equations were used to give the elevated height and time necessary to hydrodynamically inject the sample into the capillary at 2% of the total capillary volume. Placing the capillary end in the sample and applying 10 kV, was used to electrokinetically inject sample into the capillary. As seen in **Figure 3.1**, there is not a significant difference between the two injection methods. For ease of use and to facilitate rapid processing, electrokinetic injections were used in the following experiments.

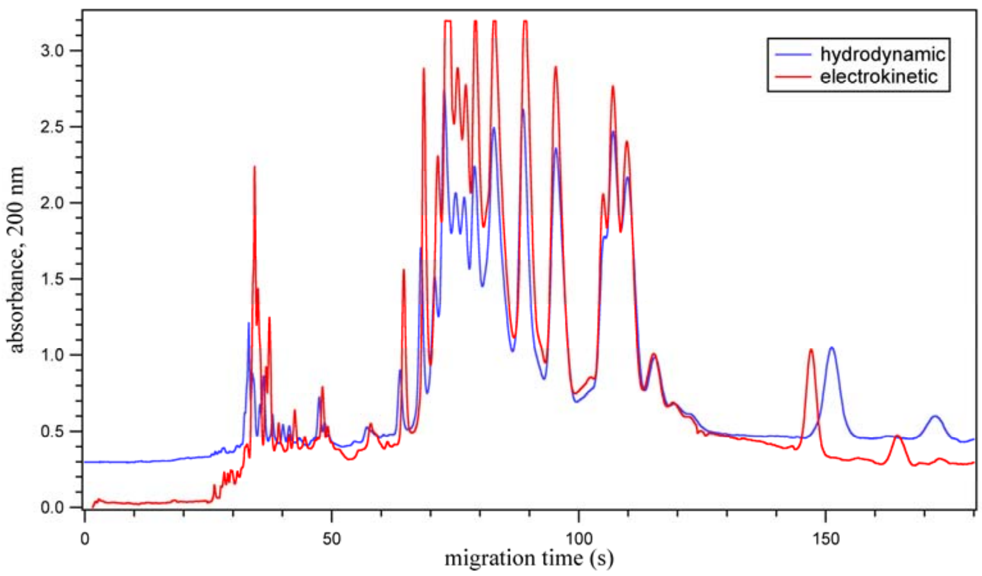

Figure 3.1 Electropherograms of the sequential hydrodynamic and electrokinetic injections of gliadin proteins of Karl 92.

3.3.2 CE Separation Reproducibility

It is imperative that the CE system be capable of performing reproducible, consecutive separations for ease of use and to simplify the normalization process using internal standards necessary for varietal identification. The system reproducibility was tested using gliadin proteins extracted from Karl 92 flour as previously described in the Materials and Methods section. **Figure 3.2** shows the remarkable sample reproducibility (<1% RSD) for ten consecutive injections of Karl 92. This is significant because the electropherograms were taken over approximately one hour. This shows that the system can maintain reproducibility over time, which is necessary for lengthy sample analyses or multiple consecutive runs. Additionally, if significant drift occurred in the electropherograms, they could not be used for cultivar identification without normalization using an internal standard.

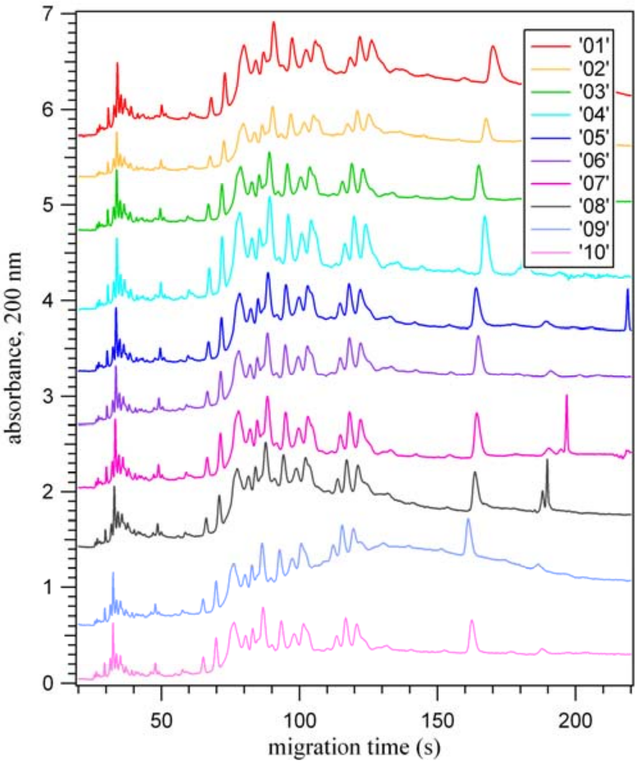

Figure 3.2 Ten consecutive separation electropherograms of Karl 92 gliadin proteins performed under the same conditions.

3.3.3 Sample Catalog and Varietal Identification

Our in-house CE system allows for shorter capillaries to be used because the reservoirs can be manually positioned. In a commercial system, the reservoirs are at set locations, requiring the use of a ~27 cm long capillary. This combined with a high conductivity buffer solution of 50 mM sodium phosphate (pH 2.5), 20% ACN, 0.05% HPMC allowed for the entire wheat protein separation for all cultivars to be completed between 180 and 275 seconds. Two examples of these separations are shown in **Figure 3.3A** and **3.3B**. These separations are a minimum of 25% faster than separations of the same cultivars that have been previously recorded in the literature.[30,32] Because wheat gliadin peak patterns vary among varieties, these separations can be used to create a catalog based on the ‘fingerprints’ of the wheat varieties from the respective electropherograms.[35] Moreover, this experiment indicates that only the first 90 seconds is necessary for varietal differentiation and thus identification (**Figures 3.3 C-G**).

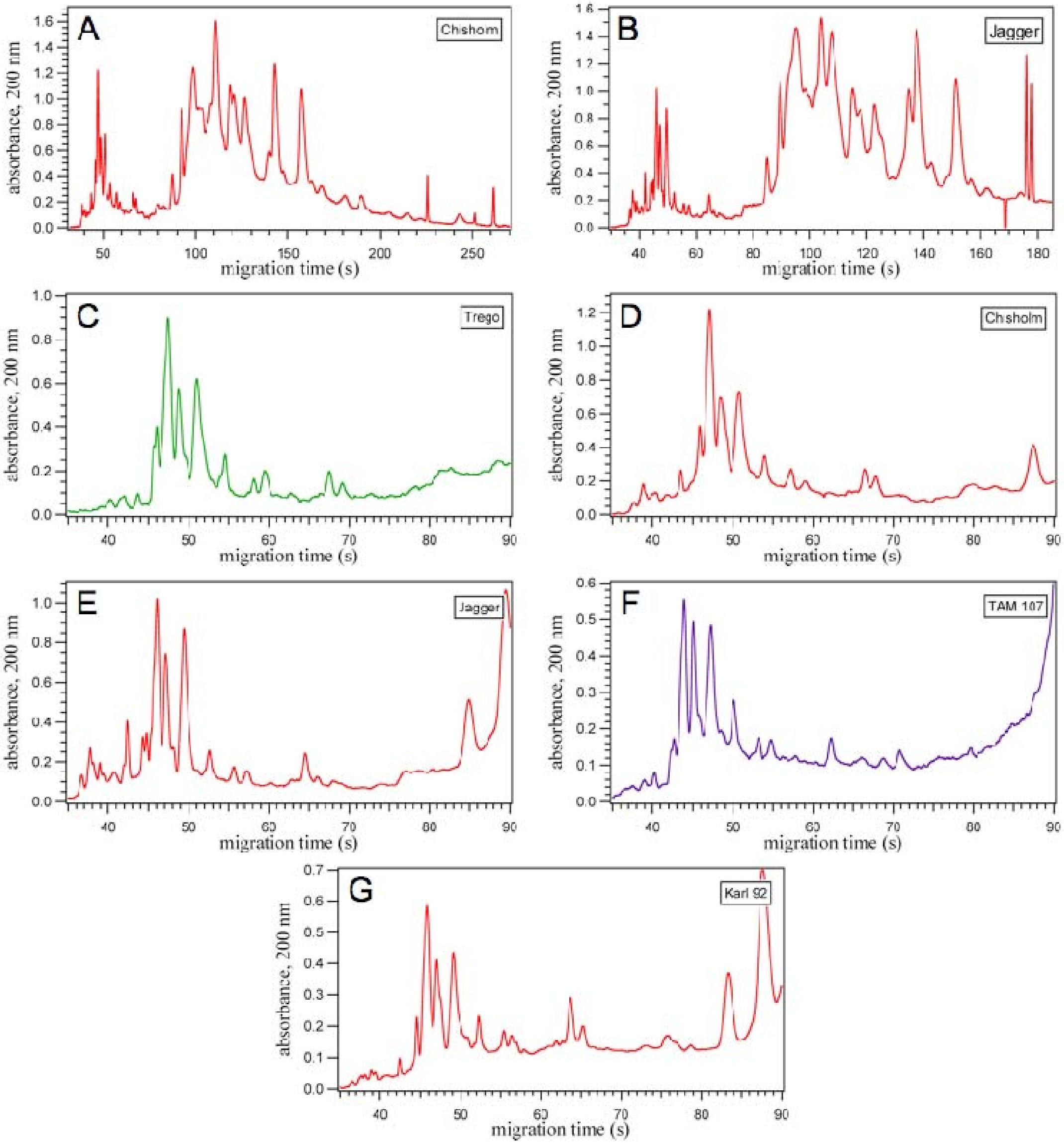

Figure 3.3 Electropherograms showing the entire separation for (A) Chisholm gliadin proteins and (B) Jagger gliadin proteins. The first 90 s of the separation from five different wheat varieties are shown in (C) through (G). The variety of wheat is given in the upper right corner of the graph.

Significant differences can be seen in the electropherograms when they are overlaid in the same graph, even between cultivars of similar genetic makeup as seen in **Figure 3.4**. Here, the electropherograms of Jagger and its genetic backcross, Karl 92, are plotted with arrows indicating obvious electropherogram pattern differences.

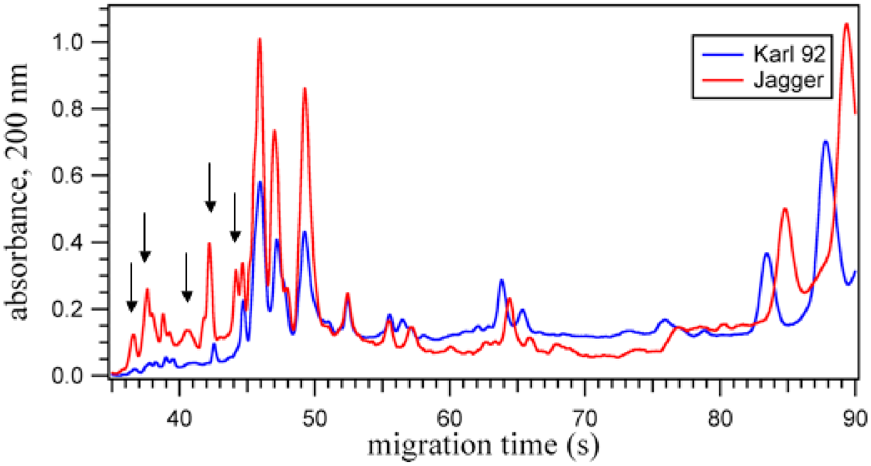

Figure 3.4 Overlapping electropherograms of Jagger and Karl 92. Arrows point out significant varietal differences between the genetically similar varieties.

It should be noted that these early peaks (< 90 s) are attributed to albumin and globulin proteins, and variation can occur across differing environments. Because of this, they are not necessarily genetic markers of cultivar. However, in these experiments it appears that they can still be used for 'fingerprinting' various cultivars. Additional experiments using wheat samples grown in different environments would be necessary to determine to what extent the environmental effects create deviations in the above cultivar identification processes.

3.4 Conclusions

From these experiments, it has been shown that wheat gliadin proteins can be easily extracted then injected into a capillary for CE separation and analysis. It has been shown that there is no significant difference between hydrodynamic and electrokinetic injections for the gliadin separations. Additionally, separations can be performed with our in-house system and buffer that significantly decrease the separation time, and thus minimize the time necessary for analysis. More than 20 Kansas wheat varieities have been analyzed with this system, yielding enough information for a positive varietal identification within 90 seconds.

CHAPTER 4 - An Integrated Portable Microchip System for Separations in Microgravity

This chapter is dedicated to our NASA collaborator, Dr. Steven R. Gonda, who passed away April 16, 2008 after a courageous battle with cancer.

4.1 Introduction

Microchip technology has been emerging as an important tool for biochemical separation and analytical analysis. Microchip platforms offer numerous advantages, including: rapid separation and analysis, small reagent consumption and waste production, high sensitivity, versatility, compact geometries, and process automation. Use of these devices allows the combination of multiple traditional bench-top handling steps onto one platform, using straight channels, tees, and crosses. This is in part due to the micrometer-size channel dimensions (generally with a maximum 50 x 50 μm, width and depth), which are comparable to that of a human hair. Micro total analysis systems (μTAS) for performing capillary electrophoresis (CE) separations of amino acids, proteins, environmental gases, etc. have been emerging as useful platforms for complete sample preparation and/or analysis.[18,36-42] Because of the numerous advantages, a few groups have constructed micro total analysis systems possessing the capability to perform capillary electrophoresis analysis in extraterrestrial gravitational environments.[39,42,43]

The primary goal of these experiments was to integrate a microfluidic device capable of sampling from a bioreactor system. These experiments show that the microfluidic device can perform rapid analysis (<12 s) and provide real time feedback during continuous, automated sampling on NASA's C-9 microgravity research aircraft. This mimic of microgravity in the aircraft was advantageous to the experiment. It allowed us to validate that our μTAS system functions repeatedly and reproducibly to perform amino acid and cell media separations in zero-*g*, lunar-*g*, Martian-*g*, and hypergravity (~1.8*g*) conditions. The advantages described above make these devices especially interesting for use in extraterrestrial environments where small, portable, rugged, and reliable devices capable of sustained remote automated operation will be required.

4.2 Materials and Methods

4.2.1 Reagents and Fluorescent Derivatization

Arginine (Arg) and Serine (Ser) and Glutamic Acid (Glu) were obtained from INC Biomedicals Inc. (Aurora, OH). BODIPY® FL CASE ester dye was obtained from Molecular Probes (Eugene, OR). Acetone, methanol, sodium tetraborate, sodium hydroxide and dimethylsulfoxide (DMSO) were obtained from Fisher (Pittsburgh, PA). 10 mM stock solutions of the amino acids were prepared in 150 mM sodium bicarbonate (pH 9). A 5 mM stock solution of BODIPY® was prepared in DMSO. 100 μL of the reactive BODIPY® stock solution were added to 900 μL of each amino acid stock solution and vortexed for 1 min. The labeling solutions were then placed in the dark for 4 hrs at room temperature. After 4 hrs the labeled amino acids were frozen until needed. All labeling and buffer solutions were made using distilled deionized water from a Barnstead Ultrapure Water System (Dubuque, IA) and filtered using 0.45μm Millex®-

LCR syringe driven filter units (Millipore Corporation; Bedford, MA). The labeled amino acids were diluted from the stock solutions above in a 10 mM sodium tetraborate solution at pH 9.1 and placed in 10 mL flight-certified cell culture bags. The amino acid combinations and concentrations are further described in the Results and Discussion section. The reGFP (100 ng/mL) control media was acquired from Dr. Steve Gonda's lab (NASA Johnson Space Center; Houston, TX).

4.2.2 Microchip Design and Fabrication

Chip designs were drawn in-house using AutoCAD LT 2002 program from Thompson Learning (Albany, NY) and electronically sent to photomask fabricators for translation and fabrication. A precision laser photoplot with a resolution of 6 200 dpc was obtained from The Photoplot Store (Colorado Springs, CO). The 1" x 2" chip design and channel dimensions are shown in **Figure 4.1**. In these experiments, the channel design incorporated a channel possessing a larger width and depth (1.2 cm x 0.35 cm) than the remaining separation channels. This fluidic channel of larger dimensions allowed for decreased fluidic resistance and decreased time required for sample switching.

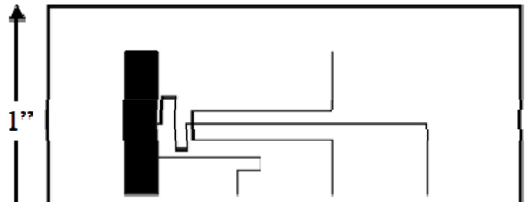

Figure 4.1 Schematic of the 1" by 2" photomask and the resultant glass chips used for the NASA separations. The flow through channel can be seen in the top portion of the image.

Microchips were fabricated using standard photolithographic and wet chemical etching techniques modified from earlier procedures.[44] Briefly, from 10.16 cm x 10.16 cm x 0.16 cm soda-lime photomask blanks coated with chrome and AZT positive tone photoresist (Telic Co.; Santa Monica, CA). The photomask blanks were patterned using the photomasks and exposing to UV light for 10 s at an energy density of 45 μJ/cm^2 using a flood exposure system (ThermoOriel; Stratford, CT). The exposed plate was then submerged in a stirred solution of Microposit Developer (Shipley Co.; Marlborough, MA) for 90 s, followed by a thorough rinse with 18 MOhm•cm water. The plate was subsequently submerged in a stirred solution of Chrome Mask Etchant (Transene, Co.; Danvers, MA) for 3 minutes, rinsed with 18 MOhm•cm water, and dried with inert gas. The exposed glass was wet chemically etched using a stirred, dilute buffered oxide etchant (BOE) (Transene Co.; Danvers, MA). The BOE (NH_4F/HF, 10:1) was diluted with water and mixed with HCl in the volumetric proportions 1:4:2, respectively. The channel dimensions were periodically measured throughout the etching process using a stylus-based surface profiler (Ambios Technology; Santa Cruz, CA). Once the separation channels were the desired depth (~20 μm), the plate was rinsed with water and dried with inert gas. A 'flow through' channel of larger dimensions was also necessary on the microfluidic platform to interface the macro external fluidics with the micro fluidics of the separation channel. To achieve this feature, all other regions of the chip designs were covered with electrical tape, and the plate was again placed into the BOE until the flow through channel reached the depth of 150 μm. This novel procedure created a smooth slope connecting the deep flow-through channel to the more shallow separation channel as can be seen in the optical microscope image and the profilometer trace in **Figure 4.2**. It should be noted that the flow-through channel dimensions are out of the profiler z-axis range (XP-2 Series Stylus Profiler; Ambios Technology; Santa Cruz, CA). This means that the scan does not remain true to the actual profile of the channel after ~0.79 mm on the graph (**Figure 4.2**), however the gradual slope at the intersection can be accurately demonstrated.

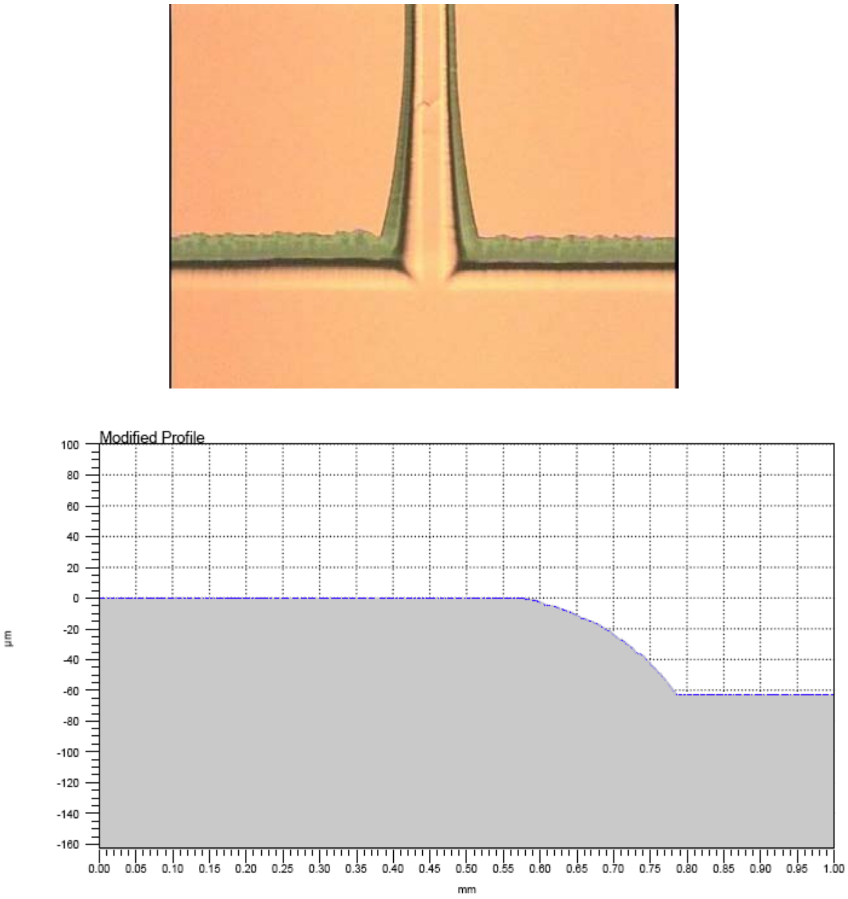

Figure 4.2 Top: Optical microscope image (10x) taken at the intersection of the flow through and separation channels, illustrating the smooth slope created between the different depths using this novel etching method. Bottom: Profilometer scan beginning inside the separation channel and leading into the flow through channel. This scan illustrates the gradual slope created during the etching process.

The remaining photoresist was removed by rinsing the plate with acetone followed by an 18 MOhm•cm water rinse. The remaining chrome was then removed by immersing the plate in a stirred solution of Chrome Mask Etchant for 10 min followed by rinses in 1M sulfuric acid and 18 MOhm•cm water. The cleaned plate was then dried with inert gas and diced into 8 individual 2.54 cm x 5.08 cm slides using a dicing and cutting saw (Model EC-400; MTI Corp.; USA). Access holes were mechanically drilled into 10.16 cm x 10.16 cm x 0.15 cm cover plates (Technical Glass Inc.; Aurora, CO), then cut into 8 individual slides in a similar manner prior to bonding.

4.2.3 Microchip Bonding

The 8 top and bottom slides were cleaned thoroughly with acetone followed by rinses with ethanol and 18 MOhm•cm water. The chips were then dried with inert gas. Next, the slides were submerged in a stirred 5M sulfuric acid solution for 5 min, rinsed with 18 MOhm•cm water, and then cleaned using the above described acetone/ethanol/water/inert gas procedure. In a laminar flow hood, the slides were immersed in a Versa-Clean Liquid soap solution (Fisher Scientific; Pittsburgh, PA), sonicated (3510 Ultrasonic Cleaner; Branson; Danbury, CT) for 15 minutes, rinsed with 18 MOhm•cm water and dried. The slides were then sonicated in acetone for 10 min, dried, and placed in the previously described dilute buffered oxide etch solution for 10 s. The slides were immediately rinsed with 18 MOhm•cm water and placed in a dilute hydrolysis solution (1:1:2 parts NH_4OH, H_2O_2, H_2O, respectively) for 12 minutes at 60 °C.[10] The slides were then rinsed with 18 MOhm•cm water and sonicated in flowing 18 MOhm•cm water for 60 s before joining. The etched slides were removed one at a time from the flowing water under a stream of 18 MOhm•cm water and placed on a

Cleanroom Wiper (DURX 670; Great Barrington, MA). The drilled cover slides were removed from the flowing water and placed on top of the respective etched slide. Binder clips were fastened on the perimeter of the chip to ensure contact between the two surfaces, and water was removed from the channels with a vacuum hose. The joined chips were placed in the oven at 95 ^{o}C for 15 min to drive out any remaining water and then annealed at 565 ^{o}C to ensure proper bonding of the cover plate to the chip surface. In the past six months, we have successfully bonded 112 of 112 microchips using this method for a bonding success rate of 100%. Four cylindrical glass reservoirs (~140 μL capacity) were attached to the separation channel outlets using Epo-tek 353ND Epoxy (Epoxy Technologies, Inc.; Billerica, MA). Additionally, two nanoport reservoirs (UpChurch Scientific; Oak Harbor, WA) where attached at each end of the flow through channel (**Figure 4.3**).

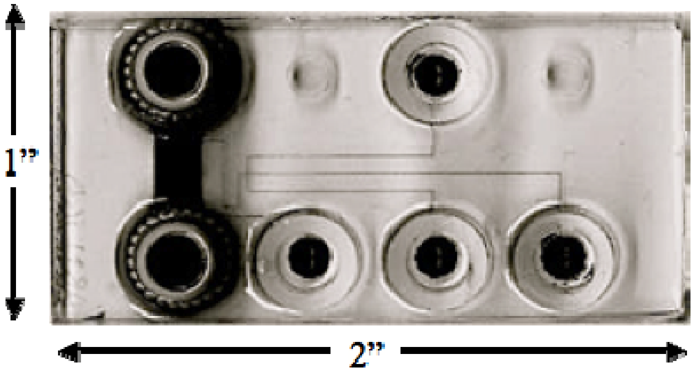

Figure 4.3 Photograph image taken of a bonded NASA chip used for experiments. The channels were filled with blank ink to make the channels visible to the eye.

4.2.4 Portable Device Design

The portable system developed for these tests was similar to that previously done in our group.[43] Briefly, the microfluidic device was contained in an ABS/PC blended box enclosure (NBA-10148; Bud Industries Inc.; Willoughby, OH)) which has exterior dimensions of 28 cm wide x 16 cm deep x 38.4 cm high as shown in **Figure 4.4**.

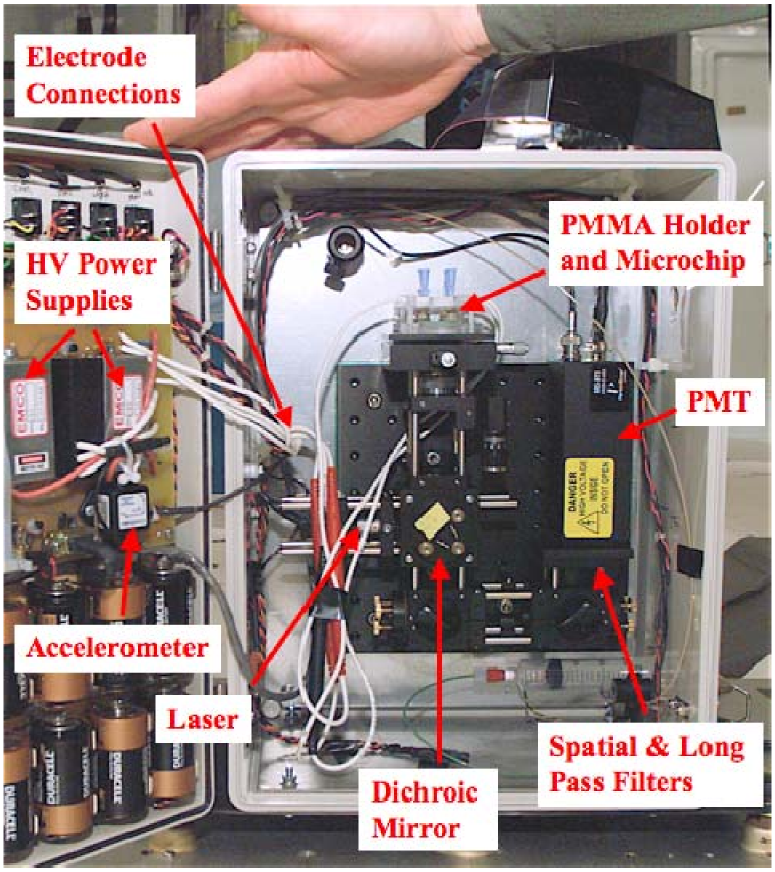

Figure 4.4 Photograph of the portable microfluidic setup flown on NASA's microgravity research aircraft with arrows depicting various components.

The box was powered from the exterior panel via a power cord to a 110V/60Hz power outlet inside the plane cabin. To monitor changes in gravity, the inside of the box door was equipped with an inertial mass measurement unit (ADXL105EM-3; Analog Devices; Norwood, MA). The microchip and separation voltage lines were fastened into an in-house machined 2-part PMMA holder. The holder attached to an x-y positioning plate (ST1XY-S; Thor Labs Inc.; Newton, NJ) positioned above a microscope objective

(CD-240-M40X; Creative Devices, Neshanic Station, NJ) that was used to focus the 473 nm excitation light of a diode pumped blue CrystaLaser (BCL-010; CrystaLaser; Reno, NV). It should be noted that the CrystaLaser replaced the laser pointer in the above photograph (**Figure 4.4**) for these experiments. The laser was mounted on the box bottom such that the same optical configuration could be used. The laser beam was reflected off a long-pass dichroic mirror (500 DRLP; Omega Optical; Brattleboro, VT) prior to being focused into the microchip channel by the microscope objective. The fluorescence from the labeled amino acids was collected by the same microscope objective, passed through the dichroic mirror, a 1.0 mm pinhole, and a 545 nm band-pass filter (545ALP; Omega Optical; Brattleboro, VT) prior to being detected at a channel photomultiplier tube (MD972; Perkin Elmer; Fremont, CA). The gain was manually controlled by a potentiometer with a locking mechanism to prevent accidental change during flight. The entire detection system was mounted in the back of the box using a Mini Breadboard (Thor Labs; Newton, NJ).

The high voltages used for making gated injections and performing the electrophoretic separations on the microchip were provided by two independent high voltage power supplies capable of 125 mA outputs at up to 8 kV (C80; EMCO High Voltage Corp.; Sutter Creek, CA). The HV output was determined by a 0-5 VDC control signal provided by a National Instruments AO card (DAQ Card AO-2DC).

A mini-pump variable flow peristaltic pump (Fisher Scientific; Pittsburg, PA) was attached outside of the box and used to provide pressure through the large flow-through channel, decreasing the time needed to completely switch samples. Sample switching was performed using two flight-certified cell culture bags connected to a 4-port switching valve using 1/16” outer diameter (0.5 mm inner diameter) PEEK tubing (UpChurch Scientific; Oak Harbor, WA). The remaining two ports on the switching valve were each directly connected to (1) a waste syringe using silicon tubing and a barbed luer lock fitting and (2) the large flow channel of the microchip using 10-32 coned inserts that thread into nanoport reservoirs (UpChurch Scientific). A diagram and photograph of the macro-to-micro fluidic system can be seen in **Figures 4.5 and 4.6**, respectively. The entire instrument was controlled by and the acceleration, current, and separation data were acquired for each run by using in-house written LabVIEW software, operated via a DELL laptop computer.

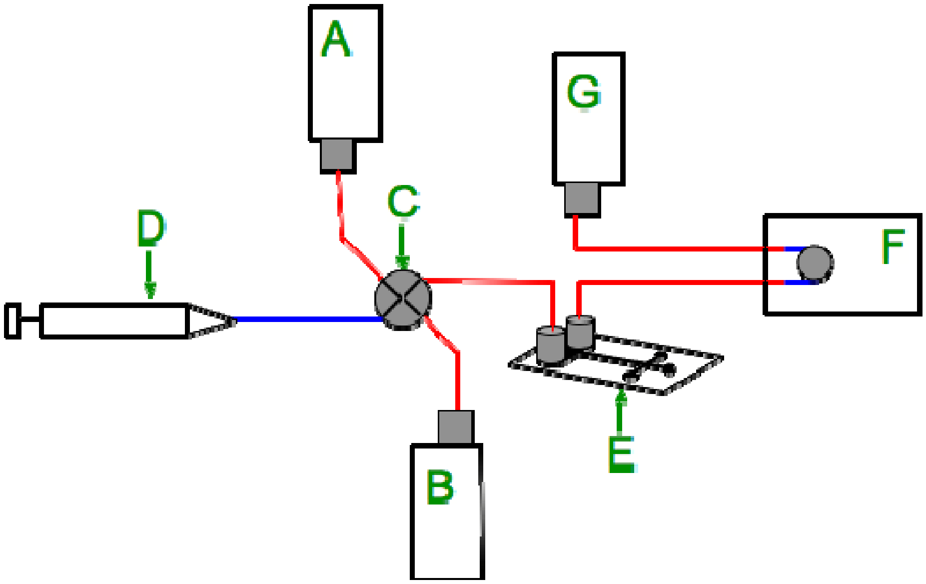

Figure 4.5 Schematic of the macro- external fluidic connections to the micro-fluidic system for performing CE separations. (A) and (B) are the sample cell culture bags connected to a waste syringe (D) and the flow-through channel of the microchip (E) using a 4-port switching valve (C). A peristaltic pump (F) is connected to the outlet of the microchip flow-through channel to increase the rate of sample switching, and the excess flows into a cell culture waste bag (G). The 1/16” o.d. PEEK tubing and the 1/16” i.d. silicon tubing is shown by red and blue lines, respectively.

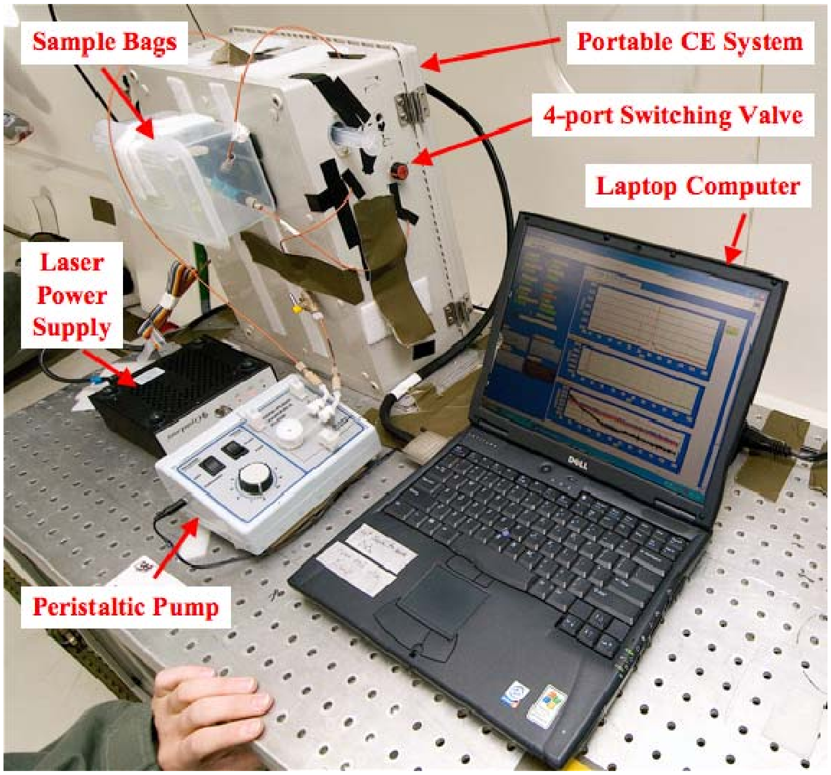

Figure 4.6 Photograph of the entire CE system setup, illustrating how the external electronic and fluidic components are interfaced with the portable CE box.

4.2.5 Chip Preparation and Operation

The chips were cleaned, prepared, and tested on the ground by pulling a 1:1 (v/v) solution of 1 M NaOH:methanol solution through the channels for 1 minute per reservoir. This step was repeated two more times using water and then run buffer, respectively. For these experiments, a 10 mM sodium tetraborate buffer (pH 9.0) was used. Once the chip was prepared, the reservoirs were partially filled with buffer, and the microchip was mounted on the PMMA holder. Before closing the holder, adhesive PDMS was affixed to each reservoir to prevent fluid leakage under microgravity environments. The electrodes were pushed through the PDMS caps to perform the CE separations. In addition, four syringe needles were inserted into each reservoir to prevent pressure heads from forming within the microchip.

4.3 Results and Discussion

The experiments were performed during two consecutive flights on NASA's C-9 reduced gravity research aircraft. Each flight duration is approximately 1.5 hours in length and consists of ~40 parabolic maneuvers as seen in **Figure 4.7** with ~30 s of ~0*g*.

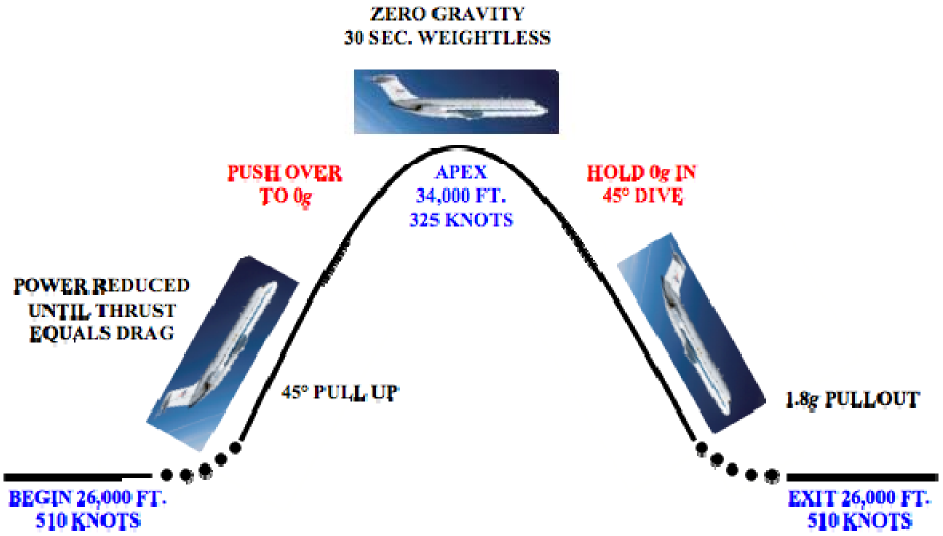

Figure 4.7 Figure illustrating the parabolic nature of NASA's C-9 microgravity research aircraft with periods of weightlessness beginning at the apex of the parabola.

The separation conditions and analytes were optimized prior to the flight to make certain that the time required for each separation was < 25 s, and complete separations could be achieved in each parabola. The separations described in these experiments were completed in < 10 s. The first flight demonstrated successful integration of a bioreactor with a microfluidic device that was capable of performing rapid online separations of amino acids. To demonstrate the sample switching within the bioreactor, two cell culture bags were filled with dilute amino acid solutions of varying composition and concentration. Sample bag 1 contained a solution of 2 μM BODIPY®-labeled arginine, serine, and glutamic acid in 10 mM sodium tetraborate (pH 9). A typical separation (Run 60; 22 August 2006) performed from sample bag 1 at ~0g is shown in **Figure 4.8**.

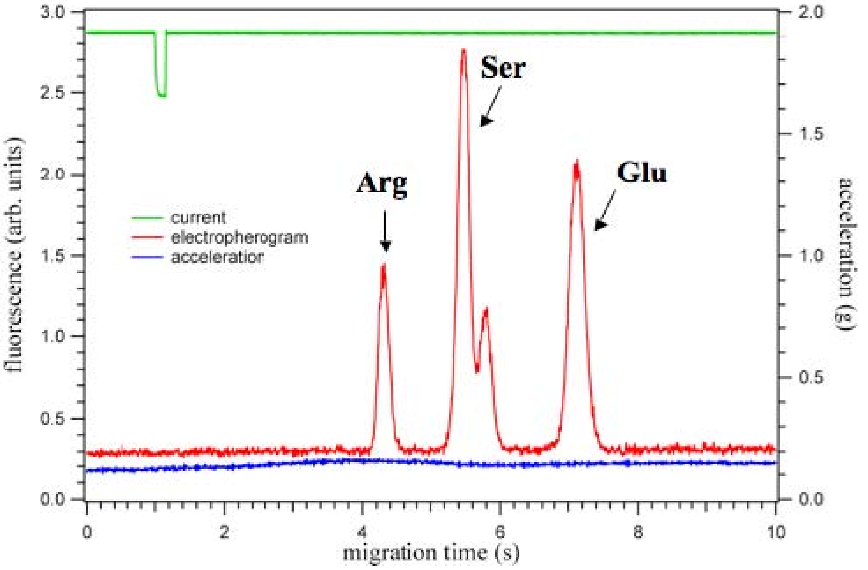

Figure 4.8 Amino acid separation (Run 60) from sample bag 1 at ~0*g* from the 22 August 2006 flight. The red, green, and blue traces are the electropherogram (left axis), separation current, and acceleration (right axis), respectively.

To emphasize the sample exchange, the amino acid concentrations were halved (to 1 μM) and glutamic acid was removed in the second sample bag. After 20 parabolas using sample bag 1 were completed, the four-way valve was switched, introducing sample bag 2 into the device. It can be seen in **Figure 4.9** that the glutamic acid peak has been removed, and the peak heights have decreased by approximately one-half of that seen in sample bag 1. This is indicative of a successful sample exchange and analytical separation within the bioreactor system.

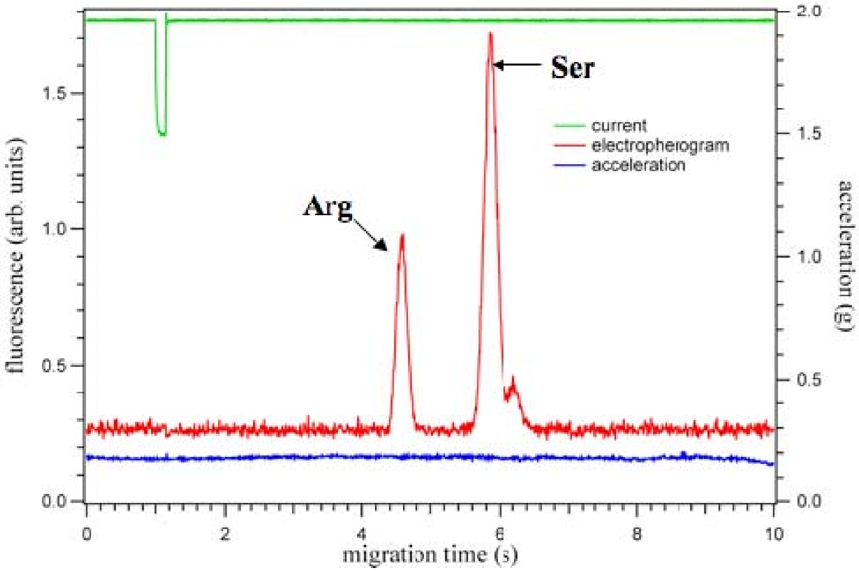

Figure 4.9 Amino acid separation (Run 308) from sample bag 2 at ~0*g* from the 22 August 2006 flight. The red, green, and blue traces are the electropherogram (left axis), separation current, and acceleration (right axis), respectively.

It should also be noted that the peak migration times do not vary significantly over the course of the runs spanning more than 40 min. The migration times for the Arg peak in Runs 60 and 308 are 4.31 s and 4.57 s, respectively. The slight shift (~5.7%) in migration times seen is most likely due to an increase in temperature in the aircraft and electronics throughout the duration of the flight. All equipment had to be powered off before the flight for safety reasons so the electronics were not allowed to properly warm up prior to data collection.

The second flight (23 August 2006) demonstrated the ability of the microfluidic device to sample from cell culture media and detect nanomolar concentrations of reGFP from the media. These experiments were performed in a similar manner to flight 1. Briefly, sample bag 1 again contained a 2 μM solution of arginine, serine, and glutamic acid in 10 mM sodium tetraborate. Sample bag 2 contained only the reGFP cell culture media. Mid-flight, the 4-port switching valve was rotated to sample from the GFP media. **Figure 4.10** shows the detection of the protein from NASA's cell media at 1.82*g* (Run 175; 23 August 2006) with a separation efficiency of 16 000 plates. Due to surface adsorption of the protein before the second set of parabolas resumed, we were unable to show a good quality separation of GFP at 0*g*.

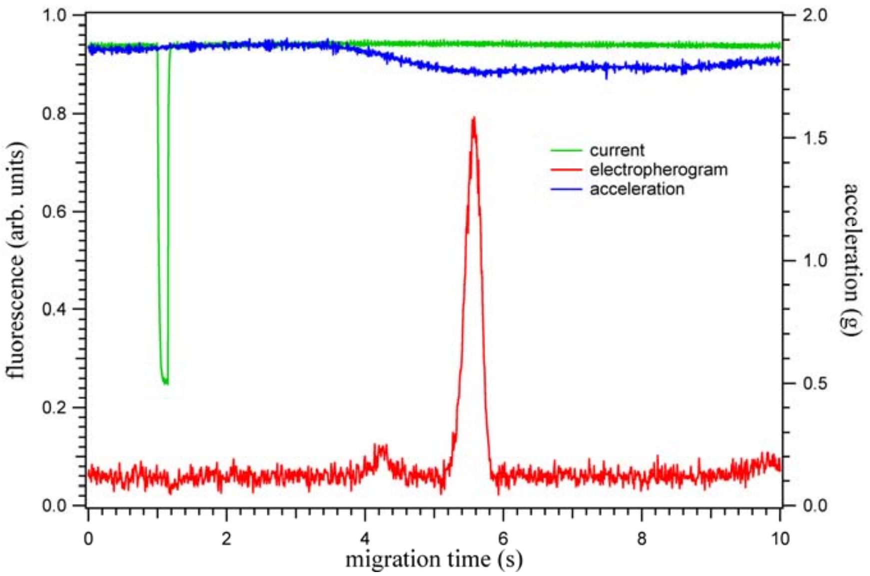

Figure 4.10 Electropherogram of reGFP run (Run 175) from sample bag 2 at ~1.82*g* from the 23 August 2006 flight. The red, green, and blue traces are the electropherogram (left axis), separation current, and acceleration (right axis), respectively.

4.4 Conclusions

These experiments demonstrate the successful integration of the large-scale external fluidics of a bioreactor-type system with the small-scale sampling and separation of a microfluidic system used for performing capillary electrophoresis separations. It was shown that the portable CE system is capable of performing automated, rapid, reliable, high-quality separations of amino acids and reGFP in microgravity and hypergravity environments. Finally, the portable CE system experienced no mechanical, electrical, or optical complications during or post flight, indicating that the CE system is adequate for hostile operating conditions similar to those found in space.

CHAPTER 5 - Preparation, Separation, Detection and Identification of Aphid Salivary Secretions

5.1 Introduction

Understanding mechanisms involved in insect feeding and salivation on host plants is crucial to determining the effects of the pest species. It is also crucial for the ability to control pest populations on various plants and crops, as many insects can adapt to become 'immune' to pest-specific insecticides. These damaging effects can be seen directly during phloem uptake, or indirectly such as in virus transmission among host plants. Currently, there are approximately 4400 aphid species (Homoptera Aphididae) known, and among those at least 250 are deemed pest species responsible for direct and indirect plant damage on crops such as potatoes, peaches, wheat, sorghum, etc.[45] It is also known that aphids can transmit more than 275 different viruses.[46,47] When feeding, the aphid stylet penetrates plant phloem sieves between the epidermal and parenchymal cells, and the aphid injects the plant with 'watery' saliva before ingesting plant sap. This salivation phenomenon was first seen in 1959 by Miles et al by visually monitoring aphid feeding in a water media.[48] This occurrence has been confirmed through the use of electrical penetration graphs (EPGs), where a circuit is constructed with the aphid and host plant, and the feeding processes can be monitored through fluctuations in the current.[49]

Due to its small size, stylet penetration causes minimal physical damage to the host plants when compared to damage caused by other tissue-feeding insects. Aphid saliva is thought to contain oxidases and depolymerization enzymes similar to those naturally occurring in plants. However, it is known that these injected salivary enzymes are capable of diverting the plants defensive, biochemical responses.[50] Aphid feeding at the molecular level is still not well understood, though research has been ongoing for decades. It is thought that multiple aspects of the aphid-plant relationship will be ‘unlocked’ through the discovery of aphid salivary components.[51] Previously, amino acids,[52] pectinases,[53] cellulase,[54] polyphenol oxidase and peroxidases[52,55-57] have been found in aphid salivary secretions. Proteins have not yet been identified in aphid salivary secretions, only enzymes (though their roles are still largely unknown) have been discovered primarily through the indirect measuring of enzymatic activity.[57] Because of the substantial similarity in salivary function within the Aphididae family, the pea aphid (*Acyrthosiphon pisum*) is the primary species used in laboratory and genetic studies due to its larger size (0.5 – 2.0 mm) and ease of rearing.

In addition to acquiring valuable information regarding aphid salivary secretion components, aphids offer other main areas of research interest, making them excellent research species. The first lies in the aphid ability to reproduce through clonal and sexual means, providing insight into the understanding of asexual reproduction in insect species.[58] Additionally, aphids possess intracellular symbiotic bacteria. It has been shown that nearly all aphid species possess *Buchnera* cells in their abdomens, and aphid survival is impossible in the absence of *Buchnera*.[58,59] Any information acquired in this realm can serve to develop a general model for understanding processes of bacteria-host symbiont relationships and infections.[60]

5.2 Materials and Methods

5.2.1 Plant Hosts and Aphid Colony

Aphid rearing was similar to the protocol previously described.[61] Briefly, pea aphids were obtained from alfalfa plants (Dr. Marina Caillaud; Cornell University). Following transport to Kansas State University, the aphids were reared in Dr. John Reese's lab on fava bean plants (*Vivia fabe*). The plants were contained in 10 cm diameter plants under high intensity sodium lights for 16 hours (with 8 hours of dark). For the following experiments, ~8000 aphids were collected (by mass and of varying ages and sizes) from the plants.

5.2.2 Reagents and Artificial Diet Preparation

Three different artificial diets: Diet 3, Complete Diet, and 15% sucrose were used in these experiments. Diet 3 consists of three amino acids (100 mM serine, 100 mM methionine, and 150 mM aspartic acid) and 15% by mass sucrose in water. The Complete Diet is more complex and more closely mimics the phloem sap of the plant. This diet includes 15% sucrose, 22 amino acids in the 0.2-12.5 mM range, vitamins (ascorbic acid, biotin, aminobenzoic acid, nicotinic acid, thiamin, etc.), metal salts, cholesterol, and choline. The 15% sucrose diet is composed of only 15% sucrose. For preparation protocols, see **Appendix A**.

5.2.3 Aphid Feeding Chamber

Throughout these experiments, two main chambers were constructed in-house and used to contain and provide the artificial diets to the aphids. The initial aphid chamber consisted of a plastic petri dish and lid with dimensions of 150 x 15 mm (Fisher Scientific; Pittsburgh, PA). A square hole (~ 9cm x 9cm) was cut into the lid for construction of a Parafilm aphid feeding area. Next, a piece of Parafilm was stretched over the square opening. An aliquot of artificial diet was placed onto the Parafilm layer, and the diet was enclosed with a secondary layer of Parafilm to prevent evaporation and/or environmental contamination. Approximately 1000 aphids were placed in the bottom of the dish, the lid placed on, and the edges sealed with a strip of Parafilm to prevent the insects from escaping. A diagram illustrating the aphid chamber assembly is shown in **Figure 5.1**. Parafilm was used to contain the aphid diets because it has been previously shown that the aphid stylet is the only organ with the ability to penetrate the Parafilm layer.[50] Optical images of this artifact can be seen in **Figure 5.2**, where the aphid stylet can be seen penetrating the Parafilm and a hole can be seen after stylet removal. Additionally, it is known that aphids are attracted to yellow coloring for feeding, so the chambers were covered using pieces of yellow construction paper. All parts of the aphid chamber were sterilized with 70% ethanol prior to assembly.

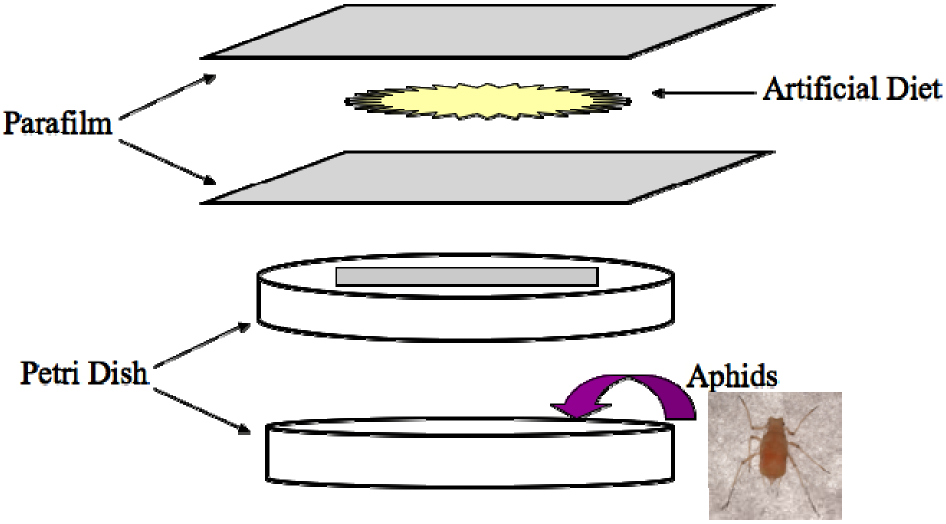

Figure 5.1 Schematic of the first generation aphid chamber used for artificial feeding experiments.

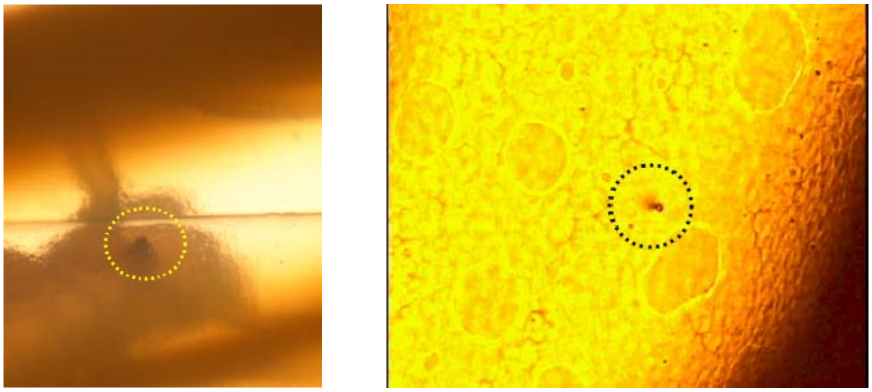

Figure 5.2 Optical images taken (left) while an aphid stylet penetrates through a Parafilm layer to feed and (right) the stylet hole that is left in the Parafilm.

The second-generation aphid chamber was also constructed in-house and consisted of a transparent 100-1000 µL pipette tip box lid (the length, width, and height were 13.3 cm x 11.5 cm x 4.8 cm, respectively). Three main differences occur in the design and assembly of this chamber. First, one end of the box is already open to attach the Parafilm feeding layers. Second, to increase ventilation within the chamber, two holes were cut into the length of the box lid (~ 3.5 cm x 12.5 cm) to which corrosion-resistant Type 304 stainless steel woven wire cloth (McMaster-Carr; Princeton, NJ) was adhered using hot glue. The wire diameter of the cloth was 0.0016” with an opening width of 0.0034,” which was more than adequate to keep the aphids contained. Images of the assembled aphid chambers were shown in **Figure 5.3**. During assembly, the aphids were placed inside the box before the initial Parafilm layer was attached. Once assembled, the aphid chamber was allowed to sit upside down for 20 minutes to allow the aphids to attach to the feeding medium. Third, the aphid chambers were covered with squares of yellow theater lighting gel (Roscoe 10; A-to-Z Theatrical; Kansas City, MO) to allow more light into the chamber (~92% transmission), better simulating sunlight. All parts of the aphid chamber were sterilized with 70% ethanol and UV light prior to assembly.

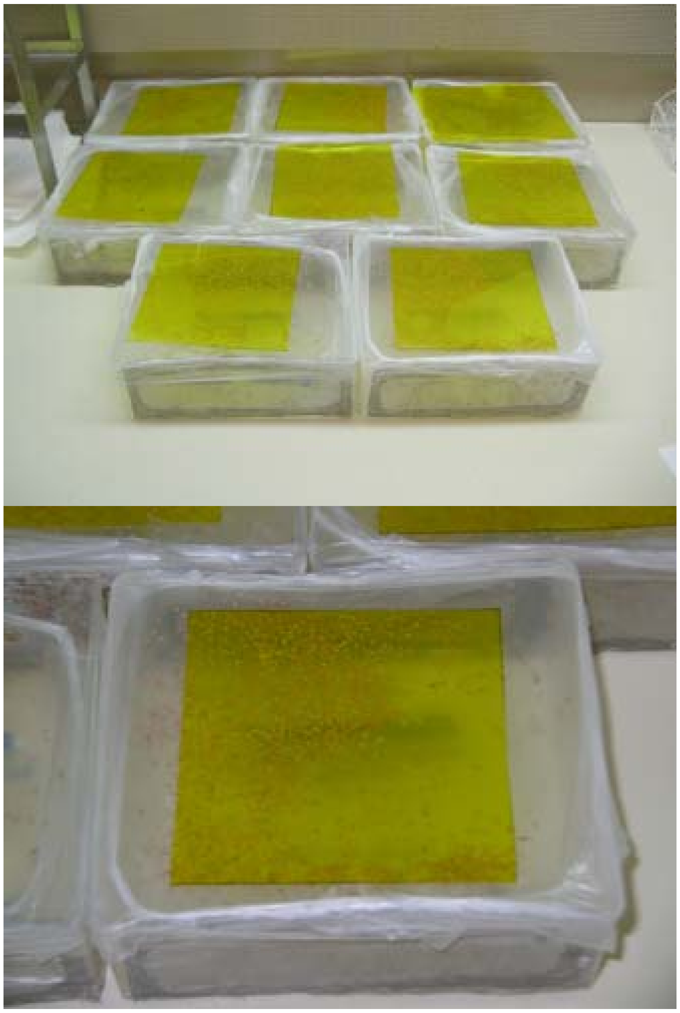

Figure 5.3 Photograph images of eight assembled second-generation aphid chambers with ~1000 aphids per chamber feeding on artificial diets (top) and a single box illustrating the aphid feeding (bottom).

5.2.4 Salivary Sample Collection, Washing, and Preconcentration

The aphid chambers were kept in a clean hood equipped with HEPA-filters (Purifier Clean Bench; Labconco; Kansas City, MO). All aphid chambers were kept under even, constant lighting for 24 or 48 hours, depending on the experiment. Throughout the optimization process, and depending on the artificial diet used, the feeding volumes ranged from 0.75 mL to 3.5 mL (see Results and Discussion for further details). Additionally, with each aphid chamber experiment, a 'blank' was also assembled in an aphid chamber and kept in the same conditions. After the desired feeding time was complete, the eight individual aphid samples from 1000 aphids were collected in sterile conditions (total aphids ~8000/collection day). This was done by carefully removing the top layer of Parafilm, removing the fed diet using a syringe, and placing it into a Falcon conical tube (Fisher Scientific; Pittsburgh, PA). Because the diet contains a large amount of sucrose, a spatula was used to gently gather the residual fed diet from the Parafilm layers. Following the collection, the Parafilm layers were then rinsed with 8 mL of distilled deionized water from a Barnstead Ultrapure Water System (Dubuque, IA), and this wash from both Parafilm layers was added to the conical tube. Because of the large volumes acquired, the samples had to be preconcentrated. This was done via centrifugal filtration using Vivaspin molecular weight cut off (MWCO) filters (Sartorius Stedim Biotech; Aubagne, France). Throughout the experiments, 3000 and 5000 MWCO filters were used with no significant differences seen. To decrease the concentration the diet media and preconcentrate the aphid salivary secretions, each sample was washed in the MWCO filters using either (1) 100 mM sodium phosphate (pH 7) containing 0.02% sodium azide and 10% acetonitrile by volume or (2) distilled deionized water and 10% acetonitrile by volume (see Results and Discussion). The washing solutions were added to the sample in appropriate volumes such that a ten-fold dilution was achieved before centrifugation, and this step was repeated 3 times per sample to achieve a 1000x decrease of the components in the diets. In some instances, the samples were lyophilized to dryness and reconstituted in a small aliquot of the washing solution to further concentrate the samples for analysis.

5.2.5 Electrophoresis

Electrophoresis experiments were performed using a 2100 Bioanalyzer System (Agilent Technologies; Santa Clara, CA) following standard preparation and operation procedures. Briefly, 5 μL of the aphid sample was mixed 1:10 with the Standard Labeling Buffer (SLB) and checked to ensure the pH is in the range 8-9. The SLB consisted of 30 mM Tris/HCl (pH 8.5). The prepared sample (and subsequent protein ladder standard) were then mixed with the Dye Solution, incubated for 30 min on ice, mixed with ethanolamine, and incubated for 10 min on ice for optimal labeling. The sample was mixed with the denaturation buffer and heated while the chip was primed and loaded with the gel and detain solutions. Finally, the sample and ladder were pipetted into the chip well, inserted into the 2100 Bioanalyzer tray, and separated. The system provided gel and chromatogram images with the corresponding masses.

5.2.6 Size Exclusion Chromatography

Size exclusion chromatography (SEC) experiments were performed using an Agilent 1100 series HPLC (Agilent; Santa Clara, CA) fitted with a BioSep-SEC-S2000 column (300 x 7.8; Phenomenex; Torrance, CA). The mobile phases consisted of 50% of A: water with 0.1% trifluoroacetic acid (TFA) and 50% B: acetonitrile with 0.1% TFA with a flow rate of 0.5 mL/min. The column temperature was held constant at 40°C, and all injection volumes used were 25 μL (with the exception of one sample that had double the volume of the other samples). Protein standard solutions were made in the aphid diet washing solution (water and 10% ACN) with a final concentration of 1 mg/mL, and the injection volumes for each were 20 μL. Alcohol dehydrogenase (MW = 150 kDa), albumin (MW = 66 kDa), carbonic anhydrase (29 kDa), and α–lactalbumin (MW = 14.2

kDa) were chosen to span a large range of molecular weights that encompass the molecular weight range of the aphid salivary components. All spectra were collected at an absorbance wavelength of 200 nm.

5.2.7 RP-HPLC Analysis and Fraction Collection

Because the early samples were not yet collected under optimized conditions, the separations were performed on a higher-sensitivity reversed phase nano-HPLC (1100 Series HPLC; Agilent; Santa Clara, CA). The mobile phases were (A) water and (B) acetonitrile, and each phase contained 0.1% trifluoroacetic acid (TFA) to serve as the ion-pairing agent. Initial separations were performed using a C-18 Jupiter column (0.3 mm x 15 cm, 5 μm, 300 A; Phenomenex; Torrance, CA) with injection volumes between 3-8 μL, a flow rate of 4 μL/min, and a column temperature of 50 °C. Using a variable wavelength detector, absorbance wavelengths of 214 nm, 254 nm, and 280 nm were used simultaneously.

Once the sample collection conditions were optimized such that the samples were concentrated enough to be detected with a typical HPLC system, an Agilent 1100 series HPLC was used for further analysis and fraction collection. For these experiments a Poroshell 300SB C-18 column was used (2.3 mm x 75 mm, 5 μm, 300 A) was used with the same mobile phases as previously described. The column was held at 50 °C, and the flow rate was 200 μL/min. In these experiments, the MWCO filters had slight sample-to-sample variation in the final preconcentration volumes, so the injection volumes were normalized to account for final sample volume differences. Using a variable wavelength detector, three absorbance wavelengths were used (214 nm, 254 nm, and 280 nm). This HPLC system was used with an automatic fraction collector to collect fraction based on time intervals. Methods and fraction collection time intervals are further described in Results and Discussion Section, as they were optimized over the course of the experiments.

5.2.8 Mass Spectrometry

Mass spectrometry experiments and analysis were done using the Biotechnology Core Facility (Kansas State University; Manhattan, KS). Protein digestion is typically done using a 1:100 ratio of trypsin to protein. Because the concentrations of proteins in our aphid samples is unknown, the tryptic digest was performed using 10 μL of 10 ng/μL trypsin and 10 μL of ammonium bicarbonate per eppendorf tube fraction and allowed to digest overnight. Following the digestion, the solution was evaporated and 10 μL of 2,5-dihydroxybenzoic acid (DHB) was added. To perform MALDI-TOF and MALDI-TOF-TOF analysis (Ultraflex II TOF/TOF; Bruker Daltonics), 2 μL of each fraction was dried on the analysis plate. In some cases, electrospray ionization mass spectrometry (ESI-MS) analysis was also possible. In these cases, the remaining fraction volumes were injected into the nano-HPLC system and sprayed into the ESI system (HCT Ultra; Bruker Daltonics).

5.3 Results and Discussion

5.3.1 Aphid Feeding

Previous experiments have shown that aphids secrete similar quantities of saliva into pure water as they do into sucrose solutions. The composition of aphid saliva may change with variations in the feeding source (ie: plants vs. artificial diets).[50,62-64]

However, it has been shown that aphids can survive and produce offspring when feeding on artificial diets, especially those containing sufficient amino acids, vitamins, trace metals, and sugars.[65] To determine which diet maintains the best aphid colony, feeding experiments were performed. In these experiments, aphid nymphs were fed Diet 3 and Complete Diets doped with 1% blue food coloring. Because the aphid bodies are slightly transparent, the abdomen was monitored for a blue change in color, indicative of feeding. The amount excrement (honeydew) production was monitored to indicate which diet they are eating a larger percentage of. It was evident by the blue coloring (**Figure 5.4**) that the aphids feed on the artificial diets and have an increased honeydew production when feeding on the complete diet.

Figure 5.4 Feeding on diets doped with 1% blue food coloring it can be noticed that (A) the aphid nymphs abdomens turn blue, indicative that they are feeding and that the aphids produce smaller quantities of honeydew when feeding on Diet 3 (B) than when feeding on Complete Diet (C).

This enhanced feeding on Complete Diet over Diet 3 was quantified by monitoring the lifespan, reproductive rate, and drops of honeydew production of 10 aphids (even aged cohorts). Three trials were completed and it is seen in **Figure 5.5** that the aphids fed on Diet 3 have complete colony death within four days. Aphids on Complete Diet live longer and have substantially more offspring (colony size doubles in one day) and honeydew production than those feeding on Diet 3.

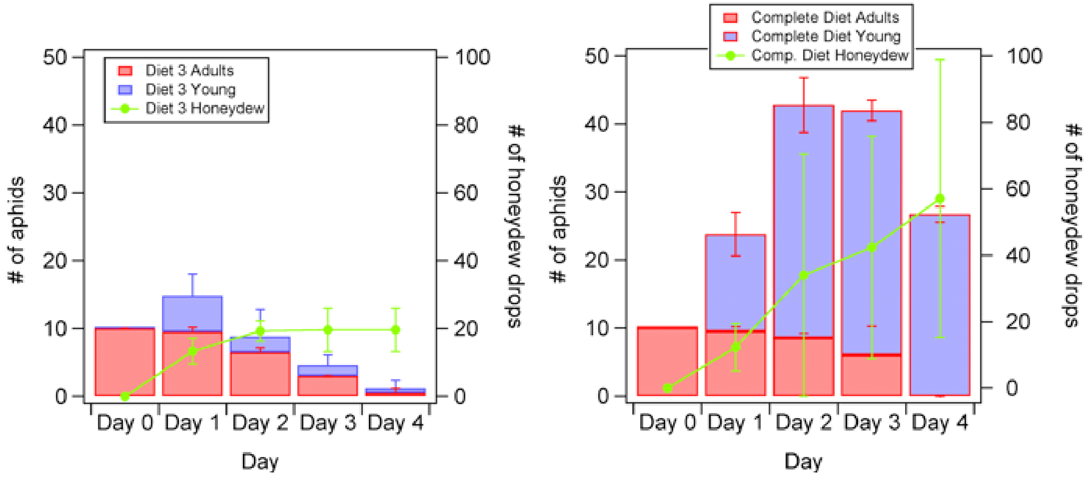

Figure 5.5 Charts comparing the number of aphids, reproduction, and honeydew production when feeding on Diet 3 (left) and Complete Diet (right). The red and blue bars represent the number of adults and the number of offspring produced, respectively. The green trace (right axis) marks the number of drops of aphid honeydew produced over four days.

5.3.2 Electrophoresis

Using the 2100 Bioanalyzer System, we were able to acquire mass information for the aphid salivary secretions. This automated system is known for its fast separation times (complete analysis in ~ 25 minutes) and the ease of use. Additionally, when run simultaneously with a standard protein ladder, the unknown sample peaks were automatically assigned mass values based on migration times of the protein standards of known masses. An electropherogram from an aphid salivary secretion sample (preparation described in the Materials and Methods section) is shown in **Figure 5.6**.

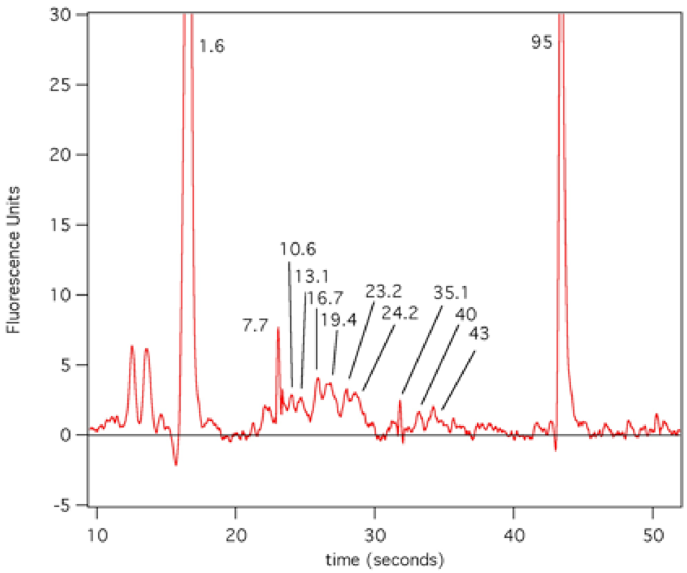

Figure 5.6 Electropherogram of aphid salivary secretions using the 2100 Bioanalyzer system. The electropherogram depicts the representative peak masses for the fluorescent bands detected on the chip as determined using the standard protein ladder.

Though the signals are somewhat low, this figure shows that there are several proteins in the 8000 aphid sample that lie in the 7.7 to 95 kDa range. These values are in close agreement with the ranges found through previous investigations in the literature (6 to 300 kDa).[50] Because our sample collection conditions were not yet optimized at the time of analysis and possible precipitation reactions can occur with the fluorescent labeling medium, there are presumably more proteins within this literature range that do not appear in the electropherogram. However, this analysis does confirm that the salivary sample contains proteins within the expected molecular weight range.

5.3.3 Size Exclusion Chromatography

Size exclusion experiments were performed as described above. From this, molecular weight ranges estimates for the aphid samples were able to be obtained and were in similar agreement with results found in the electrophoresis experiments. The SEC results for the reagents, unwashed Complete Diet, and aphid samples with blanks can be seen in **Figure 5.7**. The unwashed Complete Diet was seen to interact with the column, possibly due to the high concentrations of sucrose. This is evidenced by the elution of multiple peaks rather than one broad peak, as the diet components are small and relatively close in molecular weight range.

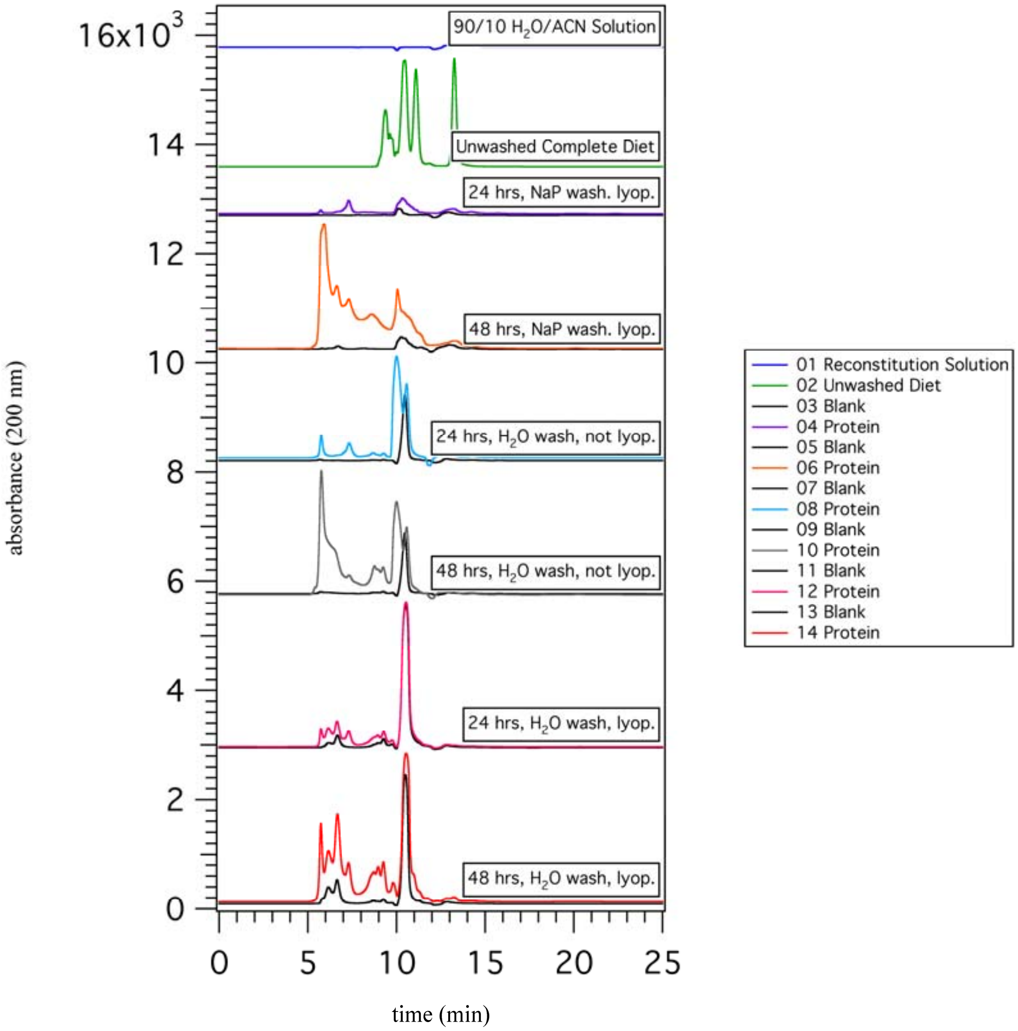

Figure 5.7 SEC results for the sample solution, unwashed complete diet, and multiple aphid samples (and their respective blanks) using 50% water + 0.1% TFA and 50% ACN + 0.1% TFA at 0.5 mL/min and 40°C.

Proteins of known molecular weights (alcohol dehydrogenase, albumin, carbonic anhydrase, and α–lactalbumin) were injected onto the system following the aphid sample and respective aphid blank LC runs. It can be seen in **Figure 5.8** that the peaks elute at noticeably different times (α–lactalbumin = 6.65 min, carbonic anhydrase = 5.97 min, albumin = 5.76 min, and alcohol dehydrogenase = 5.82).

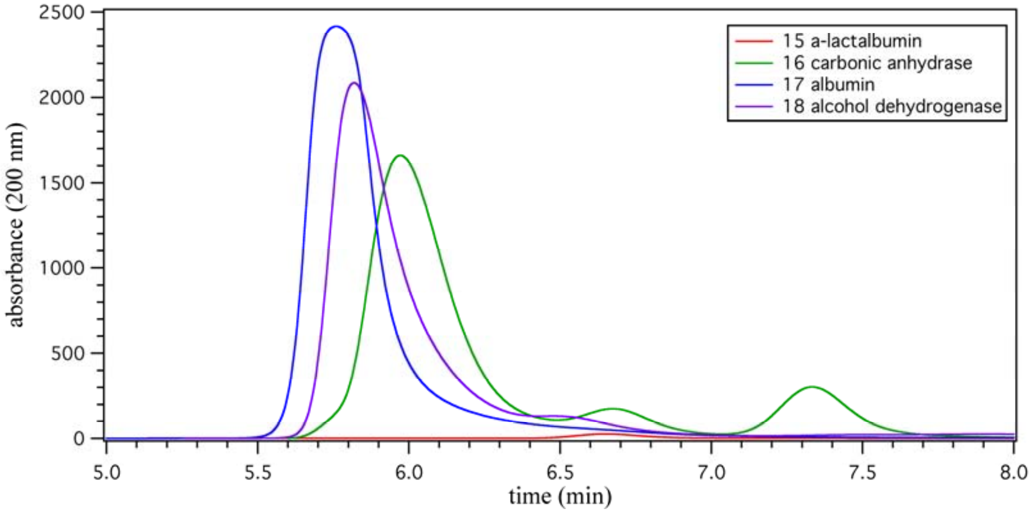

Figure 5.8 Results from the SEC analysis of the proteins (1 mg/mL) used as molecular weight markers for the molecular weight determinations of the aphid salivary components in the SEC experiments.

It is important to note that the alcohol dehydrogenase peak elutes after the albumin peak. Because alcohol dehydrogenase has the highest molecular weight, it should be the first to elute (shortest time). However, alcohol dehydrogenase is known to be an extremely unstable compound and should only be used within 6-12 months of purchase. The alcohol dehydrogenase used in this experiment was > 2 years old and has most likely decomposed over time, accounting for the unexpected peak shift. However, when the times are plotted on the aphid sample SEC results (**Figure 5.9**), it is evident that higher molecular weight components exist in all of the samples, indicative of higher molecular weight proteins. It should be noted that the sample blanks in runs 11 and 13 also possess peaks in the high molecular weight range. After further RP-HPLC and MS analysis (see following sections), it was determined that these peaks are most likely due to external contaminations of bacteria and skin cells (keratin).

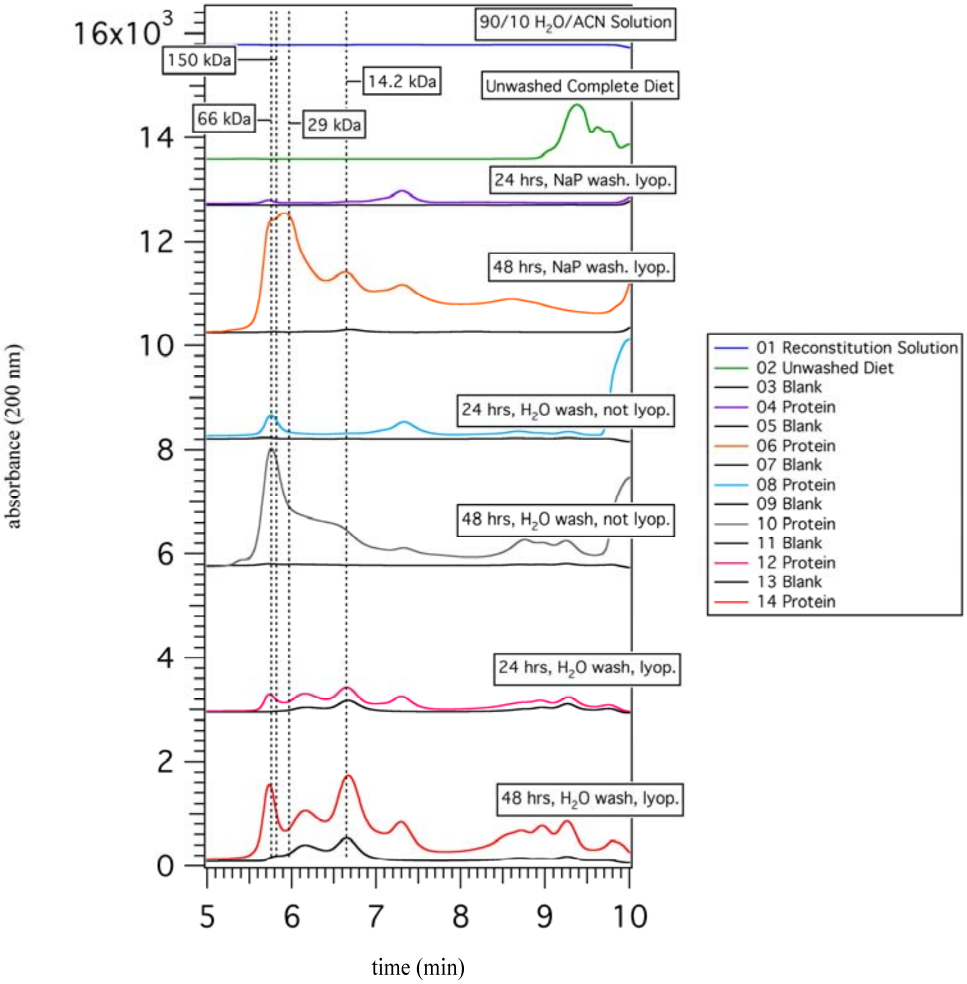

Figure 5.9 SEC results from aphid sample runs with time markers indicating the molecular weights of the chosen standards. It can be seen that many peaks exist with higher molecular weight ranges than those seen in the unwashed aphid diet.

5.3.4 RP-HPLC Separations and Concentration Enhancement

Because the feeding experiments showed that complete diet was overall a better food source for the aphids, it was initially used. Preliminary separations of the aphid salivary secretions were performed on a nano-HPLC system as previously described, and multiple peaks were seen in the chromatograms of the aphid sample as well as the blank diet samples from the same day (data not shown). Additionally, a great deal of variation existed in the chromatograms from samples collected from different days. From this, it became evident that a substantial amount of human and bacterial contamination existed in the collected samples and blanks. To remove external sources of contamination, sterilization steps using 70% ethanol and UV light were introduced and this data ignored as the peaks are most likely due to contaminations.

As the separation collection improved, separations were capable of being performed on the typical reversed phase HPLC (RP-HPLC) system described above. This was beneficial to the experimental progress as nano-HPLC systems are extremely temperamental and require constant maintenance and repair due to their miniaturized features. Of course, some drawbacks are evident when using a typical HPLC as opposed to a nano-HPLC such as decreased sensitivity due to a larger flow cell and the need for larger sample injection volumes, but these were adequate for the following experiments.

Multiple sample collection and preparation variables were investigated throughout these experiments in addition to many aphid environmental conditions. These findings will be further discussed and consist of:

1) Diet washing solutions (H_2O vs. 100 mM sodium phosphate, both containing 10% acetonitrile).

2) Addition of 10 mM calcium ions to the diet media (as opposed to no calcium).
3) Feeding periods (24 hours vs. 48 hours).
4) Artificial diet compositions (Complete Diet vs. Diet 3 vs. 15% Sucrose).
5) Type of chamber (fully enclosed Petri dishes vs. screened chambers).
6) Placing the aphid chambers in even lighting and the amount of light that is allowed into the chambers (opaque yellow paper vs. transparent yellow theater lighting gels).

Complete Diet was used to begin these experiments, as it was previously shown that the aphids feed more readily, live longer, and produce more nymphs. As expected from the minute volumes of saliva produced from the pea aphids, many sampling challenges exist, and these experiments discuss improvements in sample collection seen by peak amplitudes from typical RP-HPLC system separations. The following results are taken from ~8000 aphids/sample (feeding ~1000 aphids/chamber with a total of eight chambers and pooling them upon collection) to have adequate sample concentrations for separation detection.

Each sample was collected and preconcentrated using MWCO filters and two different sample-washing solutions, as described above. As seen in **Figure 5.10**, both Complete Diet sample traces (red and blue) possess peaks that are not seen in the sample blanks (black traces). This is indicative that the peaks observed in the sample traces are due to the aphid salivary secretions. Additionally, the samples washed with 100 mM NaP with 10% ACN, yielded much lower peak amplitudes than those samples washed with water and 10% ACN, when all other conditions were held constant. This observation was found to be consistent for Diet 3 and 15% sucrose samples as well (data not shown). In some instances using the 100 mM sodium phosphate washing solution, precipitate formation occurred. Reasons behind this have yet to be determined, as sodium phosphate solutions around pH 7 are commonly used in preparation of biological samples.[66]

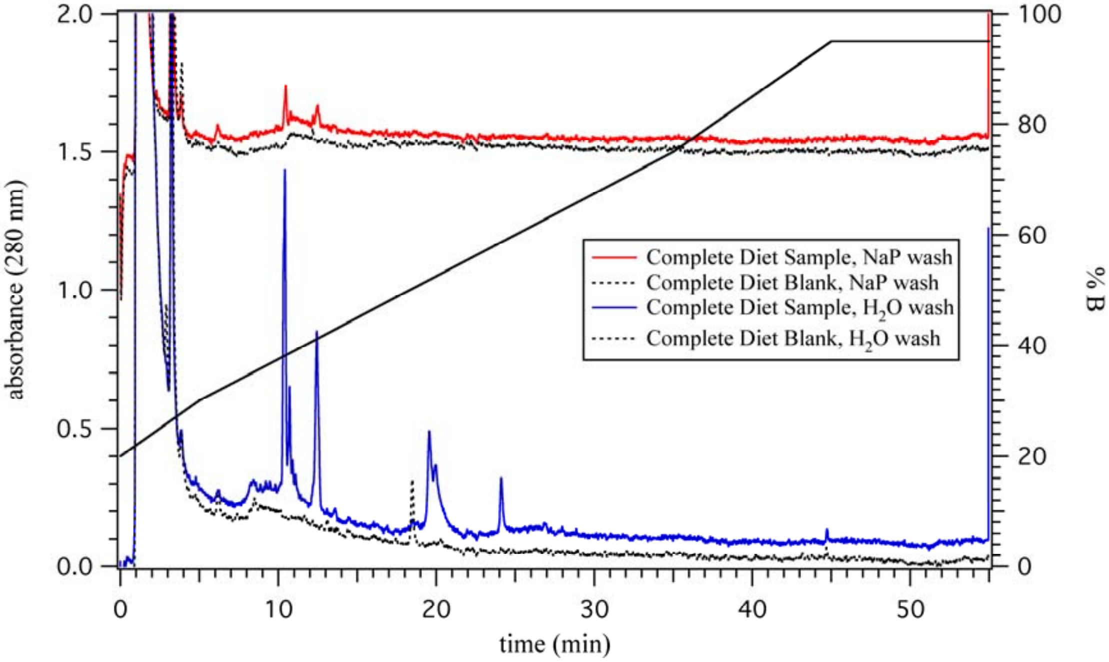

Figure 5.10 HPLC results at 280 nm for the separation of two ~8000 aphid samples and their respective blanks (blank traces) that were washed with 100 mM sodium phosphate, pH 7 + 10% ACN (red trace) and water + 10% ACN (blue trace). The HPLC gradient as a function of %B mobile phase composition is shown (right axis).

Over the course of the experiments, several environmental factors were examined in conjunction with the preconcentration conditions to improve the overall sample concentration. Initially, all experiments were carried out using fully enclosed Petri dishes, without ventilation, and covered with yellow paper squares over the diet to attract the aphids to the feeding media. The Parafilm layers were not initially rinsed during collection to reduce the possibility of introducing contaminations (prior to collection under sterile conditions). Additionally, a shelving rack was also used to house the aphid chambers, reducing the amount of space necessary for the experiments. Use of this rack caused some chambers to be in dissimilar lighting conditions from shadows due to the rack and other aphid chambers stacked above. To reduce these effects, squares of yellow theater lighting gel were used instead of the opaque, yellow paper. When this was carried out, it was evident that a larger number of aphids were feeding and producing nymphs in aphid chamber stored on the top shelf (receiving more light). Following this experiment, the aphid chambers were all set on the flow bench in even lighting from this point on. Finally, a second-generation aphid chamber was constructed using wire screens (described above) to allow air circulation within the chambers, more similar to a 'normal' feeding environment. It can be seen in **Figure 5.11** that each procedural modification (environmental and preparative) described produced a noticeable increase in the HPLC peak amplitudes of the samples from aphids fed Compete Diet over a 24-hour period. After each trial where an increase in signal was noticed, that particular step was continued throughout the remainder of the experiments.

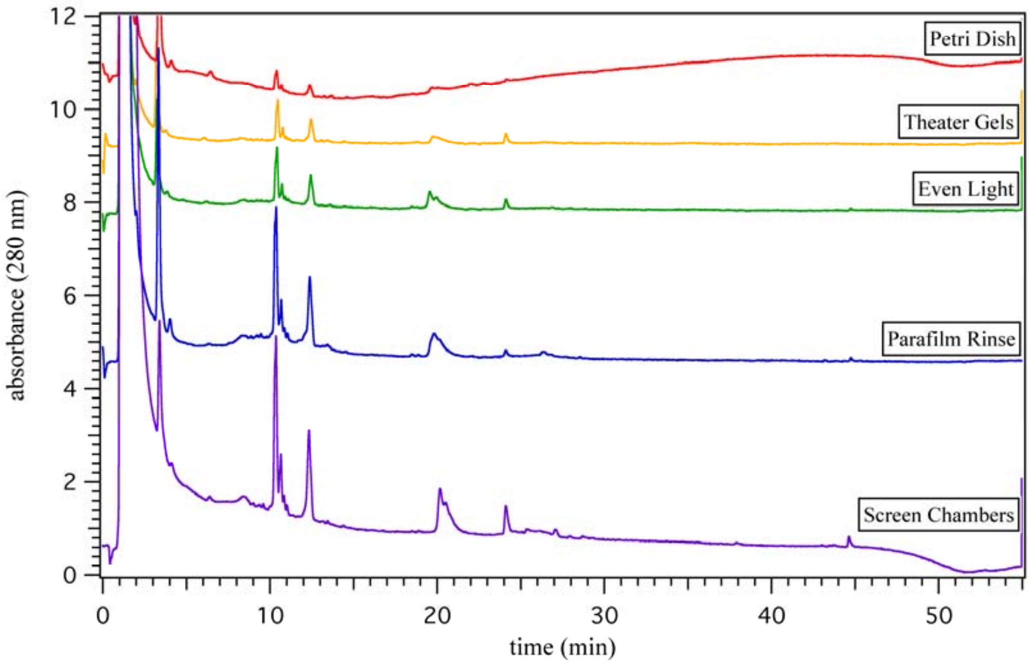

Figure 5.11 HPLC results (280 nm) showing the signal enhancement following various changes in the experimental conditions. Each change is depicted at the top right of the sample chromatogram while all other conditions remained constant. It can be seen that the signal increases by nearly 20x.

To further increase the sample concentration, 48-hour feeding times were explored. Using feeding times of 48 hours yielded an increase in the peak amplitudes by approximately two-fold for all three artificial diets. **Figure 5.12** shows the increase in peak amplitudes for a 48-hour Diet 3 sample over a 24-hour Diet 3 sample (with all other feeding conditions kept constant). It was later noticed in the mass spectrometry analysis that the Complete Diet at 48 hours contains more bacteria than the 24-hour sample.

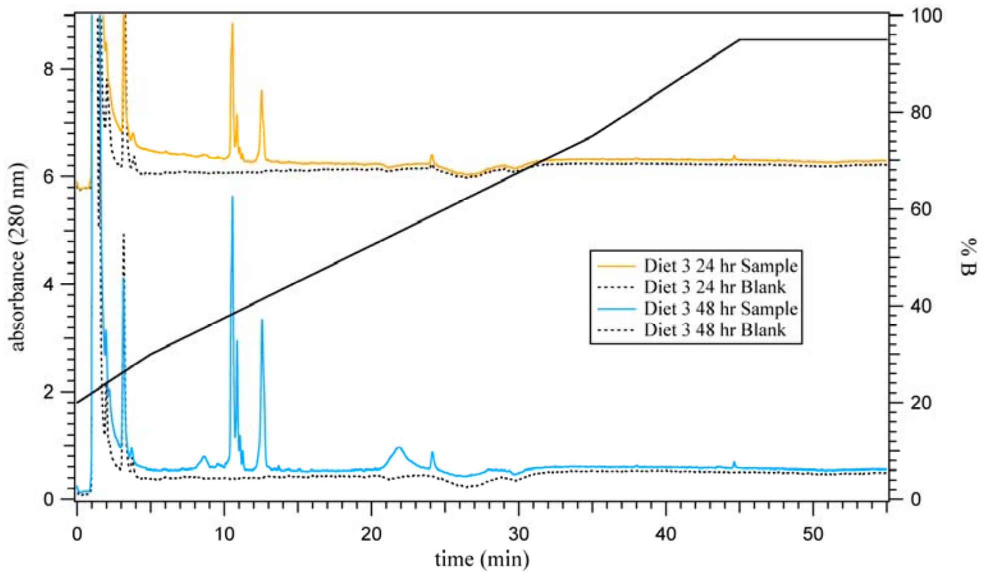

Figure 5.12 HPLC chromatograms at 280 nm of 24-hour and 48-hour Diet 3 samples (yellow and blue traces, respectively) collected at 280 nm. The data shows a > 2-fold signal increase in the 48-hour Diet 3 sample. The mobile phase gradient (black trace) is represented as a function of %B on the right axis.

It has been previously shown that pressure gradients transport materials (sugars, amino acids, proteins, signaling molecules, etc.) in the phloem sieves of plants.[67] Specifically calcium ions are thought to be important for the regulation and signaling functions of phloem sieve transport. When phloem sieves are damaged by environmental elements, pathogens, or pests, calcium channels within the plant become activated and an influx of Ca^{2+} rushes into the wounded area (sieve elements). Though the exact sequence is unknown, proteins are also transported to the wound, plugging the damaged area so that the plant can heal. This protein-plugging process is also thought to be calcium-dependent.[67-69] It has been shown that the free concentration of Ca^{2+} is between 50-70 nM and 100-200 nM in probing aphid stylets and undamaged phloem sieves, respectively.[70] Because of this phenomenon, it is thought that the aphids secret something in their saliva that (1) inhibits the influx of Ca^{2+} into the damages sieves or (2) that simply prevents the Ca^{2+}-protein binding in the wound response signaling.

For this reason, we investigated the addition of Ca^{2+} ions into the diet medias at a concentration of approximately 1 mM (dilution of a 10 mM calcium chloride stock solution). Again, all three diets were examined by collecting samples with and without Ca^{2+} ions, and the conclusions were consistent among each diet. In all cases, the HPLC peak amplitudes were substantially decreased with the addition of 1 mM Ca^{2+} ions to the feeding media. In some instances, precipitate formation was visible in the calcium samples, which could be responsible for this notable RP-HPLC signal decrease. **Figure 5.13** shows the resultant chromatograms for the Diet 3 (**top**) and 15% sucrose (**bottom**) diets with and without Ca^{2+} additions, illustrating the enhanced signal in the absence of calcium.

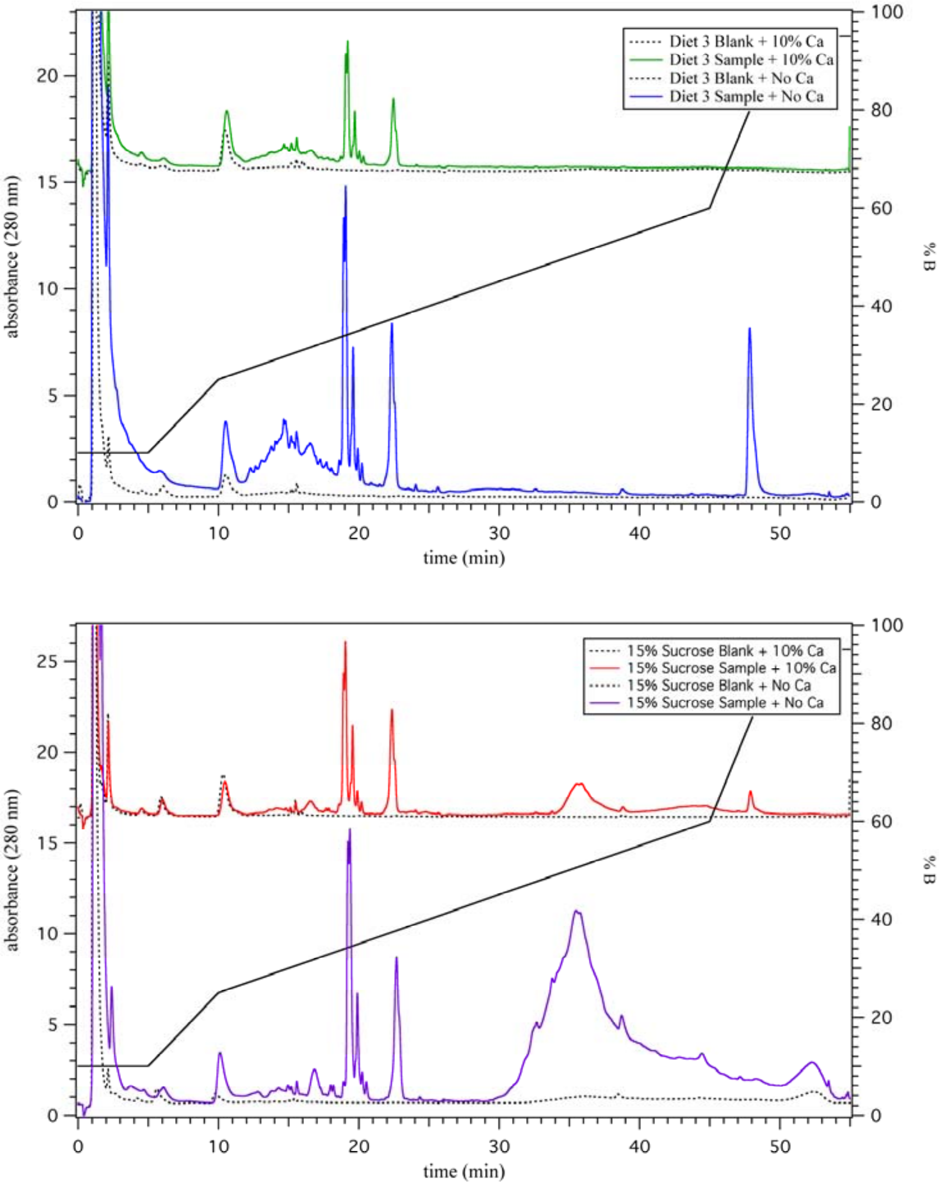

Figure 5.13 RP-HPLC chromatograms at 280 nm from samples of ~8000 aphids collected after feeding on Diet 3 (top) and 15% Sucrose (bottom), with and without the addition of 1 mM calcium ions. All samples were collected and treated in the same manner, leaving the addition of Ca^{2+} ions the only variable. Additionally, the respective sample blanks under the same conditions are shown (dashed black traces). It can be seen that the addition of calcium decreases the peak amplitude as well as the number of peaks seen in both diets. The HPLC gradient as a function of %B is shown (right axis).

A direct comparison of all three of the aphid diets is shown in **Figure 5.14** below. For all samples, the aphids were kept in the same, optimized conditions discussed above (same feeding volumes, 48-hour feed time, even lighting conditions, etc) and the sample treatment was identical (sterile conditions, water + 10% ACN washing, 3000 MWCO filter, etc.). It is evident by the increase in peak amplitudes and the number of peaks, that the aphid salivary secretions are significantly higher as the nutritional value of the diet decreases (15% Sucrose > Diet 3 > Complete Diet). It should be noted that the 15% Sucrose and Diet 3 samples contained Ca^{2+} when feeding, whereas the Complete Diet sample did not. This is to further emphasize the increase in signal enhancement in the less nutritional diets, even in the presence of Ca^{2+} ions. From these findings, we propose that the aphids increase salivation in the 'less nutritious' diet medias, which is probable because aphids continuously secrete 'watery' saliva throughout the feeding process. Perhaps aphid salivation increases when they are required to search for proper nutrients as well as existing as a necessity for the inhibition of the calcium-wound response activity in the phloem sieves.

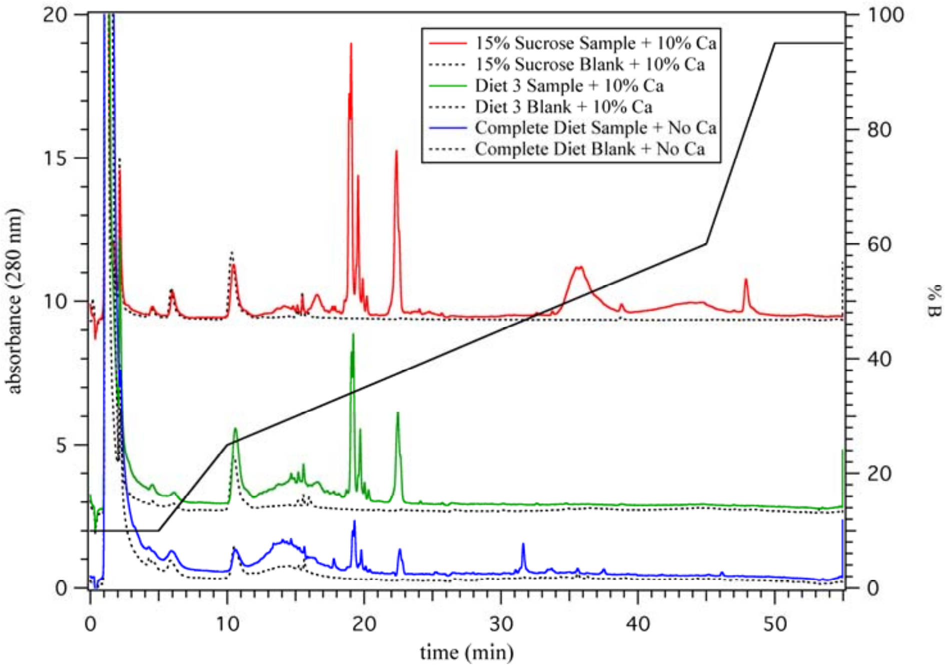

Figure 5.14 RP-HPLC chromatograms at 280 nm for all three diets collected after ~8000 aphids feeding for 48 hours. The 15% Sucrose Diet (red trace) and the Diet 3 (green trace) contain 10% of the 10mM calcium chloride solution, and the Complete Diet (blue trace) does not. The HPLC gradient is shown as a function of %B on the right axis). Even with the signal suppression of calcium, the 'less nutritional' diets provide enhanced signals over the Complete Diet without calcium.

It can be seen (**Figure 5.15**) that all three wavelengths (214 nm, 254 nm, and 280 nm) possess multiple corresponding peaks. These three wavelengths are common when monitoring protein separations, as the absorption maximum of carbonyl compounds is 280 nm, the amide group in water is 214 nm, and ringed structures (as in tryptophan) absorb at 254 nm. [71,72]

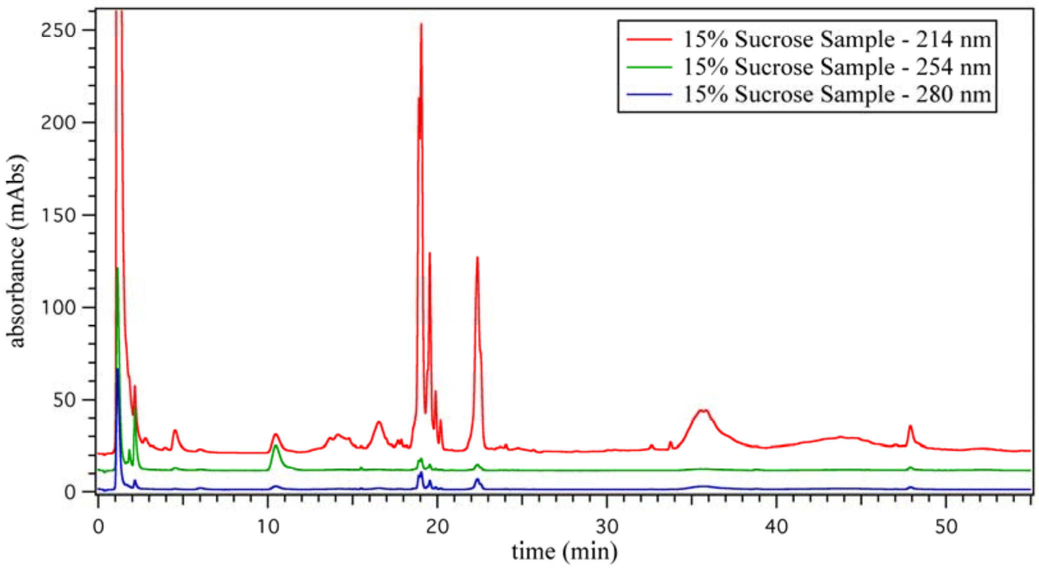

Figure 5.15 Multiple collected spectra of an ~8000 aphid 15% Sucrose sample with 10% calcium ions. Multiple corresponding peaks are seen among the wavelengths 214 nm (red trace), 254 nm (green trace), and 280 nm (blue trace) collected at one time using variable wavelength detector.

5.3.5 Mass Spectrometry Analysis

Glucose oxidase, glucose dehydrogenase, NADH dehydrogenase, α-glucosidase and α-amylase were recently discovered in the salivary secretions of the green peach aphid (*Myzus* persicae). These results were achieved by separating the proteins on a 2D SDS-PAGE followed by digestion and analysis using liquid chromatography coupled with MALDI-TOF mass spectrometry.[73]

Throughout our experiments, three types of mass spectrometry were used following the collection of multiple RP-HPLC fractions from the aphid samples. Initially, the mass spectrometry analysis herein was completed using MALDI-TOF and, when enough sample volume remained LC-MS was also carried out. These initial experiments provided significant insight into the sample components, aphid- and contamination-related, and served as a springboard in the development of improved sample collection and treatment parameters previously discussed. The digested proteins were submitted to four database searches: (1) Dr. Reeck's expressed sequence tag (EST) annotated pea aphid EST database and the NCBI database with parameters set for (2) Metazoa, (3) Other Metazoa, and (4) Bacteria. Early experiments (though the scores and sequence coverage percents were low from a mass spectrometer's standpoint) led to the discovery of many proteins (> 100) related to EST aphid sequences in Dr. Reeck's annotated pea aphid EST database. The contigs acquired from the EST database are also meaningful because some have known functions in other insects (*Apis mellifera* and *Ades aegypti*), which were also recognized in the green peach aphid experiments. Additionally, we have found exopeptidase, angiotensin converting enzyme (in two separate sets of fractions and MS analysis trials), as well as a few proteins from *Buchnera* (a bacterial symbiont in the aphid abdomen) when searching against the NCBI and EST databases. The final mass spectrometry experiments were performed using MALDI-TOF-TOF, and provided a significant increase in the obtained scores and the sequence coverage percents of the resultant protein hits (scores up to 107, and sequence coverage percents up to 39%). Additionally, significant protein hits finally resulted when searching the NCBI (Other Metazoa) database for the first time in these experiments.

Figure 5.16 shows the RP-HPLC chromatogram achieved from pooling three (~8000 aphid) samples that were kept under constant collection and treatment conditions. The samples were collected after a 24-hour 15% Sucrose Diet (no Ca^{2+}) feeding in the screened chambers and washed with a solution of water and 10% ACN. The samples and respective sample blanks were then pooled, lyophilized, reconstituted in 66 μL of the above washing solution, and injected onto the HPLC column. The designated time-interval fraction collection markings are shown, and the respective fractions are numbered 1-10.

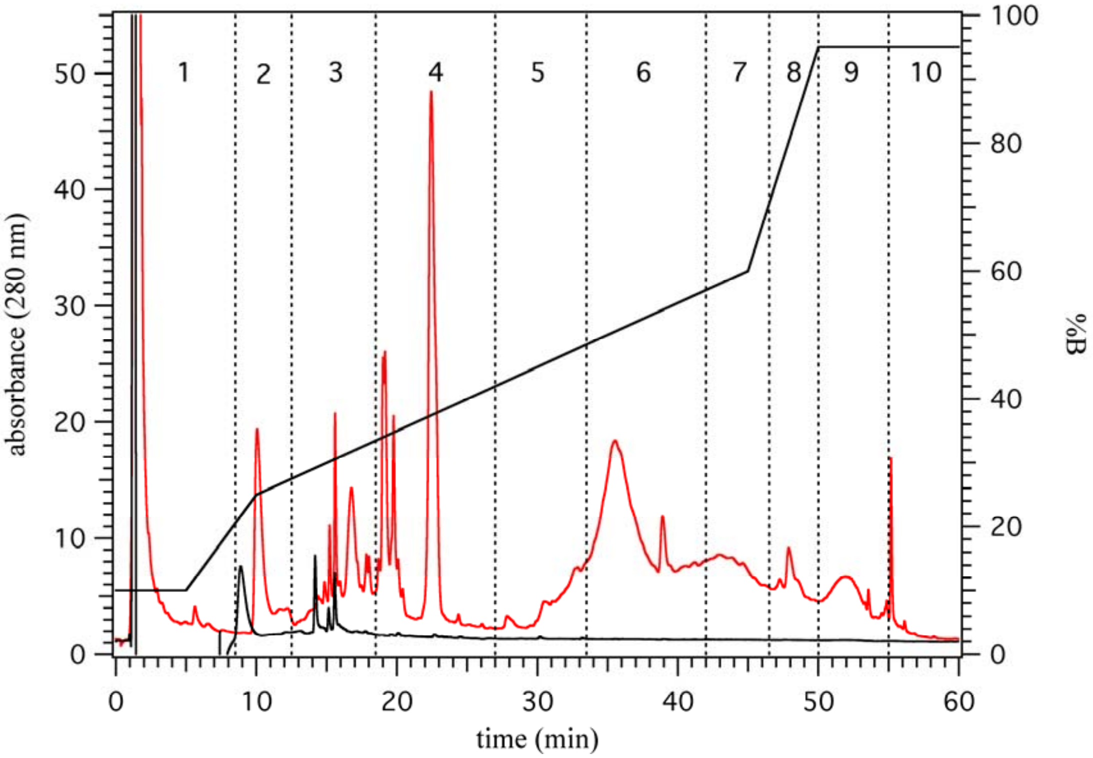

Figure 5.16 RP-HPLC chromatograms collected at 280 nm of three ~8000 aphid samples (red trace) pooled together and the pooled sample blanks (black trace). The vertical lines and numbers designate the time intervals over which the ten fractions were collected, and the mobile phase gradient is shown as a function of %B on the right axis.

Following the RP-HPLC separation, the fractions were lyophilized and given to the MS lab (KSU) where they were enzymaticlly digested into peptides using a protease (trypsin) and analyzed. **Figures 5.17** shows the MS spectrum (top) acquired from the tryptic digest of proteins in fraction 5 and the MS/MS spectrum (bottom). The MS/MS spectrum was collected from the peptide ‘VDYSAVER’.

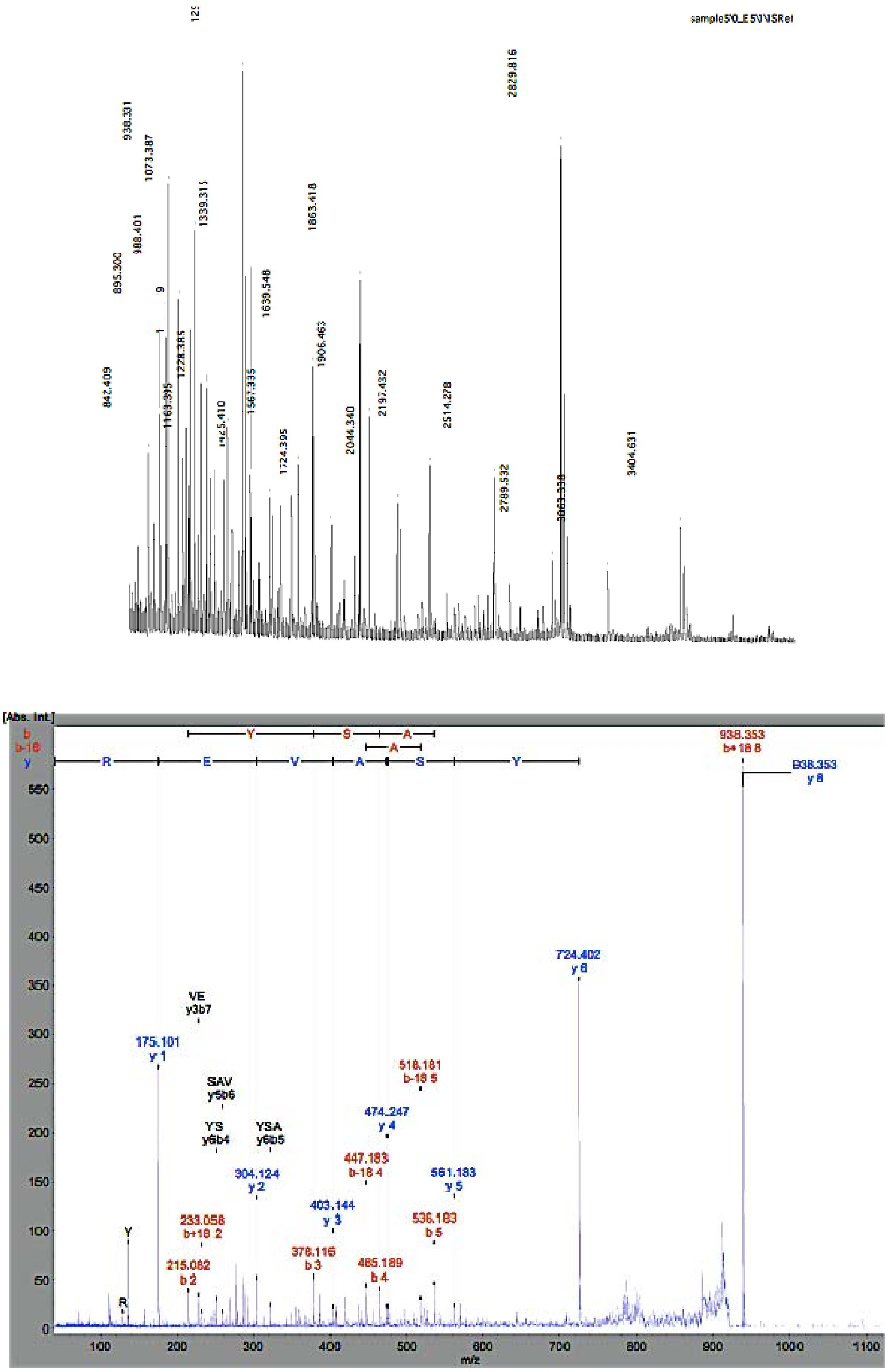

Figure 5.17 MS spectrum (top) of a tryptic digest of aphid proteins in fraction 5, and the MS/MS spectrum (bottom) collected from the peptide 'VDYSAVER'.

From the MS/MS data we were able to achieve amino acid sequence information from the peptide. The primary protein hit in this fraction using the Other Metazoa NCBI database was a match gi/19358006 (*Acyrthosiphon pisum*), which is similar to a known protein (CG1204-PA) of the *Apis mellifera*. The Mascot score for this match was 102, nominal mass 129,851 Da, and a calculated pI value of 4.62. The sequence string is shown below in **Figure 5.18**, where the matched peptides are shown red. Though the sequence coverage percent is only 4%, the matched peptides are scattered throughout the sequence, showing significant probability that the protein match is correct.

1 MRSVLILCVI IAAAVACPVS KTKDCSCGLP KICPSTWKIK TFDSQCETLA
51 FQGTWFLQMA TPTYIDQQNP LKTGLFCNSY PCTNNQLIFK DTTPCDDTDY
101 NTEYEVIDSS YNIYTQCTET QIALLCPAYG SSSKYAIFNV GSEKYYTNPI
151 AEK**YPFVDKD LFR**HKIGQGS CEREYTVAVI GADDCWKEYM VLVVINQYDN
201 FFGGDEYITW VLTRDVNPDW STYDKAYNDI KGSGLCPNYL VSVDHSFESM
251 TGPSMAVPSM APSVAVPSMA PTMPGDVDSM VQKTSVSTTS ATKSISTDCG
301 STVTSSSTST TTTSTVIIDK SSDFSSIYDI GPCDLYSPYE GLQIYK**NLDK**
351 **ETIR**RAFSGN YYMTQATPCS FYDTPKSKVG LLNTCFPACG MQLCFDDASI
401 DDWDCNTPRM VMDRGYNMRT GEVHMTRSYI SSAYSDDHPF GTVTYAFHSE
451 GYYDVPIDET DCLPLDGLIC KPPSDIYKNQ IIANIIGYKD NDYLMFCIAN
501 RYKNPLFPKK QVPLVYCYTR ER**IPSQDTMN SITQEMLR**CG LNPNYLMKID
551 QSKTIEEVFT FDKTYYESTV TSTSTTKSVV STRGLSIGSS PLQGLPSICP
601 PDWNVKTFDN QYATIAFQGI WNVQMTTPTY INGNNPLKTG LFCNSYPCTN
651 NQLIFKDTTP CDDTDYNTEY EMTDSSYNLY TQCTETQKAL LCPAYGSCSQ
701 YAIFNVGSEK YYNTAIIEK**Y PFIDKDLFR**H KIVQGTCERE YTVAVIGADD
751 CWEEYMVLAV INQYDNVFGG NK**YIIWVVTR** DANPKWSTYK KAYEDIERSG
801 LCPNYLVSVD HSLESMTGPS MAPSVAVPSI APTMPGDVDS MVQKTSVSTT
851 SATKSISTDC GSTVTSSSTS TTTTSTVIID KSSDFSSLYE LGQCDLYKDI
901 QIYKNLDKET IRRALSGKYY MTQATPCSYY NSPNSRVGIL NTCFPACGMQ
951 LCFDDTSIDD WDCNTPRMVM DRGYDMRTGE VQLTRSYISS VYSDDHPFGT
1001 VTYAFHSEGY YEGPIDEMDC LPLDGMICKP PSDIYKNQII ASIIGYKDND
1051 YLIFCIANKY KNPLFSSTPV NQVIAYTRER VPSKETIKSM TQELLQCGYN
1101 PNYLIKIDQT MYMDDDYVFE SSYYESQTSC WSSSSSSCSS STSSSTTISS
1151 SSSSSVSISC D

Figure 5.18 Sequence string for the Mascot result for the first protein hit of fraction 5. The matched peptides are shown in red.

In this same fraction, a second significant protein hit was found using the NCBI Other Metazoa database (MS/MS data above). In this hit, the match was to gi/19358006 (*Acyrthosiphon pisum*). The Mascot score for this match was 59, nominal mass 17,570 Da, and a calculated pI value of 4.68. The sequence string is shown below in **Figure 5.19**, where the matched peptides are shown red (11% sequence coverage). This protein was submitted to a BLAST search to find known proteins of similar function, but no putative domains were detected. This illustrates the difficulty of this analysis, as little is known about these proteins and the pea aphid genome sequence is not fully accessible yet.

```
  1 MAFKEIAMFS SLVVVTIISY NVLEGNAQSI KPLIDQDYCK VKASLYDLGE
 51 IGMNLMDDSQ TLNDMQREYF AGKVDYSAVE RARNELNQTK NKLFLKLIKY
101 IWATNEFEPT VNYQTADPQK LYKAMDDLEN YKDEMHADLL NSMSPTLQPT
151 VVGA
```

Figure 5.19 Sequence string for the second significant protein hit in fraction 5. The matched peptides are shown in red (11% sequence coverage).

5.4 Conclusions

These experiments demonstrate the ability to overcome small sampling challenges associated with the salivary secretions of the pea aphid (*Acyrthosiphon pisum*). An increase in salivation was observed as the diets decreased in nutritional value. Additionally, several factors were examined such as lighting, ventilation, calcium additions, and washing solutions were examined and optimized for experiments using aphids housed in artificial environments. Optimizing these conditions allowed for the identification of multiple contigs (> 100) from the EST database. Exopeptidase, angiotension converting enzyme, and a few proteins from *Buchnera* (a bacterial symbiont in the aphid abdomen) were also discovered in pea aphid saliva using RP-HPLC techniques coupled with mass spectrometry.

CHAPTER 6 - Contact Conductivity Detection of Jurkat Cells in a Microfluidic Device Using Flow Cytometry

6.1 Introduction

Flow cytometry has become a standard analytical method for cellular detection and analysis. In flow cytometry, cell suspensions are commonly focused into a small stream where the cells travel through the detection window one at a time. Microfluidic devices allow for laminar fluid flows, without mixing, that easily create confined particle or cell streams. This confined stream is commonly formed using a simple cross-pattern channel intersection with the sample suspension introduced at the top, and the sheath streams introduced from the sides. The solutions and cell suspensions can be moved using electrokinetic or pressure-driven flows.[74,75] Currently, the most common detection methods used in flow cytometry are light scattering, fluorescence, or absorption.[76-79] To optimize these detection schemes, the particles or cells must be narrowly-focused in the light path or they can miss the illumination window and not be detected. Additionally optical detection components commonly used for these setups (PMTs, APDs, lasers, mirrors, filters, etc) are generally costly and difficult to properly align. To overcome these limitations and simplify cell and particle detection in flow cytometry, electrical detection methods have been emerging.[80,81] The detectors used for electrochemical methods, specifically conductivity detection, are generally simple and composed of inexpensive electronic circuitry. Though conductivity detection is not always as sensitive as its optical counterparts, it provides adequate sensitivity for the detection of cells. In these experiments, a novel conductivity detector was constructed and used for the detection of Jurkat cells that were focused using pressure-driven flow in the channels of a PDMS-glass hybrid microfluidic device. The microfluidic platform contained a pair of gold sensing electrodes plated onto the surface of a glass slide that were used for cellular detection. Use of this detection system for cells will drastically simplify cell experiments (flow cytometry, cell trapping, etc.) that currently use complex, expensive LIF or light scattering detection components.

6.1.1 Conductivity Detection

Conductivity detection requires a minimum of two sensing electrodes, of equal geometric surface area, to make up the detection cell. The detection cell can be in the channel (or capillary) or in an end-column arrangement with the electrodes positioned in the reservoir at the end of the channel. An ac-voltage is applied to the cell to minimize Faradaic reactions that may occur at the electrode surface. In contact conductivity, the electrodes are in direct galvanic contact with the buffer solution. Here, the signal occurs in the bulk solution whereas in amperometry and potentiometry, the signal occurs on the electrode surface. This has limited the spread of contact conductivity into the realm of microchips, as glass substrates are preferable to polymers, and it becomes exceeding difficult to bond the microchip. Additionally, when using fused silica capillary, the cell construction becomes increasing complicated and time consuming. Unfortunately, even the use of an ac-voltage cannot completely prevent electrode fouling as substances can still adsorb to the surface.

6.1.2 Electronics

The most common type of periodic electrical signal when using alternating current is a sinusoidal wave, which is a result of plotting the instantaneous voltage (or current) as a function of time. A function generator is used to supply a sinusoidal input signal of a specific peak-to-peak voltage to one electrode of the detection cell. Because an ac-signal is applied, and the electrodes are in close proximity to one another, the detection cell mimics a capacitor. In an ac circuit, a capacitor resists changes in voltage. This behavior is termed capacitive reactance (X_c), and is determined by the ac frequency (*f*) and the capacitance (C), shown in Equation 6.1.[3]

$$X_C = \frac{1}{2\pi f C} \tag{6.1}$$

The resistance of the solution (R) is inversely proportional to the conductance (Equation 6) as seen in Equation 6.2.

$$L = \frac{1}{R} \tag{6.2}$$

Because the electrodes and solution act as a capactior and resistor, respectively, the impedance describes the cell behavior.[82] Impedance (Z) is made up of the resistance of the resistor (R) and the reactance of the capacitor (X_C) as shown by:

$$Z = \sqrt{R^2 + X_C^2} \tag{6.3}$$

In the presence of small spherical particles, the system models the case of a classical Coulter counter.[81] Here, the resistance change for a spherical particle in a homogeneous electric field is illustrated by:

$$\Delta R = 2\rho_{sol}\left(\frac{\arctan\dfrac{(r_p)}{\sqrt{\dfrac{A_c}{\pi}-r_p^2}}}{\pi\sqrt{\dfrac{A_c}{\pi}-r_p^2}}-\frac{r_p}{A_c}\right) \tag{6.4}$$

where ρ_{sol} is the resistivity of the phosphate buffered saline solution, A_c is the cross-sectional area of the microchannel, and r_p is the spherical particle radius. Using this equation, it can be seen that the sensitivity of the detection system can be tuned for the cell size by changing the area of the electrodes and/or the channel width.

6.2 Materials and Methods

6.2.1 Jurkat Cells and Reagents

Sodium phosphate was obtained from Fisher Scientific. All buffer solutions were made using distilled deionized water from a Barnstead Ultrapure Water System (Dubuque, IA) and filtered using 0.45μm Millex®-LCR syringe driven filter units (Millipore Corporation; Bedford, MA). Jurkat Clone E6-1 (lymphoblast) was purchased from the American Type Culture Collection (Manassas, VA). These cells were grown at 37 °C in a humidified 5.0% CO_2 incubator in RPMI-1640 media supplemented with fetal bovine serum (10%). Penicillin (100 units/ml) and Streptomycin (100 μg/ml) were added to the media to inhibit bacterial growth. A 1 mL aliquot of the cell suspension was removed from the incubator and stored at 37 °C in a dry bath until use. For use in the microchip, 0.5 mL of the cell suspension was removed and placed into an eppendorf tube. The suspension was centrifuged for 1 min at 2000 rpm, leaving a cell pellet in the bottom of the tube. The cell media solution was removed, and 1 mL of phosphate buffered saline (PBS) was added to the cells. This suspension was used for the following experiment.

6.2.2 Conductivity Detector and System Setup

The conductivity detector was designed with the help of and constructed by the Electronics Design Laboratory (EDL; Kansas State University; Manhattan, KS). An 11 MHz function generator (CFG280; Tektronix; Richardson, TX) was used to supply the sinusoidal signal with a voltage of 500 mV_{pp} and a frequency of 300 kHz. A 2-channel digital real-time oscilloscope (TDS220; Textronix; Richardson, TX) was used to monitor and measure the applied signals. The signal collection was performed using an in-house written program created using LabVIEW software (National Instruments).

6.2.3 Electrode Fabrication

The electrodes were fabricated on #2 microscope cover glass slides (Fisher Scientific; Pittsburgh, PA) because they are more robust, and metal can easily be deposited onto the surface. Using electron beam ablation (SMART LAB; KSU), 15 nm of titanium metal was deposited to serve as an adhesion layer, followed by a deposition of 150 nm of gold to become the electrode surface. Following deposition, the electrodes were fabricated using standard photolithography and wet chemical techniques similar to those previously used.[83] A thin layer of S1811 positive photoresist (MicroChem; Newton, MA) was applied to the gold surface using a spin coater. The photoresist was then baked for 1 min at 65 °C and 1 min at 115 °C, followed by 1 min cooling. Next, a photoplotted photomask (The Photoplot Store; Colorado Springs, CO) with the desired electrode pattern was laid on the photoresist surface and exposed to UV light for 4 seconds at an energy density of 45mJ/cm^2 using a flood exposure system (ThermoOriel; Stratford, CT). Following UV exposure, the slide was placed in the photoresist developing solution (dilute potassium hydroxide) for ~45 s. Here the softened photoresist was removed, leaving a protective photoresist layer over the gold in the pattern of the electrodes. Next, aqua regia (3:1, HCl:HNO$_3$) is used to remove the excess gold from the glass surface. It was found that electrode patterns are more reproducible from slide to slide if the aqua regia solution was diluted with water by 25%. The titanium was then removed using a dilute solution of buffered oxide etch (NH$_4$F/HF) and nitric acid, 2% and 0.5%, respectively. Finally, the substrate was rinsed with water then acetone to remove the protective layer of photoresist, leaving the gold electrodes on the glass surface ready for use. The electrode dimensions (width, gap, and overlap) used in this experiment were ~25 μm, ~36 μm, and ~137 μm, respectively as shown in **Figure 6.1**.

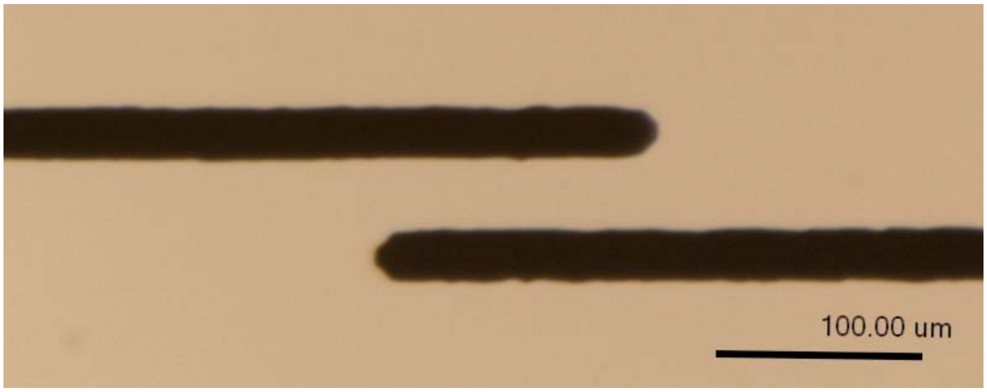

Figure 6.1 Optical image of fabricated gold electrodes used for these conductivity experiments. The annotations show the measured electrode dimensions.

6.2.4 PDMS Channel Fabrication

Microchannels were fabricated in polydimethylsiloxane (PDMS) using standard photolithography and molding procedures used previously for SU-8 and PDMS.[83] Negative molds were fabricated in SU-8 2010 (Microchem Corp,; Newton, MA) and used for casting the microchannels. The SU-8 mold was created on 4” polished silicon wafers (Silicon Inc; Boise, ID) by spin-coating it onto the surface to a thickness of ~16 μm. The SU-8 wafer was pre-baked for 4 min at 95°C. The channel-pattern photomasks were then positioned on top of the wafer and held in place with a quartz plate. Following a 5.5 s exposure at an energy density of 45mJ/cm^2 with the flood exposure system, the exposed slide was post-baked for 4 min at 115°C then cooled. The SU-8 wafer was developed by placing it in 1-methoxy-2-propanol acetate (Sigma) and gently agitated for ~45 s, until the unexposed SU-8 is removed. Finally, the developed molds were thoroughly rinsed with isopropyl alcohol and dried with nitrogen gas.

The PDMS channels were fabricated using Sylgard 184 elastomer (Dow Corning Corp.; Midland, MI). The elastomer base and curing agent were mixed 10:1 (w/w), degassed for ~30 min, and poured onto the SU-8 mold where it was cured in an 80°C oven for at least 1 hour. The PDMS can then be removed from the mold, and access holes at the channel ends can be made. The channel manifold was then positioned over the electrodes by wetting the surfaces with methanol and using a microscope to manually align the pieces. The methanol was evaporated from the channels in an oven or vacuum desicator. An optical image of the detection cell (PDMS channel over gold electrodes) used in these cell experiments can be seen in **Figure 6.2**.

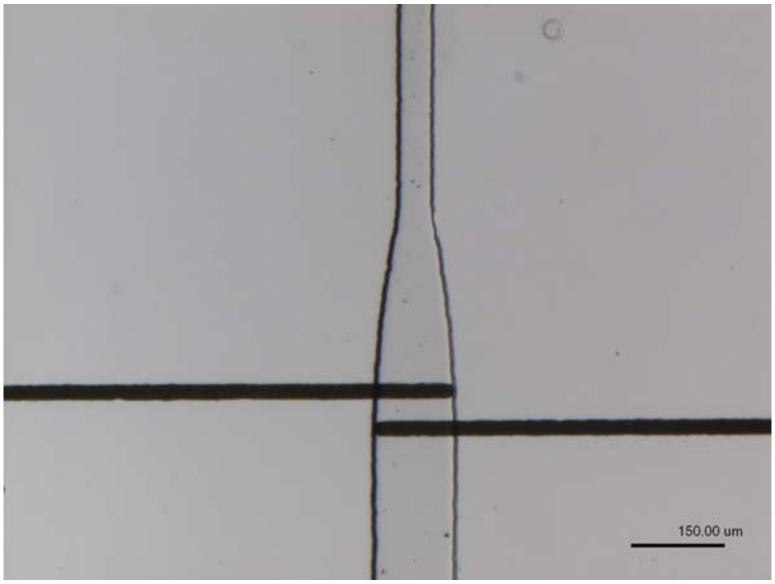

Figure 6.2 Optical microscope image of the contact conductivity detection cell taken at 7x (left) magnification. The micrometer scaling is shown in the bottom right corner.

6.3 Results and Discussion

Various electrode parameters such as orientation, length, width, gap, and thicknesses have been previously examined. It has been shown that an antiparallel arrangement is optimal as the direct capacitive coupling between the electrodes is minimized, decreasing the background signal and giving higher sensitivity. The stray capacitance is also reduced when using electrodes with a minimal overlap, however the longer parallel overlap length does not drastically hinder the S/N ratio. It has also been determined that a smaller electrode gap results in a higher analytical signal; when larger gaps are used, the resulting peaks are wider and shorter.[84]

The conductivity detector settings were optimized using pressure-driven flow of sodium phosphate solutions possessing different concentrations, and thus different conductivities. First, the microchip reservoirs were filled with water and a vacuum was applied to the exit of the separation channel. Once the chip was filled, a syringe was used to remove the water and a 25 mM solution of sodium phosphate (pH 7) was introduced. This process was repeated while varying the frequency of the detector until the largest signal change was obtained. The detector signal was optimized for these electrodes at 500 mV with an oscillation frequency of 300 kHz.

Following these tests, the Jurkat Clone E6-1 cell suspension in PBS was introduced into the sample reservoir while the vacuum continuously pulled at the exit of the focusing channel. A schematic of this hydrodynamic focusing method can be seen in **Figure 6.3**.

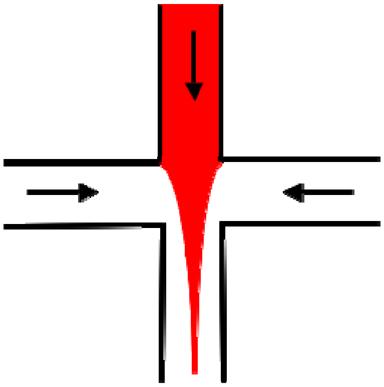

Figure 6.3 Schematic of the hydrodynamic focusing using a standard cross-channel pattern. The red and white flows illustrate the cell suspension and the other sheath flows, respectively. Arrows depict the direction of fluid flow when the vacuum is applied to the bottom channel.

It can be seen in **Figure 6.3** that the focused cells can be detected using this system. To verify that the signal changes were due to the cells, at approximately 194 s the cell suspension was removed from the sample reservoir and replaced with the PBS solution. At this point, the signal levels off and no changes are visible, indicating that the changes seen are in fact cells passing through the detection window. Additionally, when the cell region is expanded (**Figure 6.4**), the width of the signal change varies slightly. Because the electrodes span the entire width of the microchannel, these differences are most likely due to the variation in the diameter of the Jurkat cells. This can be reasoned because the cells are ~9-13 μm in diameter, and the channel depth is ~16 μm, meaning the cells cannot escape the detection window.

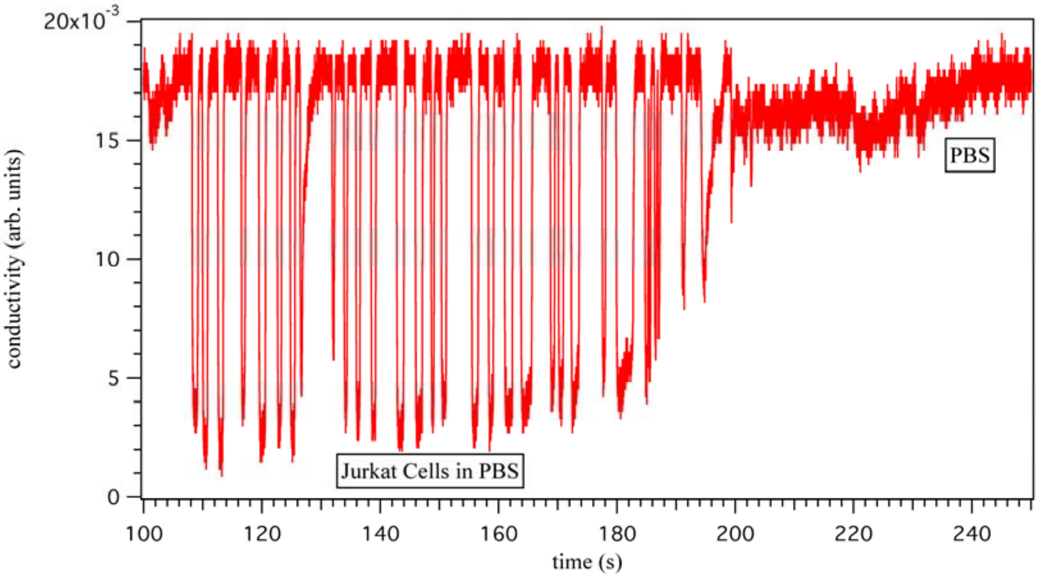

Figure 6.4 Conductivity detection response with Jurkat Clone E6-1 cells suspended in PBS. The operating parameters are 500 mV$_{pp}$ and 300 kHz. At ~194 s, the cell suspension was removed and the signal changes disappear, indicative that the changes are due to the passing cells.

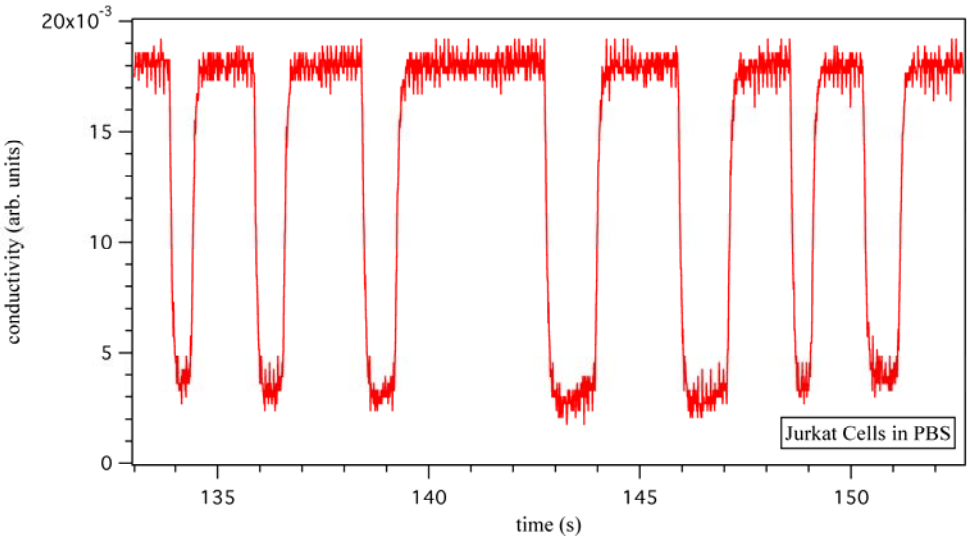

Figure 6.5 Expanded view of the Jurkat Clone E6-1 cell region. Because the channel dimensions are not significantly larger than the average cell diameter, the changes in response width can be attributed to individual cells passing through the detection window.

6.4 Conclusion

Flow cytometry is a valuable tool for the measurement and analysis of particles and cells. The use of a novel conductivity detector in contact mode has been shown to be sufficient for the detection of Jurkat Clone E6-1 cells in a solution of PBS. This system proves advantageous over its optical counterparts due to its simplicity, inexpensive components, and ease of alignment. Contact conductivity detection systems similar to this could be extremely beneficial and helpful for other microfluidic systems such as cell trapping or cell detection for cell lysis experiments. Use of contact conductivity detection yields an exceedingly simplified experimental setup, eliminating the need for additional optical components. Additionally, if the flow rate is known, the diameter of the cells (or particles) can be calculated, allowing additional cellular information to be acquired during other experiments.

CHAPTER 7 - Outlook and Future Directions

Fractions have been collected and sent for additional mass spectrometry analysis by experts in the MS field (Dr. Peter Campbell; CSIRO Entomology; Black Mountain, Australia). This will hopefully provide more accurate and reproducible MS results for the proteins and peptides in the aphid salivary secretion samples, increasing the protein score, percent sequence coverage, as well as increase the number of positive identifications. In the future, investigation into the solid salivary components of the aphid secretions may provide substantial insight into the aphid-host relationship. By removing the calcium with a chelating agent such as ethylenediaminetetraacetic acid (EDTA), it may be possible to make these proteins soluble so that they may be separated and identified using similar procedures described above.

The detection of Jurkat Clone E6-1 cells in Chapter 6, using a novel contact conductivity detection system, provides numerous directions for future research and investigation. Particularly, this novel system and parameters will greatly simplify cell trapping and lysis experiments. This detection system will enable the detection of cells and particles without the use of the current complex, optical systems. Future experiments will entail (1) testing this device in our research lab with a microchip designed for cell lysis or trapping and (2) ensuring that all cells are detected through flow optimizations. This should prove advantageous over current optical methods as it is (1) less costly, (2) more robust, (2) requires substantially less complex alignment, and (3) the detection cell spans the entire channel cross-section. Additionally, this system may be able to be further developed to construct a portable CE system for the analysis of wheat proteins.

CHAPTER 8 - References

(1) Cunico, R. L.; Gooding, K. M.; Wehr, T. *Basic HPLC and CE of Biomolecules*; 1st ed.; Bay Bioanalytical Laboratory, Inc: Richmond, 1998.

(2) Meyer, V. R. *Practical High-Performance Liquid Chromatography*; 4th ed.; John Wiley & Sons: New York, 2004.

(3) Skoog, D. A.; Holler, J. F.; Nieman, T. A. *Principles of Instrumental Analysis*; Fifth ed.; Harcourt Brace College Publishers: Philadelphia, 1998.

(4) Giddings, J. C. *Unified Separation Science*; John Wiley and Sons: New York, 1991.

(5) Linder, V.; Wu, H.; Jiang, X.; Whitesides, G. M. *Analytical Chemistry* **2003**, *75*, 2522-2527.

(6) Deng, T.; Wu, H.; Brittain, S. T.; Whitesides, G. M. *Analytical Chemistry* **2000**, *72*, 3176-3180.

(7) Hu, Y.; Werner, C.; Li, D. *Analytical Chemistry* **2003**, *75*, 5747-5758.

(8) Culbertson, C. T.; Jacobson, S. C.; Michael Ramsey, J. *Talanta* **2002**, *56*, 365-373.

(9) Atkins, P. W. *Physical Chemistry*; 3rd ed.; W.H. Freeman and Company: New York, 1986.

(10) Jacobson, S. C.; Hergenroder, R.; Koutny, L. B.; Warmack, R. J.; Ramsey, J. M. *Analytical Chemistry* **1994**, *66*, 1107-13.

(11) Seiler, K.; Fan, Z. H.; Fluri, K.; Harrison, D. J. *Analytical Chemistry* **1994**, *66*, 3485-91.

(12) Jacobson, S. C.; Ramsey, J. M. *Analytical Chemistry* **1996**, *68*, 720-3.

(13) Roman, G. T.; Hlaus, T.; Bass, K. J.; Seelhammer, T. G.; Culbertson, C. T. *Analytical Chemistry* **2005**, *77*, 1414-1422.

(14) Heiger, D. N. *High Performance Capillary Electrophoresis - An Introduction*; 2nd ed.; Hewlett-Packard Company: France, 1992.

(15) Price, A. K.; Fischer, D. J.; Martin, R. S.; Spence, D. M. *Analytical Chemistry* **2004**, *76*, 4849-4855.

(16) Kovarik, M. L.; Li, M. W.; Martin, R. S. *Electrophoresis* **2005**, *26*, 202-210.

(17) Kartalov, E. P.; Quake, S. R. *Nucleic Acids Research* **2004**, *32*, 2873-2879.

(18) Huynh, B. H.; Fogarty, B. A.; Martin, R. S.; Lunte, S. M. *Analytical Chemistry* **2004**, *76*, 6440-6447.

(19) Hansen, C. L.; Sommer, M. O. A.; Quake, S. R. *Proceedings of the National Academy of Sciences of the United States of America* **2004**, *101*, 14431-14436.

(20) Osborne, T. B. *The Proteins of the Wheat Kernel*; Carnegie Institution of Washington: Washington, D. C., 1907.

(21) Shewry, P. R.; Hamer, R. J.; Lookhart, G. L.; Bean, S. R. *Wheat Gluten Protein Analysis*; American Association of Cereal chemists: St. Paul, 2003.

(22) Lookhart, G. L.; Finney, K. F. *Cereal Chemistry* **1984**, *61*, 496-499.

(23) Kruger, J. E.; Marchylo, B. A.; Hatcher, D. *Cereal Chemistry* **1988**, *65*, 208-214.

(24) Jones, B. L.; Lookhart, G. L.; Hall, S. B.; Finney, K. F. *Cereal Chemistry* **1982**, *59*, 181-188.

(25) Dong, H.; Cox, T. S.; Sears, R. G.; Lookhart, G. L. *Crop Science* **1991**, *31*, 974-979.

(26) Lookhart, G. L.; Bean, S. R. *Cereal Chemistry* **1996**, *73*, 81-87.

(27) Lookhart, G. L.; Bean, S. R. *Cereal Chemistry* **1995**, *72*, 527-532.

(28) Jorgenson, J. W. *High performance Capillary Electrophoresis - An Introduction*; Hewlett-Packard: Waldbronn, 1992.

(29) Bean, S. R.; Lyne, R. K.; Tilley, K. A.; Chung, O. K.; Lookhart, G. L. *Cereal Chemistry* **1998**, *75*, 374-379.

(30) Bean, S. R.; Lookhart, G. L. *Cereal Chemistry* **2001**, *78*, 530-537.

(31) Bietz, J. A.; Lookhart, G. L. *Food Science & Technology (London)* **1997**, *30*, 210-213.

(32) Bean, S. R.; Lookhart, G. L. *Journal of Agricultural and Food Chemistry* **2000**, *48*, 344-353.

(33) Khaledi, M. G. *High-Performance Capillary Electrophoresis Theory, Techniques, and Applications*; John Wiley & Sons, Inc.: New York, 1998; Vol. 146.

(34) Robinson, J. W.; Frame, E. M. S.; II, G. M. F. *Undergraduate Instrumental Analysis*; 6th ed.; CRC Press, 2005.

(35) Siriamornpun, S.; Wootton, M.; Cox, J. M.; Bekes, F.; Wrigley, C. W. *Aust. J. Agric. Res.* **2001**, *52*, 839-843.

(36) Attiya, S.; Jemere, A. B.; Tang, T.; Fitzpatrick, G.; Seiler, K.; Chiem, N.; Harrison, D. J. *Electrophoresis* **2001**, *22*, 318-327.

(37) Auroux, P. A.; Koc, Y.; de Mello, A.; Manz, A.; Day, P. J. R. *Lab on a Chip* **2004**, *4*, 534-546.

(38) Jiang, L.; Lu, Y.; Dai, Z.; Xie, M.; Lin, B. *Lab on a Chip* **2005**, *5*, 930-934.

(39) Skelley, A. M.; Scherer, J. R.; Aubrey, A. D.; Grover, W. H.; Ivester, R. H. C.; Ehrenfreund, P.; Grunthaner, F. J.; Bada, J. L.; Mathies, R. A. *Proceedings of the National Academy of Sciences of the United States of America* **2005**, *102*, 1041-1046.

(40) Oh, K. W.; Park, C.; Namkoong, K.; Kim, J.; Ock, K.-S.; Kim, S.; Kim, Y.-A.; Cho, Y.-K.; Ko, C. *Lab on a Chip* **2005**, *5*, 845-850.

(41) West, J.; Becker, M.; Tombrink, S.; Manz, A. *Analytical Chemistry* **2008**, *80*, 4403-4419.

(42) Tsuda, T.; Kitagawa, S.; Yamamoto, Y. *Electrophoresis* **2002**, *23*, 2035-2039.

(43) Culbertson, C. T.; Tugnawat, Y.; Meyer, A. R.; Roman, G. T.; Ramsey, J. M.; Gonda, S. R. *Analytical Chemistry* **2005**, *77*, 7933-7940.

(44) Jacobson, S. C.; Hergenroder, R.; Koutny, L. B.; Ramsey, J. M. *Analytical Chemistry* **1994**, *66*, 1114-18.

(45) Blackman, R. L.; Eastop, V. F. *Aphids on the World's Crops*; 2nd ed.; Wiley: Chichester, 2000.

(46) Gray, S.; Gildow, F. E. *Annual Review of Phytopathology* **2003**, *41*, 539-566.

(47) Martin, B.; Collar, J. L.; Tjallingii, W. F.; Fereres, A. *Journal of General Virology* **1997**, *78*, 2701-2705.

(48) Miles, P. W. *Nature* **1959**, *183*, 756.

(49) Tjallingii, W. F. *Journal of Experimental Botany* **2006**, *57*, 739-745.

(50) Miles, P. W. *Biological Reviews* **1999**, *74*, 41-85.

(51) Will, T.; Tjallingii, W. F.; Thoennessen, A.; van Bel, A. J. E. *Proceedings of the National Academy of Sciences of the United States of America* **2007**, *104*, 10536-10541.

(52) Madhusudhan, V. V.; Miles, P. W. *Entomologia Experimentalis et Applicata* **1998**, *86*, 25-39.

(53) Adams, J. B.; McAllan, J. W. *Canadian Journal of Zoology* **1958**, *36*, 305-8.

(54) Adams, J. B.; Drew, M. *Canadian Journal of Zoology* **1964**, *41*, 489-496.

(55) Miles, P. W.; Harrewijn, P. *Entomologia Experimentalis et Applicata* **1991**, *59*, 123-134.

(56) Urbanska, A.; Tjallingii, W. F.; Dixon, A. F. G.; Leszczynski, B. *Entomologia Experimentalis et Applicata* **1998**, *86*, 197-203.

(57) Cherqui, A.; Tjallingii, W. F. *Journal of Insect Physiology* **2000**, *46*, 1177-1186.

(58) Brisson, J. A.; Stern, D. L. *BioEssays* **2006**, *28*, 747-755.

(59) Fukatsu, T.; Nikoh, N.; Kawai, R.; Koga, R. *Applied and Environmental Microbiology* **2000**, *66*, 2748-2758.

(60) Moran, N. A. *Annual Review of Entomology* **1992**, *37*, 321-48.

(61) Mutti, N. S.; Park, Y.; Reese, J. C.; Reeck, G. R. *Journal of Insect Science* **2006**, *6*, No pp given.

(62) Auclair, J. L. *Canadian Entomologist* **1964**, *96*, 241-9.

(63) Auclair, J. L. *Annals of the Entomological Society of America* **1965**, *58*, 855-75.

(64) Srivastava, P. N.; Auclair, J. L. *Annals of the Entomological Society of America* **1971**, *64*, 739-43.

(65) Akey, D. H.; Beck, S. D. *Journal of Insect Physiology* **1972**, *18*, 1901-14.

(66) Fichorova, R. N.; Richardson-Harman, N.; Alfano, M.; Belec, L.; Carbonneil, C.; Chen, S.; Cosentino, L.; Curtis, K.; Dezzutti, C. S.; Donoval, B.; Doncel, G. F.; Donaghay, M.; Grivel, J.-C.; Guzman, E.; Hayes, M.; Herold, B.; Hillier, S.; Lackman-Smith, C.; Landay, A.; Margolis, L.; Mayer, K. H.; Pasicznyk, J.-M.; Pallansch-Cokonis, M.; Poli, G.; Reichelderfer, P.; Roberts, P.; Rodriguez, I.; Saidi, H.; Sassi, R. R.; Shattock, R.; Cummins, J. E., Jr. *Analytical Chemistry* **2008**, *80*, 4741-4751.

(67) Eckardt, N. A. *The Plant Cell* **2001**, *13*, 989-92.

(68) Brauer, M.; Zhong, W.-J.; Jelitto, T.; Schobert, C.; Sanders, D.; Komor, E. *Planta* **1998**, *206*, 103-107.

(69) Will, T.; van Bel, A. J. E. *Journal of Experimental Botany* **2006**, *57*, 729-737.

(70) Evans, D. E.; Briars, S. A.; Williams, L. E. *Journal of Experimental Botany* **1991**, *42*, 285-303.

(71) Pavia, D. L.; Lampman, G. M.; Kriz, G. S. *Introduction to Spectroscpoy*; 3rd ed.; Thomson Learning, Inc.: London, 2001.

(72) Solomons, T. W. G. *Organic Chemistry*; 6th ed.; John Wiley and Sons, Inc.: New York, 1996.

(73) Harmel, N.; Letocart, E.; Cherqui, A.; Giordanengo, P.; Mazzucchelli, G.; Guillonneau, F.; De Pauw, E.; Haubruge, E.; Francis, F. *Insect Molecular Biology* **2008**, *17*, 165-174.

(74) Jacobson, S. C.; Ramsey, J. M. *Analytical Chemistry* **1997**, *69*, 3212-3217.

(75) Blankenstein, G.; Larsen, U. D. *Biosensors & Bioelectronics* **1998**, *13*, 427-438.

(76) Irish, J. M.; Kotecha, N.; Nolan, G. P. *Nature Reviews Cancer* **2006**, *6*, 146-155.

(77) Ateya, D. A.; Erickson, J. S.; Howell, P. B., Jr.; Hilliard, L. R.; Golden, J. P.; Ligler, F. S. *Analytical and Bioanalytical Chemistry* **2008**, *391*, 1485-1498.

(78) Lin, Y.-H.; Lee, G.-B. *Biosensors & Bioelectronics* **2008**, *24*, 572-578.

(79) Rosenbluth, M. J.; Lam, W. A.; Fletcher, D. A. *Lab on a Chip* **2008**, *8*, 1062-1070.

(80) Cheung, K.; Gawad, S.; Renaud, P. *Cytometry, Part A* **2005**, *65A*, 124-132.

(81) Gawad, S.; Schild, L.; Renaud, P. *Lab on a Chip* **2001**, *1*, 76-82.

(82) Guijt, R. M.; Evenhuis, C. J.; Macka, M.; Haddad, P. R. *Electrophoresis* **2004**, *25*, 4032-4057.

(83) Liu, Y.; Wipf, D. O.; Henry, C. S. *The Analyst* **2001**, *126*, 1248-1251.

(84) Kuban, P.; Hauser, P. C. *Lab on a Chip* **2005**, *5*, 407-415.

Appendix A - Artificial Diet Preparation Protocols

A.1 - 15% Sucrose Diet Preparation

The 15% sucrose diet was prepared in sterile conditions each day it was to be used. This was done by dissolving 15 grams of sucrose into 100 mL of distilled deionized water under constant stirring.

A.2 - Diet 3 Preparation

Diet 3 was prepared by dissolving 1.051 grams of methionine, 1.42 grams of serine, 1.996 grams of aspartic acid, and 15 grams of sucrose in ~60 mL of water. The pH of the diet was adjusted to pH 7 using 1.75 M potassium hydroxide, and the volume was brought up to a total of 100 mL using distilled deionized water with continuous stirring. The diet was stored at -18°C until use.

A.3 - Complete Diet Preparation

The complete diet recipe was modified from the procedures used by Akey, Beck/Douglas, and Prosser. Our Complete Diet as was prepared as follows.

7) Dissolve sucrose in ~60 mL of distilled water.
8) Add components in this order: amino acids, vitamins, salts/buffers/sterol (from crystalline stock).
9) Add trace metals from 100x stock solutions.
10) Weigh and dissolve magnesium chloride and choline chloride in the solution.
11) Add ~1.25 mL of 1.75 M potassium hydroxide and stir for 1-3 hours.

12) Slowly, over 0.5 to 1.0 hours, raise the pH of the diet to 7.5 using the 1.75 M KOH solution.

The concentrations and masses for 100 mL of Complete Diet components are shown below in **Table A.1**.

Sugars	**Conc.**	**Mass**
Sucrose	0.5M	17.1g
Amino acids and amides		
Essential amino acids		
L-Arginine HCl	12.5mM	263.34 mg
L-Histidine(Free Base)	7.5 mM	116.4 mg
L-Isoleucine (Allo Free)	7.5mM	98.4 mg
L-Leucine	7.5mM	98.4 mg
L-Lysine HCl	7.5mM	137 mg
L-Methionine	2.5mM	37.3 mg
L-Phenylalanine	2.5mM	41.3 mg
L-Threonine (Allo Free)	7.5mM	89.3 mg
L-Tryptphane	2.5mM	51.1 mg
L-Valine	7.5mM	87.8 mg
Total essencial amino acids	**65 mM**	**1020.34 mg**
Nonessential amino acids		
L-Alanine	5mM	44.5mg

L-Asparagine (Anhydrous)	12.5mM	165.15mg
L-Aspartic acid C.P.	12.5mM	166.4mg
L- Cystein HCl monohydrate	2.5mM	39.4mg
L-Cystine	0.2mM	5mg
Gamma amino butyric acid	2mM	20mg
L-Glutamic acid	7.5mM	110.33mg
L-Glutamine(Commercial)	15mM	219.2mg
Glycine	1mM	7.5mg
L-Proline	5mM	57.6mg
L-Serine	5mM	52.5mg
L-Tyrosine	0.5mM	9mg
Total nonessential amino acids	**68.7mM**	**896.58mg**
Total amino acids	**133.7mM**	**1916.92mg**
Vitamins		
p-Aminobenzoic acid	0.73mM	10mg
Ascorbic acid	5.68mM	100mg
Biotin	6uM	0.1mg
D-Calcium pantothenate	0.21mM	5mg
Folic acid	22uM	1mg
i-Inositol (meso) dihydrate	1.39mM	50mg

Nicotinic acid	0.812mM	10mg
Pyridoxine HCl	0.121mM	2.5mg
Thiamine HCl	74uM	2.5mg
Salts, Buffers and Sterol		
Calcium citrate	0.175mM	10mg
Cholesterol benzoate	50uM	2.5mg
Potassium phosphate monobasic	18.37mM	250mg
Sodium chloride	0.217 mM	12.7mg
Cupric chloride	14uM	0.254mg
Ferric chloride	49uM	1.336mg
Manganese (II) chloride	40uM	1.271mg
Zinc sulfate	30uM	0.86mg
Magnesium chloride-6H20	9.837mM	200mg
Choline chloride	3.579mM	50mg